Biology and clinical implications of the 19q13 aggressive prostate cancer susceptibility locus

Ping Gao,[1,13] Ji-Han Xia,[1,13] Csilla Sipeky,[2] Xiao-Ming Dong,[1] Qin Zhang,[1] Yuehong Yang,[1] Peng Zhang,[3] Sara Pereira Cruz,[1] Kai Zhang,[1] Jing Zhu,[3] Hang-Mao Lee,[1] Sufyan Suleman,[1] Nikolaos Giannareas,[1] Song Liu,[4] The PRACTICAL consortium,[5] Teuvo L.J. Tammela,[6] Anssi Auvinen,[7] Xiaoyue Wang,[4] Qilai Huang,[8] Liguo Wang,[9] Aki Manninen,[1] Markku H Vaarala,[10,11] Liang Wang,[3] Johanna Schleutker,[2,12] and Gong-Hong Wei[1,14,*]

[1]Biocenter Oulu, Faculty of Biochemistry and Molecular Medicine, University of Oulu, FIN-90014 Oulu, Finland

[2]Institute of Biomedicine, University of Turku, FI-20014 Turku, Finland

[3]Department of Pathology, MCW Cancer Center, Medical College of Wisconsin, Milwaukee, WI, 53226, USA

[4]State Key Laboratory of Medical Molecular Biology, Center for Bioinformatics, Institute of Basic Medical Sciences, Chinese Academy of Medical Sciences, Peking Union Medical College, Beijing, 100005, China

[5]A list of members appears in the **Supplementary Note**

[6]Department of Urology, Tampere University Hospital and Medical School, University of Tampere, FI-33521 Tampere, Finland

[7]University of Tampere, School of Health Sciences, FI-33520 Tampere, Finland

[8]School of Life Science, Shandong University, Jinan, 250012, China

[9]Division of Biomedical Statistics and Informatics, Mayo Clinic College of Medicine, Rochester, MN 55905, USA

[10]Oulu University Hospital, FIN-90014 Oulu, Finland

[11]Medical Research Center Oulu, University of Oulu and Oulu University Hospital, FIN-90014 Oulu, Finland

[12]Tyks Microbiology and Genetics, Department of Medical Genetics, Turku University Hospital, FI-20014 Turku, Finland

[13]These authors contributed equally

[14]Lead Contact

[*]Correspondence: gonghong.wei@oulu.fi (G.-H.W)

SUMMARY

GWASs have identified rs11672691 at 19q13 associated with aggressive prostate cancer (PCa). Here, we independently confirmed the finding in a cohort of 2738 PCa patients, and discovered the biological mechanism underlying this association. We found an association of the aggressive PCa-associated allele G of rs11672691 with elevated mRNA levels of two biologically plausible candidate genes *PCAT19* and *CEACAM21*, implicating in PCa cell growth and tumor progression. Mechanistically, rs11672691 resides in an enhancer element and alters the binding site of HOXA2, a novel oncogenic transcription factor with prognostic potential in PCa. Remarkably, CRISPR/Cas9-mediated single nucleotide editing showed direct effect of rs11672691 on *PCAT19* and *CEACAM21* expression, and PCa cellular aggressive phenotype. Clinical data demonstrated synergistic effects of rs11672691 genotype and *PCAT19*/*CEACAM21* gene expression on PCa prognosis. These results provide a plausible mechanism for rs11672691 associated with aggressive PCa, and hence lay the ground work for translating this finding to the clinic.

INTRODUCTION

Prostate cancer (PCa) affects millions of men worldwide, and is the second most common cancer in men and the fifth leading cause of cancer-related death, with more than 1.1 million new cases diagnosed and 300,000 deaths annually worldwide (Ferlay et al., 2015). While several risk factors have been implicated in PCa etiology and development, the genetic heritability of PCa has been estimated at 57% (Mucci et al., 2016). Our understanding of genetic predisposition to PCa has been transformed by recent genome-wide association studies (GWAS), which have thus far discovered over one hundred independent single nucleotide polymorphisms (SNPs) associated with PCa risk (Al Olama et al., 2014; Whitington et al., 2016). However, the vast majority of GWAS SNPs reside within non-coding genomic regions often far from the nearest genes (MacArthur et al., 2017; Whitington et al., 2016), thus, the molecular mechanisms underlying the causal actions and biological effects of these SNPs remain poorly understood. To date, few if any causative SNPs can be used for predicting PCa outcome.

While indolent PCa patients may be easily treated, the patients with aggressive PCa often have worse prognosis and thus need intensive treatment. Recent GWASs have identified several aggressive PCa susceptibility loci including rs11672691 at 19q13 (Amin Al Olama et al., 2013), rs35148638 at 5q14.3 and rs78943174 at 3q26.31 (Berndt et al., 2015) with potential in management for the aggressive form of the disease, though the molecular mechanisms and biological effects underlying these associations need to be investigated. A recent meta-analysis of GWAS (Amin Al Olama et al., 2013) reported that rs11672691 within intron 2 of long non-coding RNA (lncRNA)

PCAT19 (prostate cancer associated transcript 19) was not only associated with PCa predisposition but also with PCa aggressiveness. Intriguingly, the association of rs11672691 with aggressive PCa was also observed in another large cohort study (Shui et al., 2014), demonstrating that rs11672691 was associated with increased risk of PCa-specific mortality through a median follow-up of 8.3 years of 10,487 men with PCa.

In the current study, we also observed a robust association of rs11672691 with clinical features indicative of aggressive disease including high tumor stage, PSA progression and the development of castration resistant prostate cancer (CRPC) in a cohort of 2738 men with PCa, and sought to define the underlying mechanisms by which the SNP rs11672691 at 19q13 impacts PCa severity. We reported a novel association of rs11672691 genotype and the expression of two previously unknown PCa genes, *PCAT19* and *CEACAM21*. We also demonstrated the mechanisms by which the aggressive PCa risk-associated allele G of rs11672691 influenced the transcription of *PCAT19* and *CEACAM21* via enhancing chromatin binding affinity of HOXA2, a novel oncogenic transcriptional regulator with prognosis potential in PCa. Moreover, we provided direct evidence showing that rs11672691 was involved in the regulation of *PCAT19* and *CEACAM21* expression and impacted PCa tumor cellular property. Finally, we observed synergistic effects among rs11672691 genotype, *PCAT19* and *CEACAM21* expression on the prediction of PCa relapse and survival, highlighting clinical potential of this SNP as a risk stratification marker for the management of PCa patients.

RESULTS

Association of rs11672691 with clinical features of aggressive PCa

SNP rs11672691 resides in the intergenic region at 19q13 between the genes *ATP5SL* and *CEACAM21* and within *PCAT19*, an lncRNA gene (Amin Al Olama et al., 2013). To further strengthen the finding of rs11672691 in association with aggressive PCa susceptibility, we conducted an analysis of 2738 Finnish PCa cases (**Table S1**). This analysis revealed that the rs11672691 GG genotype was associated with an increased risk of developing advanced T stage (OR, 1.23, 95% CI, 1.02-1.48, p=0.03), the measure of local extent of a prostate tumor, and therefore a poorer prognosis (**Table 1**). This association predicts whether the PCa has higher chance to grow outside the prostate (T3a), to grow into the seminal vesicles (T3b) or into tissues next to prostate, such as urethral sphincter, rectum, bladder, and/or the wall of the pelvis (T4). Noteworthy, only a few prior genetic studies were able to assess association of germline genetic variants with tumor stage (Henriquez-Hernandez et al., 2014). We therefore identified, for the first time, rs11672691 as marker for PCa tumor stage progression.

We next investigated the association of rs11672691 variant with additional clinical features of PCa prognosis, namely PSA progression and the development of CRPC. We observed the association of both GG genotype (OR 1.31, 95% CI, 1.11-1.54, p=0.001) and the G carriers (OR 1.62, 95% CI, 1.13-2.32, p=0.008) of rs11672691 with PSA progression during the course of the disease, predicting worse prognosis (**Table 1**). This is in line with the observation that carriers of rs11672691 allele G have 1.75-fold odds of CRPC (95% CI, 1.00-3.05, p=0.048), progression of PCa to an incurable stage after androgen depletion therapy. Collectively, data from Finnish cohort provide further evidence that the allele G of rs11672691 is associated with several clinical features indicative of aggressive PCa risk.

Association of rs11672691 allele G with elevated expression of two plausible PCa genes *PCAT19* and *CEACAM21*

We next sought to find whether rs11672691 was associated with the expression of nearby genes, and thus performed an expression quantitative trait locus (eQTL) analysis using data from three independent cohorts (Swedish, TCGA and Wisconsin cohort) with nearly 1,000 prostate tissue samples. This analysis revealed a strong association of the aggressive PCa risk allele G at rs11672691 with higher mRNA levels of *CEACAM21* (**Figures 1A-C**). Interestingly, our analysis revealed an additional eQTL gene *PCAT19* for rs11672691 (**Figure 1D**). Consistent with this, gene level allele-specific expression (ASE) analysis in 471 benign primary prostate tissue samples (Larson et al., 2015) revealed a significant association of rs11672691 allele G with *PCAT19* upregulation ($p=8.61 \times 10^{-15}$).

PCAT19 codes an lncRNA and harbors rs11672691 in its second intron. Given that many lncRNAs play an important role in cancer initiation and progression (Gao and Wei, 2017; Kopp and Mendell, 2018), we hypothesized that *PCAT19* and *CEACAM21* may possess unknown function in PCa. To test this, we performed knockdown assays using lentivirus-mediated short hairpin (shRNA) against *CEACAM21* or *PCAT19* in multiple PCa cell models. The results showed that knockdown of *PCAT19* or *CEACAM21* markedly attenuated cell proliferation, migration and invasion in PCa cell lines 22Rv1, Du145 and LNCaP (**Figures 1E,F** and **S1**). Given the consistent observations of rs11672691 G risk allele associated with elevated *CEACAM21* expression (**Figures 1A-C**), we further pursued cellular approaches to demonstrate the effects of *CEACAM21* upregulation. Accordingly, plasmid- or lentivirus vector-based ectopic expression of CEACAM21 increased cellular proliferation (**Figures 1G** and **S2A-D**). Consistent with this, CEACAM21 overexpression significantly stimulated the growth of immortalized prostatic epithelial RWPE1 cells in 3D cultures (**Figure S2E**). We further observed higher migration and invasion capacity in the tested CEACAM21-overexpressing prostate cell lines (**Figures 1H** and **S2F-H**). To explore the mechanistic role of CEACAM21 in PCa, we performed RNA-seq analysis of CEACAM21-overexpressing RWPE1 cells (**Figure S3A**). We observed high correlation between three biological replicates and found that 924 genes were upregulated, while 915 genes were downregulated by ectopic CEACAM21 expression (DESeq2, FDR<0.01; **Figures S3B,C**). Gene set enrichment analysis on 50 "hallmark" gene sets (Subramanian et al., 2005) revealed the strongest enrichment of genes upregulated in CEACAM21 overexpression for MYC target profiles and mTORC1 signaling pathway (**Figures 1I** and **S3D**; **Table S2**). Given previous studies of MYC or mTORC1 signaling involvement in cancer (Dang, 2012; Saxton and Sabatini, 2017), our observations may implicate the role of CEACAM21 in MYC and mTORC1 activation, thereby promoting cell growth, invasion and metastasis in PCa.

We next explored whether higher RNA levels of *PCAT19* or *CEACAM21* correlated with human PCa progression in the clinical setting, and thus analyzed five independent PCa expression profile data sets (Arredouani et al., 2009; Cerami et al., 2012 Chandran et al., 2007; Ren et al., 2012; Tomlins et al., 2007). The results indicated that *PCAT19* and *CEACAM21* were highly expressed in prostate tumor tissues compared to normal prostate gland (**Figures 1J,K** and **S3E**). We observed that the mRNA levels of *CEACAM21* were significantly increased in metastatic PCa samples (**Figures 1L** and **S3F**), suggesting a potential role of *CEACAM21* in advanced prostate tumors. Thus, we investigated the association of *CEACAM21* expression with postoperative PSA recurrence by using a Kaplan-Meier analysis. The patient group with higher expression levels of *CEACAM21* had an increased risk of biochemical relapse (**Figure 1M**). Collectively, these data illustrate a significant association of the risk allele G at rs11672691 with higher expression levels of two previously unknown PCa genes *PCAT19* and *CEACAM21*, and their upregulation correlates with the development of PCa, suggesting that *PCAT19* and *CEACAM21* are plausible causative genes mediating the effect of rs11672691 on PCa severity.

rs11672691 resides in the binding site of a transcriptional complex including HOXA2

We next asked how the rs11672691 G risk allele involves in regulating the expression of *PCAT19* and *CEACAM21*. To thoroughly understand the regulatory mechanisms underlying rs11672691, we first performed genome-wide analysis of epigenome and transcription factor ChIP-seq data derived from PCa cells or tumor tissues (Kron et al., 2017; Mei et al., 2017; Whitington et al., 2016). We observed an enrichment of epigenetic marks (H3K4me1/2 and H3K27ac) for active enhancer and multiple transcription factors including AR, HOXB13 and ERG at rs11672691 region based on ChIP-seq profiles (**Figure 2A**), suggesting that this is an enhancer element. In contrast, we found no enrichment of silent epigenetic mark H3K27me3 and inactive chromatin regulator EZH2 (**Figure 2A**). We proved this result by performing enhancer reporter assays (**Figure 2B**) and the modified STARR-seq method (Liu et al., 2017) (**Figure S4A**). We next conducted imputation for SNPs in a tight linkage disequilibrium (r^2 >0.8) with lead SNP rs11672691 from the 1000 Genome Project to determine if there exists additional regulatory variants in this haplotype (Ward et al., 2012). We thus found that only rs887391 (r^2 = 0.87 with rs11672691; 36bp downstream of rs11672691) located at active gene regulatory element, the same enhancer region with rs11672691 (**Table S3**). Notably, rs887391 was previously reported to be associated with PCa risk but not at the level of GWAS significance (Hsu et al., 2009). In addition, no association was found for rs887391 with aggressiveness and other clinical characteristics of PCa. Together, these analyses suggest that rs11672691 is a likely causal regulatory SNP at this aggressive PCa susceptibility locus.

Given that regulatory SNPs with causal roles in disease susceptibility are often leading to transcription factor DNA binding variation (Deplancke et al., 2016), we next examined whether rs11672691 directly alters the DNA-binding motif of any transcription factor. We thus performed computational analysis using the Enhancer Element Locator (EEL) algorithm (Hallikas et al., 2006) and the DNA-binding position weight matrix data of human transcription factors (Jolma et al., 2013). This analysis revealed that rs11672691 maps within the binding motifs of homeodomain transcription factors including NKX3.1 and HOXA2 with the strongest match for the rs11672691-centered 13-bp genomic sequence (**Figure 2C** and **Table S4**). Interestingly, rs887391 also maps within HOXA2 DNA-binding motif (**Figure 2C**). Remarkably, the EEL prediction showed obviously increased DNA-binding affinity for aggressive PCa susceptibility G allele compared to the reference A allele at rs11672691

(**Figures 2C** and **S4B**). In contrast, rs887391 shows no obvious difference in its DNA binding affinity to HOXA2 (**Figures 2C** and **S4C**). We therefore focused the HOXA2-DNA binding variation altered by rs11672691. To assess whether the ChIP-seq-defined transcription factors at rs11672691 (**Figure 2A**) and other HOXA family members, can bind to this area, we performed microwell-based transcription factor-DNA binding assay in vitro and ChIP followed by qPCR (ChIP-qPCR) in vivo (Huang et al., 2014). The microwell-based analysis showed that HOXA2 indicated the strongest binding to the DNA sequence harboring rs11672691 compare to other tested transcription factors (**Figure 2D**). Moreover, HOXA2 showed the binding preference to allele G over allele A of rs11672691 (**Figures S4D,E**). The ChIP-qPCR results also showed the enrichment of HOXA2, ERG, HOXB13, AR, and HOXA10 at the rs11672691-containing region in multiple PCa cell lines including LNCaP, 22Rv1 and VCaP (**Figures 2E-G** and **S4F-H**), though some transcription factors such as HOXA10, ERG, and AR indicated no binding activity to the rs11672691-containing sequence in vitro (**Figure 2D**). We also performed ChIP-qPCR assays with available antibodies for HOXA9 and HOXA13, as well as HOXA10 in VCaP cells and found no enrichment (**Figures S4I,J**). Taking these studies together, we observed the strongest in vitro binding of HOXA2 at the sequence harboring rs11672691 (**Figure 2D**), and reproducible chromatin occupancy of HOXA2 at rs11672691 enhancer in all the tested PCa cell models (**Figures 2E-G**). These results suggested that HOXA2 is likely to be a driver transcription factor transforming the biological effects of rs11672691 on aggressive behavior of PCa.

To evaluate the binding preference of HOXA2 to rs11672691 in vivo, we performed ChIP followed by allele-specific qPCR (AS-qPCR) analysis or

Sanger sequencing in the PCa cells 22Rv1 that is heterozygous for this SNP (Huang et al., 2014). These analyses showed that HOXA2 was preferentially recruited to the risk G allele at rs11672691 (**Figures 2G,H**), consistent with our bioinformatics results (**Figures 2C**) and the observation of a stronger binding affinity for HOXA2 at G allele than A allele of rs11672691 in vitro (**Figures S4B,D,E**). To verify this finding independently, we performed ectopic expression of V5 tagged HOXA2 in 22Rv1 cells followed by ChIP-qPCR using anti-V5 tag antibody (**Figure 2I**). Consistently, the results showed a strong occupancy of HOXA2 at the DNA fragment harboring rs11672691 and binding preference to the G allele (**Figures 2J** and **S4K**). Together, these data indicate that HOXA2 directly binds at the rs11672691 enhancer with preference to the aggressive PCa risk-associated G allele at rs11672691.

HOXA2 **as an oncogene with prognostic potential in PCa**

The established roles and the interactions among ERG, HOXB13 and AR in PCa have been previously reported (Kron et al., 2017; Pomerantz et al., 2015; Wei et al., 2010), yet the function of HOXA2 in PCa is completely uncharacterized. We first found that *HOXA2* was an androgen-responsive gene (**Figure S5A**). To examine whether *HOXA2* implicates PCa, we performed short hairpin RNA (shRNA)-mediated knockdown of *HOXA2* in the 22Rv1 cells. Cells with shRNA against *HOXA2* showed greatly reduced cell growth compared to cells transduced with control shRNA in a proliferation assay (**Figure 3A**). This is in line with the data of genome-wide CRISPR/Cas9-based loss-of-function screen in the PCa cell line LNCaP for the identification of genes that are essential for cell viability (Aguirre et al., 2016), where *HOXA2* showed importance for the survival of LNCaP (**Figure 3B**). Next, we performed cell migration and invasion assays using the Boyden chamber with or without Matrigel. 22Rv1 cells with knockdown of *HOXA2* showed decreased cell migration and invasion (**Figures 3C** and **S5B-D**). To investigate the biological roles of *HOXA2* in PCa progression, we performed clinical correlation and prognosis analyses. The results showed that the mRNA levels of *HOXA2* were greatly upregulated in primary and metastatic PCa tumors compared to normal prostate gland (Grasso et al., 2012; Liu et al., 2006) (**Figures 3D,E**). In addition, the patient group with higher mRNA levels of *HOXA2* has increased risk for postoperative biochemical recurrence and shorter time for overall survival (Cancer Genome Atlas Research Network, 2015; Cerami et al., 2012) (**Figures 3F,G** and **S5E**). We next examined whether *HOXA2* levels possess predictive values for low- and high-risk PCa, and hence subdivided a large PCa cohort by Gleason score and compared the frequency of biochemical relapse. This analysis revealed a clear predictive value of *HOXA2* mRNA levels for biochemical relapse in the patients with a Gleason score of 7 (intermediate risk; **Figures 3H** and **S5F**), but not for the patient groups with Gleason ≤6 (low risk; **Figure S5G**) or Gleason score ≥8 disease (high risk; **Figure S5H**). The results indicate that *HOXA2* is a potential prognosis marker to distinguish PCa patients that may recur in the group with intermediate risk PCa. These observations, together with tumor cell biology experiments, illustrate that *HOXA2* is a newly-identified PCa relevant gene with potential prognosis values in PCa risk prediction, further supporting HOXA2 as an effective transcription factor transforming the regulatory effects of rs11672691 for aggressive PCa susceptibility.

HOXA2 as regulator of rs11672691 eQTL genes

Our established ChIP-qPCR results demonstrated the enrichment of HOXA2, ERG, HOXB13 and HOXA10 at the rs11672691 enhancer region (**Figures 2E-J** and **S4F-H**). Thus, we sought to investigate whether HOXA2, ERG, HOXB13 or HOXA10 affect the expression levels of rs11672691-associated genes *PCAT19* and *CEACAM21* via RNA interference-mediated knockdown assays in PCa cells. The results showed that the transcript levels of *PCAT19* or *CEACAM21* were significantly downregulated upon knockdown of *HOXA2, ERG* or *HOXB13*, respectively (**Figures 4A** and **S6A,B**), suggesting that *PCAT19* or *CEACAM21* expression are regulated by HOXA2. In contrast, knockdown of *HOXA10* showed no effect on *PCAT19* or *CEACAM21* expression (**Figure S6C**). Similar to HOXA2 (**Figure S5A**), we observed that androgen treatment induced the expression of *PCAT19* and *CEACAM21* in VCaP cells (**Figures S6D,E**). Interestingly, we found a positive correlation between the expression of *CEACAM21* or *PCAT19* and *HOXA2* in two large cohorts of clinical prostate tissue samples (Taylor et al., 2010) (**Figures 4B,C**), suggesting that HOXA2 may also regulate the expression of *PCAT19* or *CEACAM21* in the clinical setting. These findings together with ChIP-seq and microwell-based binding results indicate that *PCAT19* and *CEACAM21* are the direct targets of HOXA2, and the variation at rs11672691 may contribute to this regulatory process.

Given that rs11672691 resides within intronic region of *PCAT19*, we may expect that the alteration of HOXA2 binding thus affect *PCAT19* expression. However, *CEACAM21* is over 100kb away from rs11672691. The regulatory mechanism of the gene is unclear. Several lncRNAs have been reported to possess enhancer-like function in regulating the expression of their neighboring protein-coding genes in human cells (Orom et al., 2010). We therefore assessed whether the transcripts from *PCAT19* contribute to the regulation of *CEACAM21* expression using siRNA and shRNA assays. We found that *PCAT19* knockdown led to reduced mRNA levels of *CEACAM21* (**Figures 4D** and **S6F**). Interestingly, we also observed that the expression of *PCAT19* and *CEACAM21* are positively correlated in a cohort of 462 benign prostate tissues samples (**Figure 4E**), indicating co-expression of *PCAT19* and *CEACAM21* in association with PCa and a likely regulatory mechanism in the clinical setting.

Having demonstrated that rs11672691 resides within an enhancer region of *PCAT19* intron 2, and *PCAT19* possesses an enhancer-like function to regulate *CEACAM21* expression, we proceeded to test whether the variation at rs11672691 could directly alter *CEACAM21* promoter activity. We thus inserted the rs11672691-containing region into the upstream of *CEACAM21* promoter in an enhancer report assay. The results showed that the rs11672691-containing region with G allele has a higher enhancer activity than that with A allele to the *CEACAM21* promoter (**Figure 4F**). To examine whether there was direct chromatin interaction between rs11672691 enhancer and *CEACAM21* promoter region, we first performed quantitative chromosome conformation capture assays (3C-qPCR) (Hagege et al., 2007) with the restriction enzyme EcoR I. We used *CEACAM21* promoter region as constant fragment, and assessed its interaction with EcoR I digested chromatin fragments in this 100kb region covering rs11672691 locus in PCa cells VCaP and 22Rv1, and the breast cancer cell line MCF7. The results showed that the SNP rs11672691-containing enhancer has higher crosslinking frequencies in VCaP and 22Rv1 cells compared with MCF7 (**Figure 4G**), suggesting a PCa cell-type-specific long-range chromatin interaction between *PCAT19* and *CEACAM21*. Moreover, androgen stimulation had clear impact on the observed interaction between rs11672691 enhancer and *CEACAM21* (**Figure 4G**). Consistent with our 3C analysis, rs11672691 enhancer was found to form a strong chromatin interaction with *CEACAM21* in rs11672691-centered 1Mb window in LNCaP Hi-C data (Wang et al., 2017) (**Figure S6G**). Given that *PCAT19* knockdown led to decreased expression of *CEACAM21*, we assessed the role of *PCAT19* transcript in this chromatin interaction, and performed 3C assays in *PCAT19* knockdown 22Rv1 cells. We observed no apparent changes in locus-wide crosslinking frequencies (**Figure S6H**), suggesting that *PCAT19* transcript may play only a subtle or no role in this loop formation. Collectively, these results suggest that the G allele at rs11672691 within *PCAT19* transcriptionally regulates the expression of *CEACAM21*, and rs11672691 may directly contribute to HOXA2-mediated regulation of *PCAT19* and *CEACAM21* expression.

Direct effect of rs11672691 on its eQTL gene expression and PCa cell proliferation

To further investigate whether rs11672691 directly involves in the regulation of *PCAT19* and *CEACAM21* expression, we applied CRISPR/Cas9-mediated genome editing approach (Ran et al., 2013), and successfully converted the genotype of rs11672691 from G/A to G/G or A/A in PCa cell line 22Rv1 (**Figure 4H**). The mutated cells with rs11672691 G/G had higher transcriptional levels of *PCAT19* and *CEACAM21* than the parental cells, while their expression levels were markedly lower in 22Rv1 cells with rs11672691 AA genotype than that in parental cells (**Figure 4I**). This effect of rs11672691 enhancer on *PCAT19* was also validated in an independent study using CRISPR interference and activation assays (Hua et al., 2018). Consistently, we observed higher levels of HOXA2 chromatin occupancy at rs11672691 region in the 22Rv1 cells with rs11672691 G/G genotype than that in parental cells, and the cells with AA genotype showed the lowest enrichment of HOXA2 at rs11672691 region (**Figure 4J**). We next performed 3C experiments in the three types of cells, and found that the G/G genotype 22Rv1 cells had higher crosslinking frequencies between rs11672691 enhancer and *CEACAM21* than parental and A/A cells (**Figure 4K**).

In addition to the described molecular changes, we also observed the phenotypic difference between rs11672691 G/G, parental G/A and AA 22Rv1 cell lines under microscope. The G/G and parental 22Rv1 cells had the similar morphology, whereas A/A cells were quite different (**Figure 5A**), and the cell-cell contacts were very tight, indicating typical untransformed epithelial cell phenotype **(Figure 5A).** To determine whether there was any functional differences between the 22Rv1 cells with different genotypes for rs11672691, we analyzed their cellular proliferation and migration property. The results showed that homozygous G/G and parental G/A cells had higher proliferation rate compared to A/A clones (**Fig 5B**). Despite no difference observed between G/G and parental cells in the proliferation assays, we found an obvious promotion of wound closure in G/G and parental cells compared to the AA cells by performing wound-healing assays (**Figures 5C,D**). Collectively, these analyses provide direct lines of evidence that the risk G allele of rs11672691 contributes to enhanced expression of *PCAT19* and *CEACAM21*, and PCa cell proliferation and severity.

Synergistic prognostic effects of rs11672691 eQTLs on PCa severity

Given that the risk allele at rs11672691 was associated with higher expression of *CEACAM21* and *PCAT19* and that their upregulation correlated with PCa progression, we explored whether rs11672691 genotype directly correlated with PSA recurrence and survival status of individuals with PCa. We found that the PCa patients carrying homozygous risk genotype GG at rs11672691 correlated with increased frequency of biochemical relapse in the analysis of a large PCa cohort (**Figure 5E**). We observed the correlation in a similar direction with PSA recurrence and metastasis-free survival in an independent collection of Finnish PCa patients (**Figures 5F-H**). These results are well consistent with previous large cohort studies (Amin Al Olama et al., 2013; Shui et al., 2014), showing that the variant G at rs11672691 confers increased risk for aggressive PCa susceptibility.

We next performed Kaplan-Meier analysis and examined the association of *CEACAM21* and *PCAT19* expression with clinical variables indicating tumor aggressiveness in PCa patients with different rs11672691 genotype. We found that higher mRNA levels of *CEACAM21* were strongly correlated with increased risk of biochemical relapse in the patients carrying rs11672691 GG genotype (**Figures 6A** and **S7A**). In contrast, no similar association was found in the patients with rs11672691 GA or AA genotype (**Figure 6B**). Though *PCAT19* expression data alone showed no association with biochemical relapse of PCa patients (**Figure 6C**), the patient group with GG genotype and higher expression levels of *PCAT19* was strongly correlated with increased risk for PSA recurrence (**Figures 6D** and **S7B**). Together, these integrated analyses showed that the GG genotype at rs11672691 is associated with poor prognosis of PCa patients, and indicates synergistic effects with the expression data of *CEACAM21* or *PCAT19* to predict PCa clinical outcomes.

DISCUSSION

We present an integrated study of the mechanisms and the clinical implications underlying the 19q13 aggressive PCa risk locus. We identify an oncogenic regulatory circuit among several novel genes including *HOXA2*, *CEACAM21* and *PCAT19* underlying the association of rs11672691 with aggressive PCa and potentially driving disease progression to advanced stage.

Patients with aggressive PCa are typically treated by androgen deprivation therapy (Bishr and Saad, 2013). Although the ADT treatment is initially effective and can prolong the survival time of PCa patients, a high rate of patients will eventually relapse and begin to show signs of CRPC with high mortality rate (Bishr and Saad, 2013; Mills, 2014). Rs11672691 at 19q13 is associated with fatal PCa. Thus, characterizing the regulatory mechanisms of this association may provide more clues to aggressive PCa diagnosis and treatment. We reveal that rs11672691 is an enhancer variant and synergizes with HOXA2 to drive the expression of its eQTL genes *PCAT19* and *CEACAM21*. The biological function of *CEACAM21* in cancer is totally unknown. *CEACAM21* is a transmembrane protein-coding gene and belongs to the carcinoembryonic antigen gene family with several members playing roles in cell adhesion, invasion and metastasis (Amin Al Olama et al., 2013; Blumenthal et al., 2007), which may give some clues on how *CEACAM21* confers susceptibility to aggressive PCa. Interestingly, *CEACAM21* has been found to be a novel schizophrenia susceptibility gene (Alkelai et al., 2012), emphasizing its association with additional types of disease.

As reviewed extensively elsewhere (Gao and Wei, 2017), recent studies reported the association of lncRNAs with PCa and other types of cancer susceptibility. Notably, in a recent work (Guo et al., 2016), the PCa risk variant of rs7463708 was found to disrupt the binding of ONECUT2 and increased the expression of *PCAT1*, a well-studied PCa-associated lncRNA (Gao and Wei, 2017). These findings defined the relationships between lncRNAs and SNPs within major part of human genome with non-protein-coding capacity. In current study, we find a new lncRNA *PCAT19* as a plausible PCa susceptibility gene with high levels of expression in malignant tumors of the prostate. Furthermore, we provide evidence that this lncRNA could regulate the expression of a newly identified oncogene *CEACAM21* but not a loop formation between rs11672691 enhancer and *CEACAM21*. Together with an independent study of the rs11672691 effect on *PCAT19* expression (Hua et al., 2018), the data imply an alternative mechanism by which the rs11672691 enhancer may effect indirectly through *PCAT19* on *CEACAM21* expression. Moreover, unknown or known transcription factors such as HOXA2, HOXB13, AR and ERG, as well as NKX3.1 and YY1 (Hua et al., 2018) may facilitate loop formation at rs11672691 locus to regulate *PCAT19* and *CEACAM21* gene expression. Clinically, the expression levels of *PCAT19* or *CEACAM21* may synergize with rs11672691 genotypes to predict PCa severity.

One daunting challenge with mechanistic assessment of common, noncoding SNPs is having direct evidence to support the effect of each variant on gene expression and disease phenotype. Here we modified the existing CRISPR/Cas9 genome editing protocol (Ran et al., 2013) to change the genotype of rs11672691, and revealed a direct role of rs11672691 allele G in enhanced chromatin binding of HOXA2, elevated expression of *CEACAM21* and *PCAT19*, and tumor cellular property. The other genome editing methods such as TALEN have also been successfully applied to change the genotype of the SNPs, e.g. rs339331 (Spisak et al., 2015), which was found to enhance chromatin binding of HOXB13 and elevate *RFX6* expression driving PCa progression (Huang et al., 2014). In comparison with TALEN, CRISPR/Cas9 is much more efficient, accurate and easy to optimize for single nucleotide editing.

Our study may have clinical implications and translational value to benefit patients. We show that risk genotype of rs11672691 contributes to an elevated expression of *CEACAM21* and *PCAT19*. We also show that increased expression of the two genes and *HOXA2* are associated with poor prognosis and their knockdown reduces invasion and migration of PCa cells. Thus, the findings may allow better prognostic prediction and distinguishing a more lethal phenotype to identify high-risk group patients that need radical treatment regimens because of their poorer treatment outcomes. Clearly, *CEACAM21* and *PCAT19* are not only PCa susceptibility genes but also responsible for PCa aggressive phenotype. To date, there is no known therapeutic compound that directly targets these genes. Identification of such a compound will be important for more effective targeted therapies. Whether inhibition of the expression or function of these genes and their products affect tumor cell growth in clinical setting is an important topic for future studies.

In summary, we provide several lines of evidence together with clinical follow-up analysis to show biological roles of rs11672691 connecting with a regulatory circuit of HOXA2, *PCAT19* and *CEACAM21* for PCa cell growth and invasion, and their expression in association with disease progression. A major remaining question will be how this regulatory circuit directly or indirectly initiates PCa. Genetically engineered pre-clinical mouse models and patient-derived tumor grafts seem warranted to test this hypothesis.

ACKNOWLEDGMENTS

We thank Johanna Myllyharju, Kalervo Hiltunen, Peppi Karppinen, and Taina Pihlajaniemi for study support; Antti Viklund, Jaana Träskelin, Katri Pylkäs, Leena Keskitalo, Meeri Otsukka, Veli-Pekka Ronkainen, BCO Sequencing and Imaging Core for technical service; Fredrik Wiklund, Johan Lindberg, and Thomas Whitington for eQTL data; CSC-IT Center for Computing server and TCGA Research Network. This work was funded by Academy of Finland (284618/279760 to G.-H.W., 251074/310115 to J.S.); UO Strategic Funds (G.-H.W.); Jane and Aatos Erkko Foundation (G.-H.W.); Finnish Cancer Foundation (G.-H.W. and J.S.); Sigrid Juselius Foundation (J.S.); Turku University Hospital (M3002/M4807 to J.S.); and National Institute of Health (R01CA157881 to L.W.).

AUTHOR CONTRIBUTIONS

G.-H.W. conceptualized, designed and supervised the project. P.G., J.-H.X., X.-M.D., and Y.Y. assisted by S.S., N.G., and Q.H. performed the experiments. C.S., T.L.J.T., A.A., and J.S. generated PCa cohort data. Q.Z. did bioinformatics analysis. H.-M.L. did ChIP-seq reanalysis. L.G.W analysed TCGA RNA-seq data. P.Z., J.Z., and L. W. contributed to eQTL analysis. S.P.C., K.Z., and A.M. contributed to 3D cell culture and phenotyping. S.L. and X.W. did STARR-seq. M.H.V. provided PCa clinical data. G.-H.W., and P.G. wrote the manuscript with help from J.-H.X., C.S., Q.Z., A.M., and input from other co-authors.

DECLARATION OF INTERESTS

The authors declare no competing interests.

REFERENCES

Aguirre, A.J., Meyers, R.M., Weir, B.A., Vazquez, F., Zhang, C.Z., Ben-David, U., Cook, A., Ha, G., Harrington, W.F., Doshi, M.B.*, et al.* (2016). Genomic Copy Number Dictates a Gene-Independent Cell Response to CRISPR/Cas9 Targeting. Cancer. Discov. *6,* 914-929.

Al Olama, A.A., Kote-Jarai, Z., Berndt, S.I., Conti, D.V., Schumacher, F., Han, Y., Benlloch, S., Hazelett, D.J., Wang, Z., Saunders, E.*, et al.* (2014). A meta-analysis of 87,040 individuals identifies 23 new susceptibility loci for prostate cancer. Nat. Genet. *46,* 1103-1109.

Alkelai, A., Lupoli, S., Greenbaum, L., Kohn, Y., Kanyas-Sarner, K., Ben-Asher, E., Lancet, D., Macciardi, F., and Lerer, B. (2012). DOCK4 and CEACAM21 as novel schizophrenia candidate genes in the Jewish population. Int. J. Neuropsychopharmacol. *15,* 459-469.

Amin Al Olama, A., Kote-Jarai, Z., Schumacher, F.R., Wiklund, F., Berndt, S.I., Benlloch, S., Giles, G.G., Severi, G., Neal, D.E., Hamdy, F.C.*, et al.* (2013). A meta-analysis of genome-wide association studies to identify prostate cancer susceptibility loci associated with aggressive and non-aggressive disease. Hum. Mol. Genet. *22,* 408-415.

Arredouani, M.S., Lu, B., Bhasin, M., Eljanne, M., Yue, W., Mosquera, J.M., Bubley, G.J., Li, V., Rubin, M.A., Libermann, T.A., *et al.* (2009). Identification of the transcription factor single-minded homologue 2 as a potential biomarker and immunotherapy target in prostate cancer. Clin. Cancer Res. *15,* 5794-5802.

Berndt, S.I., Wang, Z., Yeager, M., Alavanja, M.C., Albanes, D., Amundadottir, L., Andriole, G., Beane Freeman, L., Campa, D., Cancel-Tassin, G.*, et al.* (2015). Two susceptibility loci identified for prostate cancer aggressiveness. Nat. Commun. *6,* 6889.

Bishr, M., and Saad, F. (2013). Overview of the latest treatments for castration-resistant prostate cancer. Nat. Rev. Urol. *10,* 522-528.

Blumenthal, R.D., Leon, E., Hansen, H.J., and Goldenberg, D.M. (2007). Expression patterns of CEACAM5 and CEACAM6 in primary and metastatic cancers. BMC Cancer *7,* 2.

Cancer Genome Atlas Research Network. (2015). The Molecular Taxonomy of Primary Prostate Cancer. Cell *163,* 1011-1025.

Cerami, E., Gao, J., Dogrusoz, U., Gross, B.E., Sumer, S.O., Aksoy, B.A., Jacobsen, A., Byrne, C.J., Heuer, M.L., Larsson, E.*, et al.* (2012). The cBio cancer genomics portal: an open platform for exploring multidimensional cancer genomics data. Cancer. Discov. *2,* 401-404.

Chandran, U.R., Ma, C., Dhir, R., Bisceglia, M., Lyons-Weiler, M., Liang, W., Michalopoulos, G., Becich, M., and Monzon, F.A. (2007). Gene expression profiles of prostate cancer reveal involvement of multiple molecular pathways in the metastatic process. BMC Cancer *7,* 64.

Dang, C.V. (2012). MYC on the path to cancer. Cell *149,* 22-35.

Deplancke, B., Alpern, D., and Gardeux, V. (2016). The Genetics of Transcription Factor DNA Binding Variation. Cell *166,* 538-554.

Ferlay, J., Soerjomataram, I., Dikshit, R., Eser, S., Mathers, C., Rebelo, M., Parkin, D.M., Forman, D., and Bray, F. (2015). Cancer incidence and mortality worldwide: sources, methods and major patterns in GLOBOCAN 2012. Int. J. Cancer *136,* E359-86.

Gao, P., and Wei, G.H. (2017). Genomic Insight into the Role of lncRNA in Cancer Susceptibility. Int. J. Mol. Sci. *18,* pii: E1239.

Grasso, C.S., Wu, Y.M., Robinson, D.R., Cao, X., Dhanasekaran, S.M., Khan, A.P., Quist, M.J., Jing, X., Lonigro, R.J., Brenner, J.C.*, et al.* (2012). The mutational landscape of lethal castration-resistant prostate cancer. Nature *487,* 239-243.

Guo, H., Ahmed, M., Zhang, F., Yao, C.Q., Li, S., Liang, Y., Hua, J., Soares, F., Sun, Y., Langstein, J.*, et al.* (2016). Modulation of long noncoding RNAs by risk SNPs underlying genetic predispositions to prostate cancer. Nat. Genet. *48,* 1142-1150.

Hagege, H., Klous, P., Braem, C., Splinter, E., Dekker, J., Cathala, G., de Laat, W., and Forne, T. (2007). Quantitative analysis of chromosome conformation capture assays (3C-qPCR). Nat. Protoc. *2,* 1722-1733.

Hallikas, O., Palin, K., Sinjushina, N., Rautiainen, R., Partanen, J., Ukkonen, E., and Taipale, J. (2006). Genome-wide prediction of mammalian enhancers based on analysis of transcription-factor binding affinity. Cell *124,* 47-59.

Henriquez-Hernandez, L.A., Valenciano, A., Foro-Arnalot, P., Alvarez-Cubero, M.J., Cozar, J.M., Suarez-Novo, J.F., Castells-Esteve, M., Fernandez-Gonzalo, P., De-Paula-Carranza, B., Ferrer, M.*, et al.* (2014). Single nucleotide polymorphisms in DNA repair genes as risk factors associated to prostate cancer progression. BMC Med. Genet. *15,* 143-014-0143-0.

Hsu, F.C., Sun, J., Wiklund, F., Isaacs, S.D., Wiley, K.E., Purcell, L.D., Gao, Z., Stattin, P., Zhu, Y., Kim, S.T.*, et al.* (2009). A novel prostate cancer susceptibility locus at 19q13. Cancer Res. *69,* 2720-2723.

Hua, T.J., Ahmed, M., Guo, H., Zhang, Y., Chen, S., Soares, F., Lu, J., Zhou, S., Wang, M., Li, H., *et al.* (2018). Risk SNPs mediated promoter-enhancer switching promotes prostate cancer progression through lncRNA PCAT19.

Huang, Q., Whitington, T., Gao, P., Lindberg, J.F., Yang, Y., Sun, J., Vaisanen, M.R., Szulkin, R., Annala, M., Yan, J.*, et al.* (2014). A prostate cancer susceptibility allele at 6q22 increases RFX6 expression by modulating HOXB13 chromatin binding. Nat. Genet. *46,* 126-135.

Jolma, A., Yan, J., Whitington, T., Toivonen, J., Nitta, K.R., Rastas, P., Morgunova, E., Enge, M., Taipale, M., Wei, G.*, et al.* (2013). DNA-binding specificities of human transcription factors. Cell *152,* 327-339.

Kopp, F., and Mendell, J.T. (2018). Functional Classification and Experimental Dissection of Long Noncoding RNAs. Cell *172,* 393-407.

Kron, K.J., Murison, A., Zhou, S., Huang, V., Yamaguchi, T.N., Shiah, Y.J., Fraser, M., van der Kwast, T., Boutros, PC., *et al.* (2017). TMPRSS2-ERG fusion co-opts master transcription factors and activates NOTCH signaling in primary prostate cancer. Nat Genet. *49*:1336-1345.

Larson, N.B., McDonnell, S., French, A.J., Fogarty, Z., Cheville, J., Middha, S., Riska, S., Baheti, S., Nair, A.A., Wang, L., *et al.* (2015). Comprehensively evaluating cis-regulatory variation in the human prostate transcriptome by using gene-level allele-specific expression. Am. J. Hum. Genet. *96,* 869-882.

Liu, P., Ramachandran, S., Ali Seyed, M., Scharer, C.D., Laycock, N., Dalton, W.B., Williams, H., Karanam, S., Datta, M.W., Jaye, D.L., *et al.* (2006). Sex-determining region Y box 4 is a transforming oncogene in human prostate cancer cells. Cancer Res. *66,* 4011-4019.

Liu, S., Liu, Y., Zhang, Q., Wu, J., Liang, J., Yu, S., Wei, G.H., White, K.P., and Wang, X. (2017). Systematic identification of regulatory variants associated with cancer risk. Genome Biol. *18*, 194.

Love, M.I., Huber,W., and Anders, S. (2014). Moderated estimation of fold change and dispersion for RNA-seq data with DESeq2. Genome Biol. *15,* 550.

MacArthur, J., Bowler, E., Cerezo, M., Gil, L., Hall, P., Hastings, E., Junkins, H., McMahon, A., Milano, A., Morales, J., Pendlington, Z.M., *et al.* (2017). The new NHGRI-EBI Catalog of published genome-wide association studies (GWAS Catalog). Nucleic Acids Res. *45*, D896-D901.

Martin, M. (2011). Cutadapt removes adapter sequences from high-throughput sequencing reads. EMBnet.Journal *17,*

Mei, S., Qin, Q., Wu, Q., Sun, H., Zheng, R., Zang, C., Zhu, M., Wu, J., Shi, X., Taing, L., *et al.* (2017). Cistrome Data Browser: a data portal for ChIP-Seq and chromatin accessibility data in human and mouse. Nucleic Acids Res. *45*, D658-D662.

Mills, I.G. (2014). Maintaining and reprogramming genomic androgen receptor activity in prostate cancer. Nat. Rev. Cancer. *14,* 187-198.

Mucci, L.A., Hjelmborg, J.B., Harris, J.R., Czene, K., Havelick, D.J., Scheike, T., Graff, R.E., Holst, K., Moller, S., Unger, R.H.*, et al.* (2016). Familial Risk and Heritability of Cancer Among Twins in Nordic Countries. JAMA *315,* 68-76.

Orom, U.A., Derrien, T., Beringer, M., Gumireddy, K., Gardini, A., Bussotti, G., Lai, F., Zytnicki, M., Notredame, C., Huang, Q., *et al.* (2010). Long noncoding RNAs with enhancer-like function in human cells. Cell *143,* 46-58.

Pomerantz, M.M., Li, F., Takeda, D.Y., Lenci, R., Chonkar, A., Chabot, M., Cejas, P., Vazquez, F., Cook, J., Shivdasani, R.A.*, et al.* (2015). The androgen receptor cistrome is extensively reprogrammed in human prostate tumorigenesis. Nat. Genet. *47,* 1346-1351.

Ran, F.A., Hsu, P.D., Wright, J., Agarwala, V., Scott, D.A., and Zhang, F. (2013). Genome engineering using the CRISPR-Cas9 system. Nat. Protoc. *8,* 2281-2308.

Ren, S., Peng, Z., Mao, J.H., Yu, Y., Yin, C., Gao, X., Cui, Z., Zhang, J., Yi, K., Xu, W.*, et al.* (2012). RNA-seq analysis of prostate cancer in the Chinese population identifies recurrent gene fusions, cancer-associated long noncoding RNAs and aberrant alternative splicings. Cell Res. *22,* 806-821.

Rhodes, D.R., Yu, J., Shanker, K., Deshpande, N., Varambally, R., Ghosh, D., Barrette, T., Pandey, A., and Chinnaiyan, A.M. (2004). ONCOMINE: a cancer microarray database and integrated data-mining platform. Neoplasia *6,* 1-6.

Saxton, R.A., and Sabatini, D.M. (2017). mTOR Signaling in Growth, Metabolism, and Disease. Cell *168,* 960-976.

Schroder, F.H., Hugosson, J., Roobol, M.J., Tammela, T.L., Ciatto, S., Nelen, V., Kwiatkowski, M., Lujan, M., Lilja, H., Zappa, M.*, et al.* (2009). Screening and prostate-cancer mortality in a randomized European study. N. Engl. J. Med. *360,* 1320-1328.

Shui, I.M., Lindstrom, S., Kibel, A.S., Berndt, S.I., Campa, D., Gerke, T., Penney, K.L., Albanes, D., Berg, C., Bueno-de-Mesquita, H.B.*, et al.* (2014). Prostate cancer (PCa) risk variants and risk of fatal PCa in the National Cancer Institute Breast and Prostate Cancer Cohort Consortium. Eur. Urol. *65,* 1069-1075.

Spisak, S., Lawrenson, K., Fu, Y., Csabai, I., Cottman, R.T., Seo, J.H., Haiman, C., Han, Y., Lenci, R., Li, Q.*, et al.* (2015). CAUSEL: an epigenome- and genome-editing pipeline for establishing function of noncoding GWAS variants. Nat. Med. *21,* 1357-1363.

Subramanian, A., Tamayo, P., Mootha, V.K., Mukherjee, S., Ebert, B.L., Gillette, M.A., Paulovich, A., Pomeroy, S.L., Golub, T.R., Lander, E.S., *et al.* (2005). Gene set enrichment analysis: a knowledge-based approach for interpreting genome-wide expression profiles. Proc. Natl. Acad. Sci. U. S. A. *102,* 15545-15550.

Taylor, B.S., Schultz, N., Hieronymus, H., Gopalan, A., Xiao, Y., Carver, B.S., Arora, V.K., Kaushik, P., Cerami, E., Reva B., *et al.* (2010). Integrative genomic profiling of human prostate cancer. Cancer Cell. 18:11-22.

Tomlins, S.A., Mehra, R., Rhodes, D.R., Cao, X., Wang, L., Dhanasekaran, S.M., Kalyana-Sundaram, S., Wei, J.T., Rubin, M.A., Pienta, K.J., *et al.* (2007). Integrative molecular concept modeling of prostate cancer progression. Nat. Genet. *39,* 41-51.

Wang, L., Wang, S., and Li, W. (2012). RSeQC: quality control of RNA-seq experiments. Bioinformatics *28,* 2184-2185.

Wang, Y., Zhang, B., Zhang, L., An, L., Xu, J., Li, D., Choudhary, M.N., Li, Y., Hu, M., Hardison, R., *et al.* (2017). The 3D Genome Browser: a web-based browser for visualizing 3D genome organization and long-range chromatin interactions. bioRxiv

Ward, L.D. and Kellis, M. (2012). HaploReg: a resource for exploring chromatin states, conservation, and regulatory motif alterations within sets of genetically linked variants. Nucleic Acids Res. *40*, D930-934.

Wei, G.H., Badis, G., Berger, M.F., Kivioja, T., Palin, K., Enge, M., Bonke, M., Jolma, A., Varjosalo, M., Gehrke, A.R.*, et al.* (2010). Genome-wide analysis of ETS-family DNA-binding in vitro and in vivo. EMBO J. *29,* 2147-2160.

Whitington, T., Gao, P., Song, W., Ross-Adams, H., Lamb, A.D., Yang, Y., Svezia, I., Klevebring, D., Mills, I.G., Karlsson, R.*, et al.* (2016). Gene regulatory mechanisms underpinning prostate cancer susceptibility. Nat. Genet. *48,* 387-397.

Zhang, K., Myllymaki, S.M., Gao, P., Devarajan, R., Kytola, V., Nykter, M., Wei, G.H., and Manninen, A. (2017). Oncogenic K-Ras upregulates ITGA6 expression via FOSL1 to induce anoikis resistance and synergizes with alphaV-Class integrins to promote EMT. Oncogene *36,* 5681-5694.

Figure 1. Candidate gene identification by eQTL analysis at the 19q13 aggressive PCa risk locus. (**A-D**) The aggressive PCa risk allele G at rs11672691 associates with increased expression of *CEACAM21* (A-C) and *PCAT19* (D) in prostate tissues. Linear model P values assessed by Matrix eQTL. (**E-F**) *PCAT19* or *CEACAM21* promotes PCa cell proliferation measured by XTT colorimetric assays (mean ± SD of triplicate experiments), and aggressiveness by migration and invasion assays (mean ± SEM of triplicate experiments) in 22Rv1 cells infected with control or gene-specific shRNAs. (**G**) Ectopic CEACAM21 expression promotes 22Rv1 cell proliferation (mean ± SD of triplicate experiments). (**H**) CEACAM21 overexpression enhances RWPE1 cell migration and invasion (mean ± SEM of triplicate experiments). In E-H, *P < 0.05, **P < 0.01, ***P < 0.001, Student's t test. (**I**) GSEA plot testing the enrichment of differentially expressed genes between CEACAM21 overexpressing versus control RWPE1 cells. (**J**) *PCAT19* or **(K,L)** *CEACAM21* transcript levels upregulated in human primary or metastasis PCa. P values by Mann-Whitney U-tests. (**M**) Higher levels of *CEACAM21* correlate with increased risk of biochemical recurrence in a cohort of PCa patients. P value assessed by a log-rank test. See also **Figures S1-S3** and **Table S2.**

Figure 2. The risk allele G of rs11672691 enhances HOXA2 chromatin binding. (**A**) ChIP-seq tracks showing the enrichment of active enhancer marks, silent epigenetic signature, and transcription factors at the rs11672691 region. (**B**) Reporter assays showing enhancer activity of the pGL3 promoter vector inserted with the rs11672691-containing or control DNA fragments. (**C**) rs11672691 and rs887391 reside within HOXA2 DNA-binding motifs. (**D**) Binding affinity of HOX A family members, HOXB13, AR, FOXA1, and ERG to the rs11672691 surrounding sequence competed with the counterparts

harboring G or A allele. (**E**) ChIP-qPCR confirmation of transcription factor binding at rs11672691 region. (**F**) ChIP-qPCR results showing HOXA2 binding at rs11672691 in LNCaP cells. (**G**) ChIP-AS-qPCR indicating allele-specific binding of HOXA2 at rs11672691 in 22Rv1 cells. (**H**) HOXA2 prefers the binding to G allele than A allele at rs1672691 confirmed by ChIP Sanger sequencing. (**I**) Western blot result of V5 tagged HOXA2 expression in 22Rv1. (**J**) ChIP-AS-qPCR for HOXA2 enrichment at the rs11672691 region in HOXA2 overexpressing and control cells. Error bars, SD (B, D-G, J), n = 3 technical replicates. **P* < 0.05, ***P* < 0.01, ****P* < 0.001, Student's *t* tests. See also **Figure S4, Tables S3-S6**

Figure 3. Effect of *HOXA2* on PCa cell growth, metastasis and patient prognosis. (**A**) Depletion of *HOXA2* reduces PCa cell proliferation, mean ± SD of triplicate experiments. (**B**) Genome-wide loss-of-function screening of the essential genes for cell survival. Lower ATARiS scores demonstrate elevated dependency of cell viability on given genes. *AR*, *HOXB13*, *MYC* and *BRD4* are known to be important for PCa cell growth and survival, and *TP53* vice versa. (**C**) The number of 22Rv1 cells infected with control or *HOXA2* shRNAs in invasion assay. Mean ± SEM of triplicate experiments. In A and C, **P* < 0.05, **P < 0.01, ***P < 0.001, Student's t test. (**D** and **E**) Elevation of *HOXA2* mRNA levels in human primary or metastasis PCa. P values examined by Mann-Whitney U-tests. (**F** and **G**) Higher levels of *HOXA2* correlate with increased risk of biochemical recurrence (F) and reduced time for overall survival (G) in PCa patient cohorts. (**H**) Higher levels of *HOXA2* shows predictive values for biochemical recurrence in patient group with Gleason Score 7 (intermediate risk). P values determined by a log-rank test (F-H), and Cox regression analysis (F and H). See also **Figure S5.**

Figure 4. Direct effect of rs11672691 on *PCAT19* and *CEACAM21* expression. (**A**) Depletion of *HOXA2* diminishes the mRNA levels of *PCAT19* and *CEACAM21*. **(B** and **C)** Scatter plots showing an expression correlation between *HOXA2* and *CEACAM21* or *PCAT19* in prostate tissues. (**D**) *PCAT19* knockdown results in decreased expression of *CEACAM21*. (**E**) Scatter plot displaying a correlation between *PCAT19* and *CEACAM21* expression in human prostate. (**F**) Reporter assay showing contribution of the G compared with the A allele at rs11672691 to an increased enhancer (E) activity for *CEACAM21* promoter (P). Error bars, SD from five technical replicates. (**G**) 3C analysis of chromatin interactions between *CEACAM21* and rs11672691 locus within nearly 100 kb region (chr19:41982282-42079092). (**H**) Sanger sequencing of CRISPR/Cas9-modified and parental 22Rv1 cells. (**I**) Analysis of *PCAT19* and *CEACAM21* expression in mutated and parental 22Rv1 cells. (**J**) Chromatin enrichment of HOXA2 at the rs11672691 site measured by ChIP-qPCR. (**K**) 3C measurement of chromatin interactions between *CEACAM21* promoter and rs11672691 locus in the CRISPR/Cas9 modified and parental 22Rv1 cells. NS, non-significant. In A,D,G,I,J, and K, data shown are mean ± SD of triplicate experiments, **P < 0.01, ***P < 0.001, ****P < 0.0001, Student's t test. See also **Figure S6** and **Table S7.**

Figure 5. Effect of rs11672691 genotype on PCa cell growth, aggressive behavior and patient prognosis. (**A**) The phenotype of each 22Rv1 cell lines analyzed by microscopy under culture for two days. (**B**) Cell proliferation analysis of CRISPR/Cas9-modified and parental 22Rv1 cells, mean ± SD of triplicate experiments. (**C**) Representative images showing wound healing assay for migration ability of 22Rv1 cells with different genotypes of rs11672691. (**D**) Quantification of percentage fraction of original wound closure in triplicate

plates. Migration was assessed every 10 h. Error bars, SD from three biological replicates. In B, D, *P < 0.05, **P < 0.01, ***P < 0.001, Student's *t* test. (**E** and **F**) Association analyses show that the patient group with rs11672691 GG genotype correlates with increased risk for biochemical recurrence in two independent cohorts of PCa patients. (**G** and **H**) Survival analyses show that the patients carrying rs11672691 GG genotype are more likely to get metastasis disease earlier. In E-H, P values examined by a log-rank test.

Figure 6. Synergistic effect of rs11672691 genotype and *CEACAM21* or *PCAT19* expression on PCa patient prognosis. (**A** and **B**) *CEACAM21* indicates strong predictive value in the patient group with rs11672691 GG genotype (**A**), but not in the group with rs11672691 AA or GA genotype (**B**). (**C** and **D**) *PCAT19* shows no prognostic value in a cohort of PCa patients (**C**), but the PCa patient group carrying rs11672691 GG genotype with higher *PCAT19* expression tumors indicates a significant association with increased risk of biochemical relapse (**D**). The P values were assessed by a log-rank test (**A-D**) and Cox regression analysis (**A** and **D**). See also **Figure S7.**

Table 1. Association of rs11672691 variant with aggressive PCa compared to nonaggressive PCa as defined by selected clinical variables, See also **Table S1**

Core clinical variables of aggressive PCa	**rs11672691 genotype**[a]	**OR (95% CI)**	***P***
PSA[b] > 100	GG	1.32 (0.92-1.88)	0.13
	GG+GA	1.86 (0.81-4.27)	0.15
Gleason score ≥ 8	GG	1.08 (0.86-1.34)	0.51
	GG+GA	1.35 (0.86-2.11)	0.19
Tumor stage T3/T4	GG	**1.23 (1.02-1.48)**	**0.03**
	GG+GA	1.22 (0.85-1.76)	0.28
Lymph node, yes	GG	0.72 (0.25-2.09)	0.55
	GG+GA	1.17 (0.15-8.97)	0.88
Metastasis, yes	GG	1.14 (0.65-1.99)	0.66
	GG+GA	1.08 (0.81-1.46)	0.60
Fatal PCa, yes[c]	GG	**1.26 (0.99-1.60)**	**0.065**
	GG+GA	1.39 (0.85-2.29)	0.193
Additional clinical features of aggressive PCa			
PSA progression, yes	GG	**1.31 (1.11-1.54)**	**0.001**
	GG+GA	**1.62 (1.13-2.32)**	**0.008**
CRPC[d], yes	GG	1.22 (0.95-1.56)	0.120
	GG+GA	**1.75 (1.00- 3.05)**	**0.048**

a, AA genotype represented the reference group in the analyses

b, Diagnostic PSA level, ng/mL

c, Prostate cancer specific mortality (PCSM)

d, CRPC, Castration Resistant Prostate Cancer

P<0.05 considered to be significant, bold

Figure S1. Experimental analysis of *PCAT19* and *CEACAM21* function in PCa cell proliferation and metastasis, Related to Figures 1E and 1F

(**A**) Quantitative RT-PCR analysis of the mRNA levels of *PCAT19* in the PCa cells 22Rv1, DuCaP and LNCaP infected with lentiviral particles carrying different shRNAs against *PCAT19*. Error bars, ± SD from three technical replication. (**B** and **C**) *PCAT19* promotes PCa cell growth measured by XTT colorimetric assay (absorbance at 450nm (OD450); mean ± SD of triplicate experiments), and metastasis behaviors by migration and invasion assays (mean ± SEM of triplicate experiments) in the PCa cell lines DuCaP (**B**) and LNCaP (**C**) infected with control shRNA or the shRNAs against *PCAT19*. In A-C, **P* < 0.05, ***P* < 0.01, ****P* < 0.001 were assessed using two-tailed Student's *t* test. (**D** and **E**) Representative images of migration (**D**) and invasion (**E**) assays for 22Rv1, DuCaP and LNCaP cells infected with control and *PCAT19* shRNAs. Scale bars, 100 µm. (**F**) The mRNA levels of *CEACAM21* in the PCa cells 22Rv1, DuCaP and LNCaP infected with lentiviral particles carrying *CEACAM21*-specific shRNAs. Data shown are mean ± SD of three technical replicates. (**G** and **H**) Depletion of *CEACAM21* inhibits PCa cell proliferation measured by XTT colorimetric assay (absorbance at 450nm (OD450); mean ± SD of triplicate experiments), and aggressive behaviors by migration and invasion assays (mean ± SEM of triplicate experiments) in the PCa cell lines DuCaP (**G**) and LNCaP (**H**) infected with control shRNA or the different shRNAs against *CEACAM21*. In A-C, **P* < 0.05, ***P* < 0.01, ****P* < 0.001 were evaluated by two-tailed Student's *t* test. (**I** and **J**) Representative images of migration (**I**) and invasion (**J**) assays for the tested PCa cell lines, including 22Rv1, DuCaP and LNCaP infected with control and *CEACAM21*-specific shRNAs. Scale bars, 100 µm.

Figure S2. Ectopic expression of CEACAM21 enhances PCa cell growth and proliferation, and elevates PCa cell invasive behaviors, Related to Figures 1G and 1H

(**A**) Overexpression of CEACAM21 in the human PCa cell lines, including 22Rv1, LNCaP, DuCaP and RWPE1. CEACAM21 protein levels were determined by western blot analysis. Lanes 1, 3, 5, 7, empty vector-transfected cells as experimental controls. Lanes 2, 4, 6, 8, cells transfected with expression vectors containing CEACAM21. (**B**) Cell growth and viability were analyzed by XTT assays in the four tested PCa cell models. (**C**) Similar to the experiments shown in A, except that the overexpression of CEACAM21 was mediated by lentivirus expression constructs. (**D**) XTT proliferation assay showing the effect of CEACAM21 overexpression on cell growth rate. In B and D, **P* < 0.05, ***P* < 0.01, ****P* < 0.001, were examined by two-tailed Student's *t* test. (**E**) CEACAM21 overexpression stimulates the growth of RWPE1 cells in 3D cyst culture. Left panel: Confocal slices of control (lenti-control) and CEACAM21 overexpressing (lenti-CEACAM21) RWPE1 cysts. Note that both types of cysts have large central lumens while the overall size of CEACAM21 cysts is obviously larger. Cysts were grown for one week followed by fixation, permeabilization and staining with DAPI (nucleus, blue) and TRITC-Phailloidin (Actin, red). Scale bar is 100 µm. Right panel: Cyst areas of the two RWPE1 cell samples were measured (n=60 cysts each condition) as described in supplementary materials and methods. The data are shown as average cyst area ± SD. Statistical significance was assessed using two-tailed Student's t test. *** represents P < 0.0001. (**F** and **G**) Transient transfection (**F**) or lentivirus expression construct-mediated (**G**) overexpression of CEACAM21 enhance the migration and invasion of the tested PCa cell lines of 22Rv1, LNCaP and

DuCaP (mean ± SEM of triplicate experiments). Error bars, ± SD of triplicate experiments. *P < 0.05, **P < 0.01, were assessed using two-tailed Student’s *t* test. Accordingly, representative images of migration and invasion assays are shown. (**H**) Representative images of migration (upper panel) and invasion (lower panel) assays for RWPE1 cells infected with lenti control vector or CEACAM21 lenti expression constructs. Scale bars, 100 µm.

Figure S3. RNA-seq analysis of RWPE1 cells with ectopic expression of CEACAM21, and the analysis of *PCAT19* and *CEACAM21* expression levels in cancerous and normal tissues of PCa patients, Related to Figures 1I-1L

(**A**) CEACAM21 overexpression in the human immortalized prostatic epithelial RWPE1 cells. CEACAM21 protein expression was determined by western blot analysis. Lanes 1-3, lentivirus empty vector-transfected cells as experimental controls. Lanes 4-6, cells transfected with lentivirus vectors haboring CEACAM21. (**B**) Raw RPKM expression correlation among three biological replicates of controls and experiments, respectively, from RWPE1 RNA-seq data. (**C**) Heat maps for expression level of genes down- or upregulated by CEACAM21 overexpression in RWPE1 cells. The number of genes determined by RNA-seq (DESeq2, FDR < 0.01). (**D**) GSEA was performed on RNA-seq from RWPE1 cells with CEACAM21 overexpression by using the hallmark gene sets. Enrichment plot indicates elevated expression of MYC gene sets upon CEACAM21 overexpression in RWPE1 cells. (**E**) *PCAT19* and (**F**) *CEACAM21* mRNA expression were elevated in human prostate tumors than that in normal prostate gland. The P values were calculated using Mann-Whitney U-tests.

Figure S4. Enhancer reporter, DNA-binding assays and ChIP-qPCR were performed to determine the key transcription factor occupancy at the region harboring rs11672691, Related to Figure 2

(**A**) rs11672691 enhancer activity was determined by the modified self-transcribing active regulatory region sequencing (STARR-seq) assays. (**B** and **C**) Prediction of the affinity of HOXA2 binding to the difference alleles of rs11672691 (**B**) and rs887391 (**C**). (**D** and **E**) Relative binding affinity of HOXA2 to the DNA sequences with rs11672691. In D, Error bars, ± SD of six replicate experiments. (**F** and **J**) ChIP-qPCR for HOXA9, HOXA13, HOXB13, AR, and HOXA10 chromatin binding at the rs11672691 containing region in 22Rv1 or VCaP cell lines. (**K**) ChIP followed by allele-specific quantitative PCR (qPCR) validation of overexpressed HOXA2 binding at rs11672691 in 22Rv1 cells. In F-K, Error bars, ± SEM of three technical replicates. NS, non-significant. $^*P < 0.05$, $^{**}P < 0.01$, $^{***}P < 0.001$, were assessed using two-tailed Student's *t* test.

Figure S5. Examination of the role of *HOXA2* in PCa development and prognosis, Related to Figure 3

(**A**) The mRNA level of *HOXA2* was induced upon DHT treatment in VCaP cells. (**B**) The number of 22Rv1 cells infected with control shRNA or *HOXA2* shRNA in migration assays. (**C** and **D**) Representative images of migration (**C**) and invasion (**D**) assays for 22Rv1 cells infected with control and *HOXA2* shRNA. Scale bars, 100 µm. Error bars, ± SEM from triplicate experiments. $^*P < 0.05$, $^{**}P < 0.01$, $^{***}P < 0.001$, *P* values were assessed using two-tailed Student's *t* tests. (**E** and **F**) Multivariate analysis of the risk for BCR-free survival in a large cohort of PCa patients with the expression data of *HOXA2* and other clinical variables. (**G** and **H**) In comparison with the data shown in **Figure 3H**, *HOXA2* expression data shows no predictive values for biochemical recurrence in the patient group with Gleason Score 6 (low risk) or Gleason Score ≥8 (high risk).

Figure S6. Regulation of *PCAT19* and *CEACAM21* expression, and long-range chromatin looping formed between *PCAT19* and *CEACAM21* loci, Related to Figure 4

(**A** and **B**) Knockdown of *HOXB13* (shRNA) (**A**) or *ERG* (siRNAs) (**B**) in VCaP cells diminishes the mRNA levels of *PCAT19* and *CEACAM21*. (**C**) Knockdown of *HOXA10* in 22Rv1 cells has no effect on the mRNA levels of *PCAT19* or *CEACAM21*. (**D** and **E**) DHT stimulation induces slight upregulation of *PCAT19* (**D**) and obvious elevation of *CEACAM21* mRNA levels (**E**) in VCaP cells. (**F**) The mRNA levels of *CEACAM21* decreased upon knockdown of *PCAT19* in VCaP cells. Error bars, ± SD from three technical replicates. **P* < 0.05, ***P* < 0.01, ****P* < 0.001, two-tailed Student's *t* test. (**G**) The virtual 4C mode of the 3D Genome Browser reveals a strong interaction of the SNP rs11672691 (red line) with CEACAM21 region (the highest peak) in LNCaP. Here the remote chromatin interaction effect of SNP rs11672691 was explored by plotting the virtual 4C from LNCaP Hi-C data set (Wang et al., 2017). (**H**) 3C analysis of chromatin interactions between *CEACAM21* and rs11672691 loci in 22Rv1 cells with or without shRNA-mediated depletion of *PCAT19* expression. Graphic data shows the relative crosslinking frequencies of *CEACAM21* promoter (anchor fragment) and the other cutting sites of EcoRI in this nearly 100 kb region (chr19:41982282-42079092) in 22Rv1 cells measured by 3C-qPCR. Data shown are mean ± SD of triplicate experiments.

Figure S7. Multivariate analysis of prostate cancer biochemical recurrence, Related to Figure 6

(**A** and **B**) Multivariate analysis of the risk for BCR-free survival in a large cohort of PCa patients with the expression data of *CEACAM21* (**A**) or *PCAT19* (**B**) with additional clinical variables.

STAR METHODS

Detailed methods are provided in the online version of this paper and include the following:

KEY RESOURCES TABLE

CONTACT FOR REAGENT AND RESOURCES SHARING

EXPERIMENTAL MODEL AND SUBJECT DETAILS

Cell Lines

Study Subjects

METHOD DETAILS

SNP genotyping and sequencing

eQTL analysis

Genotyping of rs11672691 in prostate cancer cell lines

Quantitative RT-PCR

Microwell-based transcription factor-DNA binding assay

Chromatin immunoprecipitation

Transfection and luciferase enhancer reporter assay

Western Blot assays

siRNA transfection

Lentiviral constructs, lentivirus production and infection

Cell viability and proliferation assays

Invasion and migration assays

3D culture of RWPE1 cells

Wound healing assays

Single nucleotide mutation using CRISPR/Cas9

Quantitative analysis of chromosome conformation capture assays

Analysis of prostate cancer TCGA expression data

Differential gene expression

Survival analysis for prostate cancer prognosis

Multivariate analysis

Expression correlation

RNA-Seq

QUANTIFICATION AND STATISTICAL ANALYSIS

DATA AND SOFTWARE AVAILABILITY

STAR METHODS

KEY RESOURCES TABLE

REAGENT or RESOURCE	SOURCE	IDENTIFIER
Antibodies		
Rabbit polyclonal anti-AR	Santa Cruz Biotechnology	Cat#sc-816x
Rabbit polyclonal anti-HOXB13	Santa Cruz Biotechnology	Cat#sc-66923x
Rabbit polyclonal anti-ERG	Santa Cruz Biotechnology	Cat#sc-353X
Rabbit polyclonal anti-HOXA2	Santa Cruz Biotechnology	Cat#sc-28596 X
Rabbit IgG	Santa Cruz Biotechnology	Cat#sc-2027X
Mouse IgG	Santa Cruz Biotechnology	Cat#sc-2025X
Mouse monoclonal anti-HOXA10	Santa Cruz Biotechnology	Cat#sc-271428X
Mouse monoclonal anti-V5	Invitrogen (Thermofishcer)	Cat#R960-25
Mouse monoclonal anti-V5-HRP	Invitrogen (Thermofishcer)	Cat#R961-25
Rabbit polyclonal anti-HOXA13	Abcam	Cat#ab26084
Rabbit polyclonal anti-HOXA9	EMD Millipore	Cat#07-178
Goat anti-mouse IgG (H+L) secondary antibody, HRP	Thermo Fisher	Cat#32430
Goat anti-rabbit IgG (H+L) secondary antibody, HRP	Thermo Fisher	Cat#32460
Bacterial and Virus Strains		
DH5α™ Chemically Competent cells	This paper	N/A
Stbl3™ Chemically Competent cells	This paper	N/A
Chemicals, Peptides, and Recombinant Proteins		
5α-Dihydrotestosterone (DHT) solution	From Olli A. Jänne lab (University of Helsinki)	N/A
EcoRI-HF	New England Biolabs	Cat#R3101M
T4 DNA Ligase	New England Biolabs	Cat#M0202M
T4 DNA Ligase Reaction Buffer	New England Biolabs	Cat#B0202S
Phalloidin-TRITC	Merck	Cat#P1951
DAPI	Merck	Cat#D9542
DMEM	Invitrogen	Cat#31966021

RPMI1640	Merck	Cat#R8758
EMEM	ATCC	Cat#30-2003
Keratinocyte-Serum Free Medium	Invitrogen	Cat#17005-042
Dihydrotestosterone	Merck	Cat#D-073-1ML
SYBR Select Master Mix	Applied Biosystems	Cat#4472908
Lipofectamine 2000	Thermo Fisher Scientific	Cat#11668030
Lipofectamine 3000	Thermo Fisher Scientific	Cat#L3000015
cOmplete™, Mini, EDTA-free Protease Inhibitor Cocktail	Roche	Cat#04693159001
Dynabead protein G	Invitrogen	Cat#10004D
X-treme GENE™ HP DNA Transfection Reagent	Roche	Cat#06366236001
SuperSignal West Femto Maximum Sensitivity Substrate	Thermo Fisher Scientific	Cat#34094
Lipofectamine RNAiMAX Transfection Reagent	Invitrogen	Cat#13778030
Low glucose DMEM	Invitrogen	Cat#21885025
Wright-Giemsa	Merck	Cat#WG16-500ml
Matrigel Growth Factor Reduced (GFR) Basement Membrane Matrix	Corning	Cat#354230
35 mm, high Glass Bottom dish	IBIDI	Cat#81158
Cell Proliferation Kit II	Roche	Cat#11465015001
Culture-Insert 2 Well 24	IBIDI	Cat#80241
Polybrene	Merck	Cat#H9268
Puromycin	Merck	Cat#P9620
Exonuclease I and FastAP	Thermo	Cat#EF0651
2x Phusion Master Mix with HF Buffer	Thermo	Cat#F531
Quanti tech probe PCR mix	QIAGEN	Cat#204343
Critical Commercial Assays		
RNeasy Mini Kit	QIAGEN	Cat#74106
PureLink® RNA Mini Kit	Invitrogen	Cat#12183018A
RNase-Free DNase	QIAGEN	Cat#79254

High-Capacity cDNA Reverse Transcription Kit	Applied Biosystems	Cat#4368814
Renilla luciferase assay system	Promega	Cat#E2820
MinElute PCR Purification Kit	QIAGEN	Cat#28006
Dual-Glo® Luciferase Assay System	Promega	Cat#E2940
Deposited Data		
Data of Figures 1I and S5D see Table S2	This paper	N/A
SNP imputation for rs11672691 with variants r2 >= 0.8 see Table S3	This paper	N/A
Data of Figures 2C and S7B-E see Table S4	This paper	N/A
Raw RNA-seq data	This paper	European Nucleotide Archive: PRJEB25719
cDNA microarray assay of gene expression profiling	Arredouani et al., 2009	GEO: GSE55945
Genome-wide CRISPR/Cas9 screening of cancer cell survival genes	Aguirre et al., 2016	http://wwwbroadinstituteorg/achilles
cDNA microarray assay of gene expression profiling	Chandran et al., 2007	GEO: GSE6752
Processed RNA-seq data	Cancer Genome Atlas Research Network, 2015	http://www.cbioportal.org/
Oncomine database	Rhodes et al., 2004	https://www.oncomine.org/resource/login.html
Processed and raw cDNA microarray data	Grasso et al., 2012	GEO: GSE35988
Processed and raw ChIP-seq data	Kron et al., 2017	GEO: GSE96652
Raw STARR-seq data	Liu et al., 2017	GEO: GSE94140
Processed and raw cDNA microarray data	Liu et al., 2006	ArrayExpress: E-TABM-26
Processed ChIP-seq data	Mei et al., 2017	http://cistrome.org/db/#/
Raw RNA-seq data	Ren et al., 2012	ArrayExpress: E-MTAB-567
Processed and raw cDNA microarray data	Taylor et al., 2010	GEO: GSE21032

Processed and raw cDNA microarray data	Tomlins et al., 2007	GEO: GSE6099
Processed ChIP-seq data	Whitington et al., 2016	http://tomwhi.github.io/prcagwas/
Experimental Models: Cell Lines		
22Rv1	ATCC	Cat#CRL-2505
LNCaP	ATCC	Cat#CRL-1740
DuCaP	From Olli A. Jänne lab (University of Helsinki)	Cat#RRID:CVCL_2025
COS-1	ATCC	Cat#CRL-1650
RWPE1	ATCC	Cat#CRL-11609
VCaP	ATCC	Cat#CRL-2876
MCF7	ATCC	ATCC® HTB-22™
293T Cells	ATCC	Cat#CRL-11268
Oligonucleotides		
Control siRNA: AGGUAGUGUAAUCGCCUUG	This paper	N/A
PCAT19 siRNA1: CCAUUGGAGAUACUCAUUA	This paper	N/A
PCAT19 siRNA2 UCAAGAAGAUGCUCAUCUA	This paper	N/A
AllStars Negative Control siRNA	Qiagen	Cat#SI03650318
ERG-siRNA1	Qiagen	Cat#SI03064726
ERG-siRNA2	Qiagen	Cat#SI03089443
Control-shRNA	Functional Genomics Unit (University of Helsinki)	Cat#SHC002
HOXB13-shRNA	Functional Genomics Unit (University of Helsinki)	Cat#TRCN0000020846
HOXA2-shRNA1	Functional Genomics Unit (University of Helsinki)	Cat#TRCN0000015061
HOXA2-shRNA2	Functional Genomics Unit (University of Helsinki)	Cat#TRCN0000015058

CEACAM21-shRNA1	Functional Genomics Unit (University of Helsinki)	Cat#TRCN0000146920
CEACAM21-shRNA2	Functional Genomics Unit (University of Helsinki)	Cat#TRCN0000150236
CEACAM21-shRNA3	Merck	Cat#TRCN0000371717
CEACAM21-shRNA4	Merck	Cat#TRCN0000371716
CEACAM21 shRNA5 Forward: CCGGGCTAATCGCAGCATATGTAATCTCGAGATTACATATGCTGCGATTAGCTTTTTG	This paper	N/A
CEACAM21 shRNA Reverse: AATTCAAAAAGCTAATCGCAGCATATGTAATCTCGAGATTACATATGCTGCGATTAGC	This paper	N/A
HOXA10 shRNA1	Functional Genomics Unit (University of Helsinki)	Cat#TRCN0000015248
HOXA10 shRNA2	Functional Genomics Unit (University of Helsinki)	Cat#TRCN0000015252
Control shRNA Forward: CCGGCAACAAGATGAAGAGCACCAACTCGAGTTGGTGCTCTTCATCTTGTTGTTTTTG	This paper	N/A
Control shRNA Reverse: AATTCAAAAACAACAAGATGAAGAGCACCAACTCGAGTTGGTGCTCTTCATCTTGTTG	This paper	N/A
PCAT19 shRNA1 Forward: CCGGGCCGACCAATTAATGACATATCTCGAGATATGTCATTAATTGGTCGGCTTTTTG	This paper	N/A
PCAT19 shRNA1 Reverse: AATTCAAAAAGCCGACCAATTAATGACATATCTCGAGATATGTCATTAATTGGTCGGC	This paper	N/A
PCAT19 shRNA2 Forward: CCGGGCTTGCTCTCTGGATAGCAATCTCGAGATTGCTATCCAGAGAGCAAGCTTTTTG	This paper	N/A

PCAT19 shRNA2 Reverse: AATTCAAAAAGCTTGCTCTCTGGATAGCAATCTCGAGATTGCTATCCAGAGAGCAAGC	This paper	N/A
PCAT19 shRNA3 Forward CCGGTACTCTGCTGCTGTGATTAAACTCGAGTTTAATCACAGCAGCAGAGTATTTTTG	This paper	N/A
PCAT19 shRNA3 Reverse: AATTCAAAAATACTCTGCTGCTGTGATTAAACTCGAGTTTAATCACAGCAGCAGAGTA	This paper	N/A
PCAT19 shRNA4 Forward: CCGGCAGCACAAGTCATTCAGGTTTCTCGAGAAACCTGAATGACTTGTGCTGTTTTTG	This paper	N/A
PCAT19 shRNA4 Reverse: AATTCAAAAACAGCACAAGTCATTCAGGTTTCTCGAGAAACCTGAATGACTTGTGCTG	This paper	N/A
PCAT19 shRNA5 Forward: CCGGAATGTGCCTACAGTTACTACTCTCGAGAGTAGTAACTGTAGGCACATTTTTTTG	This paper	N/A
PCAT19 shRNA5 Reverse AATTCAAAAAAATGTGCCTACAGTTACTACTCTCGAGAGTAGTAACTGTAGGCACATT	This paper	N/A
PCAT19 shRNA2 For 3C Forward: CCGGAAGAAGATGCTCATCTATGTACTCGAGTACATAGATGAGCATCTTCTTTTTTTG	This paper	N/A
PCAT19 shRNA2 For 3C Reverse: AATTCAAAAAAAGAAGATGCTCATCTATGTACTCGAGTACATAGATGAGCATCTTCTT	This paper	N/A
Primer for site-mutagenesis of rs11672691 Forward: CGTGAAACCGACAGAACACTTATTACACTTTTTGTGAGCTC	This paper	N/A
Primer for site-mutagenesis of rs11672691 Reverse: GAGCTCACAAAAAGTGTAATAAGTGTTCTGTCGGTTTCACG	This paper	N/A
Primer for cloning of rs11672691-centered fragment into pGL3 promoter vector Forward: CTAGCTAGCAGCGAGCCACCGCATAAGCA	This paper	N/A

Primer for cloning of rs11672691-centered fragment into pGL3 promoter vector Reverse: CCGCTCGAGTGGCCCTCCCACCTAGCCTT	This paper	N/A
Primer for cloning of rs11672691-centered fragment into pGL3 Basic vector Forward: CGGCTAGCCGATTAAGGGTCTCGTTACTA	This paper	N/A
Primer for cloning of rs11672691-centered fragment into pGL3 Basic vector Reverse: CCCTCGAGCCACGTCACCTCCCATAAA	This paper	N/A
Primer for cloning of *CEACAM21* promoter into pGL3 promoter vector Forward : TCTTCTCGAG ATCCTCCCGAGACCTC	This paper	N/A
Primer for cloning of *CEACAM21* promoter into pGL3 promoter vector Reverse : GAGGAAGCTTTGGTTCTCCTTAGACGCTC	This paper	N/A
Primer for cloning of CEACAM21 coding region into pcDNA3.1/V5-His A Forward: AATAAAGCTTATGGGGCCCCCCTCAGCT	This paper	N/A
Primer for cloning of CEACAM21 coding region into pcDNA3.1/V5-His A Reverse: GAAGCTCGAGGGAGATGGAGCTGTCAGAGG	This paper	N/A
Primer for cloning of V5-CEACAM21 into pLVET-IRES-GFP vector Forward: AGCTTTGTTTAAACATGGGGCCCCCCTCAGCT	This paper	N/A
Primer for cloning of V5-CEACAM21 into pLVET-IRES-GFP vector Reverse: AGCTTTGTTTAAACATGGGGCCCCCCTCAGCT	This paper	N/A
Primers for ChIP-qPCR and RT-qPCR, see Table S5	This paper	N/A
Primers for transcription factor-DNA binding assays, see Table S6	This paper	N/A
Primers for 3C-qPCR experiments, see Table S7	This paper	N/A
Recombinant DNA		
pGEN-MCS-Renilla	Wei et al., 2010	N/A
pcDNA3.1/V5-His A	Invitrogen	Cat#V81020
pLVET-IRES-GFP	Zhang et al., 2017	N/A
pGL3-Basic	Promega	Cat#E1751
pGL3-Promoter Vector	Promega	Cat#E1761

pLKO.1 Puro Vector	Addgene	Cat#8453
pSpCas9n (BB)-2A-Puro (PX462)	Feng Zhang Lab at MIT	N/A
pGL4.75 [hRluc/CMV]	Promega	Cat#E6931
Software and Algorithms		
HaploReg v4.1	Ward and Kellis. 2012	http://archive.broadinstitute.org/mammals/haploreg/haploreg.php
FastQC	Babraham Bioinformatics Institute	https://www.bioinformatics.babraham.ac.uk/projects/fastqc/
Matrix eQTL	R Bioconductor	https://bioconductor.org/
Trimmed mean of M-values (TMM)	R Bioconductor	https://bioconductor.org/
Cutadapt	Martin. 2011	https://cutadapt.readthedocs.io/en/stable/
Tophat2	Center for Computational Biology at Johns Hopkins University	https://ccb.jhu.edu/software/tophat/index.shtml
HTSeq	Bioconductor	https://htseq.readthedocs.io/en/release_0.9.1/
DESeq2	Love et al., 2014	https://bioconductor.org/packages/release/bioc/html/DESeq2.html
GSEA	Subramanian et al., 2005	http://software.broadinstitute.org/gsea/index.jsp
CRISPR design tool	Feng Zhang Lab at MIT	http://crispr.mit.edu/
BLOCK-iT™ RNAi Designer	Thermo Fisher Scientific	https://rnaidesigner.thermofisher.com/rnaiexpress/

Enhancer Element Locator	Hallikas et al., 2006	https://www.cs.helsinki.fi/u/kpalin/EEL/
edgeR	R Bioconductor	http://bioconductor.org/packages/release/bioc/html/edgeR.html
R Version 3.4.1	R	https://www.r-project.org/

CONTACT FOR REAGENT AND RESOURCES SHARING

Further information and requests for resources and reagents should be directed to and will be fulfilled by the Lead Contact, Dr. Gong-Hong Wei (gonghong.wei@oulu.fi).

EXPERIMENTAL MODEL AND SUBJECT DETAILS

Cell Lines

22Rv1, LNCaP, VCaP, RWPE1, COS-1, and 293T cell lines were originally purchased from ATCC, and DuCaP was a gift from Olli Janne's lab at University of Helsinki. All cell lines were confirmed to be mycoplasma free during our study. All the cells were cultured at 37 °C, with 95 % air and 5 % CO_2. VCaP, COS-1, 293T and DuCaP was grown in DMEM (Invitrogen), LNCaP and 22Rv1 were grown in RPMI1640 (Merck), MCF7 was grown in EMEM (ATCC). RWPE1 cells were grown in Keratinocyte-Serum Free Medium. Keratinocyte-SFM Kit including epidermal growth factor (EGF), and Bovine Pituitary extract (BPE) supplements was purchased from Invitrogen (17005-042, Invitrogen). 10 % FBS and 1% of Penicillin/Streptomycin were supplied to the base medium. In order to study AR activity we cultured the VCaP, LNCaP and 22Rv1 cells in charcoal stripping media up to at least 48 hours. AR activity was induced by treating cells with 100 nM dihydrotestosterone (DHT). For ectopic expression, we inserted *HOXA2* or *CEACAM21* into pcDNA3.1 V5-HisA vector (Invitrogen), and the CEACAM21-V5 subcloned into pLVET-IRES-GFP vector (Zhang et al., 2017).

Study subjects

Cancer cases and controls genotyped in this study were nested population- and hospital-based samples of Finnish origin. Written informed consent was obtained from each study subject. The study protocol was approved by the research ethics committee at Pirkanmaa Hospital District (Tampere, Finland) and by the National Supervisory Authority for Welfare and Health (VALVIRA). For rs11672691 variant, 2738 unselected non-familial eligible prostate cancer cases were analyzed. Control subjects (n=2427) were derived from the control group of the Finnish arm of The European Randomized Study of Screening for Prostate Cancer (ERSPC) (Schroder et al., 2009). Control subjects were population-matched healthy individuals who had undergone PSA screening. Their disease status is annually evaluated from the records of the Finnish Cancer Registry. Clinical information on study participants, including PSA at diagnosis, Gleason score, stage of disease (TNM), prostate cancer specific mortality, PSA progression and presence of castration resistance prostate cancer (CRPC), was obtained through in-person interviews or medical or death records. Aggressive disease was defined as PSA >100 ng/mL, or Gleason score ≥8, or tumor stage T3/T4, or tumor in nodes (N1), or metastasis present (M1), or prostate cancer-associated death (**Table 1**). The study was conducted according to the guidelines and regulations of the Helsinki Declaration (1975).

METHOD DETAILS

SNP genotyping and sequencing

Genotyping of germline blood DNA for rs11672691 was carried out by the Prostate Cancer Association Group to Investigate Cancer Associated Alterations in the Genome (PRACTICAL) Consortium using custom Illumina iSelect SNP genotyping array platform, which was designed as part of the Collaborative Oncological Gene-Environment Study (COGS), according to the manufacturer's instructions. Individuals were excluded from the study based on strict quality control criteria, including overall genotype call rate <95%, low or high heterozygosity, genotypically non-European origin, samples that were XX or XXY and therefore not genotypically males (XY), samples not concordant with previous genotyping within PRACTICAL, genotypes for the duplicate sample that appeared to be from a different individual, and cryptic duplicates where the phenotypic data indicated that the individuals were different.

eQTL analysis

We tested for eQTL associations between genotypes of rs11672691 and gene expression levels of *CEACAM21* and *PCAT19* using data from TCGA, Swedish and Wisconsin cohorts, which comprised of 389, 94, and 462 prostate samples, respectively. Association between genotype and gene expression was analyzed using the Matrix Expression Quantitative Trait Loci (Matrix eQTL) R package, parameters "useModel = modelLINEAR", "errorCovariance = numeric ()" were used. We applied the principal-component analysis covariates for the TCGA cohort. R was used to perform the statistical tests and plot figures for the association between SNP genotypes and gene expression levels. The transcriptional profilings were assessed by Illumina Expression BeadChip in

Swedish human prostate tissue samples, while RNA-seq in TCGA samples. The Stockholm and TCGA cohorts were genotyped on Illumina Omni 2.5 and Affymetrix SNP array 6, respectively.

Genotyping of rs11672691 in prostate cancer cell lines

The rs11672691 centered fragment 235 bp was amplified by primers (F: CCAGCGATTAAGGGTCTCGT1, R: TCCCATAAAATGGCCACGCTC). The 2x Phusion Master Mix with HF Buffer (F531, Thermo) were applied for PCR reactions. PCR products were cleaned with Exonuclease I and FastAP (# EF0651, Thermo) to remove unincorporated primers and degrade unincorporated nucleotides. Then the cleaned products with forward primer were sent for Sanger Sequencing.

Quantitative RT-PCR

RNA was isolated from cultured cell lines using RNeasy Mini Kit (QIAGEN) or PureLink® RNA Mini Kit (Invitrogen), while DNA in these samples were removed by RNase-Free DNase (QIAGEN). The High-Capacity cDNA Reverse Transcription Kit (Applied Biosystems) was used to synthesize cDNA from 2 ug RNA. The SYBR Select Master Mix (Applied Biosystems) was used in the Quantitative RT-PCR reactions. High specificity primers were selected from at least three pairs of primers for each target. Primer sequences used in this experiment can be found in **Table S5.**

For the analysis of mRNA levels, each gene was analyzed at least in triplicate and the data was normalized against an endogenous *ACTB* (β-actin) control. For ChIP-qPCR, all target primers had three technical replicates and the data were normalized to the control regions, then the relative enrichment of the target antibodies at target DNA fragment were determined by compared with the background (IgG control).

Microwell-based transcription factor-DNA binding assay

This experiment was performed according to the previous protocol (Wei et al., 2010). Full-length protein coding region or DNA-binding domain of human genes were amplified from human cDNA library (Stratagene) and cloned into pGEN-MCS-*Renilla* vector, and expressed in COS-1 cells by Lipofectamine 2000-mediated transfection (Thermo). Lysis buffer (600 mM NaCl and 1 % (wt/vol) Triton X-100 in PBS) was used to extract protein lysates from the cells. Subsequently, the mixture containing double-stranded biotinylated consensus oligo (8.3 µl of 1 µM oligo), Poly(dI-dC)•Poly(dI-dC) (5 µl of 1 µg/µl stock) and competitor , consensus or scrambled oligo (25 µl of 10 µM oligo)) was prepared and incubated at room temperature for 1 h. Then the diluted cell lysate was added into the mixture and incubated at room temperature for 2h. Binding reaction of scramble oligo without biotinylated consensus oligo was set up as background control. The oligo-cell-lysate reaction mix was eventually added into the StrepMax streptavidin-coated 96-well plates (Thermo Scientific) and incubated another 2 h at room temperature. After washing step with high-stringency binding buffer (5 mM NaCl and 20 mM HEPES, pH 7.05), the luciferase activity was determined using Renilla luciferase assay system (Promega) by a Multilabel Reader VICTOR3 V (PerkinElmer Inc.). The relative affinity of the competitor oligo in relation to the consensus oligo was calculated with the following equation:

$$\text{Kd sample/Kd consensus} = \{[(\text{Lsample/Lconsensus})-1]/[(\text{Lscrambled/Lconsensus})-(\text{Lsample/Lconsensus})]\} \times (\text{Lscrambled/Lconsensus}) +1$$

The positional weight matrix scores were calculated by dividing the inverse of the values by the sum of the inverses of the corresponding position. The oligos used for binding assay are listed in **Table S6**.

Chromatin immunoprecipitation (ChIP)

The cells were cross-linked in final concentration of 1 % formaldehyde for 10 min at room temperature. The final concentration of 125 mM glycine was added to stop the reaction. Cell pellets were collected and snap frozen in liquid nitrogen for next step experiments (the cell pellets can also be stored at -80 °C). Cell pellets were suspended in hypotonic lysis buffer (20 mM Tris-Cl, pH 8.0, with 10 mM KCl, 10 % glycerol, 2 mM DTT, and cOmplete protease inhibitor cocktail (Roche)) and incubated up to 50 min to isolate nuclei. The nuclei were washed twice with cold PBS and suspended in SDS lysis buffer (50 mM Tris-HCl, pH 8.1, with 0.5 % SDS, 10 mM EDTA, and cOmplete Protease Inhibitor). An average size of 400bp of chromatin was prepared by sonication (Q800R sonicator, Q Sonica). 70 µl of Dynabead protein G (Invitrogen) slurry per each reaction was washed twice with blocking buffer (0.5 % BSA in IP buffer), followed by 10 h incubation with 7 µg of indicated antibodies against the target proteins or control IgG in 1000 µl of 0.5% BSA in IP buffer (20 mM Tris-HCl, pH8.0, with 2 mM EDTA, 150 mM NaCl, 1%Triton X-100, and Protease inhibitor cocktail). After removal of the supernatant, the fragmented chromatin lysate (200-250 µg) diluted in 1.3 ml of IP buffer was added onto bead/antibody complexes with incubation at 4 °C for at least 12 h. Next, the complex was washed once with wash buffer I (20 mM Tris-HCl, pH 8.0, with 2 mM EDTA, 0.1 %SDS, 1 % Triton X-100, and 150 mM NaCl) and once with buffer II (20 mM Tris-HCl pH, 8.0, with 2 mM EDTA, 0.1 % SDS, 1 % Triton X-100, and 500 mM NaCl), followed by two times of washing with buffer III (10 mM Tris-HCl, pH 8.0, with 1 mM EDTA, 250 mM LiCl, 1 % Deoxycholate, and 1 % NP-40) and buffer IV (10 mM Tris-HCl, pH 8.0, and 1 mM EDTA), respectively. Then, 100ul of extraction buffer (10 mM Tris-HCl, pH 8.0, 1 mM EDTA, and 1 % SDS) was added to extract the DNA-protein complexes from the beads. Proteinase K (5 µl from 20mg/ml stock) and NaCl final 0.3 M were added into the complexes incubating overnight at 65 °C to reverse the crosslinks of protein-DNA interactions. Finally, DNA was purified with MinElute PCR Purification Kit (Qiagen) and the target DNA fragments were analyzed by qPCR.

Transfection and luciferase enhancer reporter assay

DNA fragments surrounding rs11672691 (G allele or A allele) were inserted into the pGL3 Promoter vector upstream of SV40 promoter. The SV40 promoter was subsequently replaced by *CEACAM21* promoter region (800 bp around the transcriptional start site (TSS) of *CEACAM21*). The internal Renilla control plasmid pGL4.75 [hRluc/CMV] (Promega) and the target plasmids were reverse co-transfected into LNCaP cells using X-treme GENE™ HP DNA Transfection Reagent (Roche) according to the protocol provided by the manufacturer. The experiments were carried out on the 96-well white plates. 100 µl of 3×10^5

LNCaP cells / ml was added per well. After 48 h, luciferase activity was measured with Dual-Glo® Luciferase Assay System (Promega). All data was obtained from at least three replicate wells and statistical analyses were performed with a two-tailed Student’s t test.

Western Blot assays

Cell pellets were collected and resuspended in lysis buffer (600mM Nacl, 1% Triton X-100 in PBS, 1× protease inhibitor). 30 µg of total protein lysates of each sample was separated by electrophoresis in 10 % SDS-PAGE gels and transferred onto 0.45 µm PVDF transfer membranes using a Semi-Dry transfer cell (Trans-Blot SD, Bio-Rad). Membranes were blocked for 1 h at room temperature using blocking buffer (5 % nonfat milk in TBST) and incubated with antibodies against V5 Tag, or V5-HRP (Invitrogen), or β-actin (Santa Cruz). Next, membranes were washed three times using TBST, 5 min each. With the exception for V5-HRP in Western blot assays, HRP-conjugated anti-rabbit IgG or anti-mouse IgG was used as secondary antibody (Invitrogen) followed by a 45 minutes incubation and washing as described above. Chemiluminescence signal was developed with SuperSignal West Femto Maximum Sensitivity Substrate (Thermo Fisher Scientific).

siRNA transfection

50-60 % confluent 22Rv1 cells or 60-70 % confluent VCaP cells were seeded in 6-well plates. 24 h later, siRNA was transfected into the cells using Lipofectamine RNAiMAX Transfection Reagent (Invitrogen) according to manufacturer's instructions. Medium was changed after 24 h and the cells were collected after 48 h.

Lentiviral constructs, lentivirus production and infection

The shRNA constructs targeting *HOXA2*, *HOXB13*, *CEACAM21, PCAT19*, and *HOXA10* were ordered from Functional Genomics Unit (University of Helsinki) or designed by BLOCK-iT™ RNAi Designer (Thermo Fisher Scientific) and inserted into pLKO.1 Vector (Addgene). Third generation lentiviral vectors were packaged using 293T cells. Briefly, 65-75 % confluent 239T cells were trypsinized and seeded into 3.5-cm plates, 24 h later the growth medium was changed with 1 ml pre-warmed low glucose DMEM (Invitrogen) containing 10 % FBS, 0.1 % penicillin and streptomycin. Cells were co-transfected with indicated shRNA construct or overexpression construct (1.5 µg each), pVSVG (envelope plasmid, 0.5 µg), pMDLg/pRRE (packaging plasmid, 0.5 µg) and pRSV-Rev (packaging plasmid, 0.5 µg) plasmids using Lipofectamine 2000 according to the manufacturer's instructions. The medium was replaced with fresh medium 24 h post transfection and afterwards the virus-containing medium was collected every 12 h up to six times. Lentivirus was passed through 0.45 µm filter unit, snap frozen in liquid nitrogen and stored at -80 °C. For viral transduction, the target cells were seeded in 6-well at a density of 60-70 %. 16-20 h later, cell culture medium was replaced with lentivirus-containing medium with final 8 µg/ml polybrene (Sigma). For lentivirus-mediated knockdown, 24 h later, virus was removed and replaced by normal medium containing final 1 µg/ml puromycin (Sigma). When uninfected control cells completely died, the target cells were cultured in normal growth medium with 0.5 µg/ml puromycin.

For lentivirus-mediated overexpression, 22Rv1, LNCaP, DuCaP, and RWPE1 cell lines stably expressing GFP, or CEACAM21-IRES-GFP were generated by lentiviral transduction and the GFP-expressing cells were sorted positively by fluorescence activated cell sorting (FACS) using BD FACSAria™ flow cytometer (BD Biosciences).

Cell viability and proliferation assays

Cells were resuspended and seeded into 96-well cell culture plates (2 × 10^3 for 22Rv1, LNCaP and RWPE1, 1 × 10^3 for DuCaP per well, respectively). Cell viability and proliferation was determined by using Cell Proliferation Kit II (Roche). The data was collected at the indicated time points by measuring the absorbance at 450 nm according to the manufacturer's instructions. Values were obtained from triplicate wells and statistical significance was calculated using two-tailed Student's t-test.

Invasion and migration assays

Cells were detached by trypsinization and resuspended into growth medium without serum or growth factor (2.5 × 10^5 cells/ml 22Rv1 or LNCaP, 1 × 10^5 cells/ml DuCaP, 5 × 10^5 cells/ml RWPE1). 200 µl of cell suspension was transferred into 8-µm Transwell inserts (Corning Costar) with or without 100 µl Matrigel (diluted with serum free medium to 250 µg/ml) (Corning) coating. The lower chambers were filled with 700 µl of normal growth medium. After 36 h, the cells were fixed in 3.7 % formaldehyde, permeabilized with methanol and stained with Wright-Giemsa (Merck). Cells on the upper surface of the membranes were removed using a cotton swab. Invasive cells that migrated to the bottom surface of the filters were quantified by counting the numbers of cells that penetrated the membrane in eight or twelve microscopic fields (acquired at 20 X magnification) per membrane. A two-tailed Students' t-test was employed to perform statistical analysis from three replicate inserts.

3D culture of RWPE1 cells

The RWPE1 cell lines were prepared for Matrigel overlay cultures as described previously (Zhang et al., 2017). Shortly, 100 µl of Matrigel (Corning) was layered onto a 3.5 cm high glass bottom cell culture-dish (IBIDI) and allowed to solidify for 30 minutes at + 37°C (5% CO2). RWPE1 control and CEACAM21 overexpression cells were grown to ~70% confluency, trypsinized and counted. Ten thousand cells per sample were resuspended into 200 µl of ice-cold Keratinocyte-SFM containing 2% (v/v) of Matrigel and 2% of FBS. Resuspended cells were seeded onto Matrigel-coated dishes and incubated for 15 minutes at + 37°C after which 1 ml of Keratinocyte-SFM medium containing 2% Matrigel was added. Matrigel-containing medium was subsequently refreshed every two days. One week later, cells were fixed, stained using DAPI (Merck) and filamentous actin (Merck), and analyzed by using an Olympus FluoView FV1000 confocal microscope equipped with 20 x UPLSAPO objective, NA: 0.75. The area of each cyst in the field of view was analyzed by Image J software using the "Particle Analysis" tool with selected sizes defined to range from 5000 μm^2 upwards. Statistical analysis was assessed using two-tailed Student's *t* test.

Wound healing assays

Cells were seeded into 24 well plates with ready-to-use culture-Inserts 2-Well (IBIDI) and allowed to grow near confluence. Then the inserts were removed and cells were washed twice with PBS. 1 ml of culture medium was added into each well. The wound areas were imaged at 10 h intervals using Zeiss Spinning Disc Confocal Microscope. The area of the wound in each well was analysed using image J software.

Single nucleotide mutation using CRISPR/Cas9

Two pairs of oligos (sgRNA1-top: CACCGAAGTGTAATAAGTGTTCTGT, sgRNA1-bottom: AAACACAGAACACTTATTACACTTC; sgRNA2-top: CACCGAAGTGTAATGAGTGTTCTGT; sgRNA2-bottom: AAACACAGAACACTCATTACACTTC) were designed using online CRISPR design tool (http://crispr.mit.edu/). rs11672691 (A or G) centered DNA fragments were cloned into pGL3 basic vector to generate repair templates. Most of the experiment was performed according to the previous protocol (Ran et al., 2013). One sgRNA-expressing plasmid was used for cutting the target region in this experiment instead of using two sgRNA-expressing plasmids as suggested in the protocol (Ran et al., 2013). Briefly, annealed oligos for sgRNAs were inserted into pSpCas9n (BB)-2A-Puro (PX462) V2.0 (a gift from Feng Zhang Lab at MIT). Transfection was performed in 22Rv1 cells with 70 % confluency. 300 ng of indicated Cas9 plasmid (pSpCas9n (sgRNA)) and 300 ng of targeting plasmid were co-transfected into cells using Lipofectamine 3000. Medium was changed after 24 h. 48 h later, 0.8 µg/ml puromycin (Sigma) was added into transfected cells. After non-transfected cells died, the remaining transfected cells were trypsinized and sorted using FACS to establish single cell clones. The single cells were seeded into 96-well plates and checked during 9-14 days to rule out non-single clones. Finally, the single clones were picked up for subculture and genotyping.

Quantitative analysis of chromosome conformation capture assays

Quantitative analysis of chromosome conformation capture assays (3C-qPCR) were performed as described previously (Hagege et al., 2007). All the primers used in this experiment are listed in **Table S7**. Briefly, cells were trypsinized and resuspended in PBS with 10 % FBS. 10-million of cells were fixed in 10 ml of PBS with 10 % FBS and 1 % formaldehyde for 10 min at room temperature. The crosslinking reaction was quenched with 0.57 ml of 2.5 M glycine (ice cold). The cell pellets were washed with cold PBS and resuspended in 5 ml of cold lysis buffer (10 mM Tris-HCl, pH 7.5; 10 mM NaCl; 0.2 % NP-40; 1×complete protease inhibitor). 22Rv1 cells and VCaP cells were incubated for 13 min in lysis buffer, MCF7 cells for 11 min. Then the nuclei were collected by centrifugation and used for digestion. EcoR I was applied to digest chromatin DNA and the digestion efficiency was verified. The well-digested nuclear lysate will be used in the ligation step. After ligation and reverse crosslinking, DNA was purified and washed by 70 % ethanol. In order to remove DTT, DNA pellet was dissolved in 400 ul water, then 1200 ul 100 % ethanol was added. DNA pellets were picked using pipette tips to separate it from DTT. The concentration of 3C DNA samples was examined by SYBR-based qPCR and diluted to 100 ng/µl. 1 µl of the ligation products, 5µl of Quanti tech probe PCR mix (QIAGEN), 1 µl of Taqman probe (1.5 µM), 1µl of Test + Constant primer (5 µM) and 2 µl

ddH_2O were used for TaqMan qPCR. We amplified the fragments across each of nine EcoR I cut sites and mix them together as control template. We performed standard curve of each primer using serial dilution of control template. Intercept and slope values from the standard curve were used to quantify the ligation product using the following equation: Value = $10^{(Ct-intercept)/slope}$. These values were finally normalized to *ERCC3* (loading control).

Analysis of prostate cancer TCGA expression data

Gene level expression value (reads per million or RPM) was estimated as following: Gene level fragment count was estimated using RSeQC (Wang et al., 2012). The method of trimmed mean of M-values (TMM) in R was applied to normalize library size. Common dispersion and RPM was estimated using the edgeR package in R.

Differential gene expression

We examined differential gene expression across normal prostate, tumor and metastatic tissues of several cohorts from the cBioPortal for Cancer Genomics (Cerami et al., 2012) and Oncomine database (Rhodes et al., 2004). Mann-Whitney U test or Kruskal-Wallis H test was used to assess the statistical significance of gene expression in the course of disease development. R was applied to perform statistical analyses and plot figures. For microarray-based expression profiling, we selected probes with lowest p values.

Survival analysis for prostate cancer prognosis

We assessed the impact of gene expression levels of *CEACAM21, HOXA2, PCAT19* and rs11672691 genotypes on prostate cancer prognosis and survival. We applied the Kaplan–Meier survival analysis in several cohorts from The Cancer Genome Atlas (TCGA) (Cerami et al., 2012), Oncomine database (Rhodes et al., 2004) and Oulu University Hospital. Patients were stratified into two groups based on the mean of gene expression or by the genotype of rs11672691. For the association between rs11672691 genotypes and the prognosis survival, we tested in several scenarios considering both gene expression data and rs11672691 genotype. We used the Cox proportional hazards model to assess the hazard ratio (HR). R package "Survival" was employed in the analyses.

Multivariate analysis

We investigated the association of the PCa patient overall survival with gene expression and clinical variables including Gleason score, PSA, T stage, N stage and age. We performed multivariate Cox proportional hazard analyses on various cohorts as described above. Samples were stratified into two groups with higher and lower expression by comparing to the mean values of gene expression levels. The clinical relevance of overall survival and covariates were performed in several different scenarios.

Expression correlation

We tested the linear correlation among the expression levels of *CEACAM21, PCAT19* and *HOXA2* in benign prostate and tumor issues in several cohorts from Oncomine database (Rhodes et al., 2004). Both Pearson and Spearman correlations were applied. Statistical tests and figures were made in R.

RNA-Seq

Agilent Bioanalyzer 2100 (Agilent Technologies) and Eukaryote Total RNA Nano Kit (Agilent), and Qubit RNA Broad Range kit (Life Techologies) were used to assessing the quality and quantity of total RNA, which were prepared from CEACAM21 overexpressing and control RWPE1 cells each with three biological replicates. The RNA integrity number of the samples ranged from 9.8 to 10.1 µg total RNA was used for library preparation using Illumina's TruSeq® Strnd mRNA Library preparation kit (Illumina) following the manufacturer's instructions. Quantification and quality assessment of libraries were performed by using the Bioanalyzer 2100 in combination with DNA 1000 Kit (Agilent), Qubit Broad Range DNA-kit (Life Technologies) and qPCR KAPA Library quantification kit (Kapa Biosystems). Illumina NextSeq550 platform in high-output, single-ended, 76 cycle mode, followed by FASTQ generation within BaseSpace (Illumina) was used to sequence the libraries. Sequencing resulted in approximately 40.7 Gb of data with average Q30 values of 96.41%. We checked the quality of reads with FastQC, followed with Cutadapt (Martin, 2011) for quality control. TopHat2 software was used to align reads to human reference genome hg19. We then quantified the mapped reads using HTSeq-count script in R Bioconductor. Bioconductor package DESeq2 (1.16.1) (Love et al., 2014) was employed to identify differentially expressed genes. We then preformed the gene set enrichment analysis (GSEA) on the hallmark gene sets using GSEAPreranked test (Subramanian et al., 2005). The pre-ranked gene list was created by sign(logFC)*-log(p-value), and then being sorted in a descending order. Enrichment statistic was set to “classic”, Max size: exclude larger sets was set to 5000, and 1000 permutations, while all other parameters remained as default. R was applied to perform statistical analyses and figure plots.

QUANTIFICATION AND STATISTICAL ANALYSIS

The Hardy-Weinberg equilibrium equation was used to determine whether the proportion of each genotype obtained was in agreement with the expected values as calculated from the allele frequencies. We conducted case-control unconditional logistic regression analyses to measure the association between the rs11672691 variant and prostate cancer risk or selected clinical features listed above by estimation of per allele odds ratio (OR) and its 95% confidence interval (CI). P-values were 2-sided and $p<0.05$ was considered to indicate a statistically significant result. Statistical analyses were performed with IBM SPSS version 22 (SPSS Inc, Chicago, USA) and STATA unless otherwise specified.

SPSS v20 (IBM Corporation) was used to assess the statistics of Quantitative real time PCR results and cell proliferation assays. Significance was examined by Student’s *t*-test (two-tailed), significant differences were considered when $P < 0.05$.

DATA AND SOFTWARE AVAILABILITY

RNA-seq raw data reported in this paper was deposited in the European Nucleotide Archive with the study accession number: PRJEB25719 (https://www.ebi.ac.uk/ena/submit/sra).

Supplementary Note

COGS acknowledgement and funding

This study would not have been possible without the contributions of the following: Per Hall (COGS); Douglas F. Easton, Paul Pharoah, Kyriaki Michailidou, Manjeet K. Bolla, Qin Wang (BCAC), Andrew Berchuck (OCAC), Rosalind A. Eeles, Douglas F. Easton, Ali Amin Al Olama, Zsofia Kote-Jarai, Sara Benlloch (PRACTICAL), Georgia Chenevix-Trench, Antonis Antoniou, Lesley McGuffog, Fergus Couch and Ken Offit (CIMBA), Joe Dennis, Alison M. Dunning, Andrew Lee, and Ed Dicks, Craig Luccarini and the staff of the Centre for Genetic Epidemiology Laboratory, Javier Benitez, Anna Gonzalez-Neira and the staff of the CNIO genotyping unit, Jacques Simard and Daniel C. Tessier, Francois Bacot, Daniel Vincent, Sylvie LaBoissière and Frederic Robidoux and the staff of the McGill University and Génome Québec Innovation Centre, Stig E. Bojesen, Sune F. Nielsen, Borge G. Nordestgaard, and the staff of the Copenhagen DNA laboratory, and Julie M. Cunningham, Sharon A. Windebank, Christopher A. Hilker, Jeffrey Meyer and the staff of Mayo Clinic Genotyping Core Facility

Funding for the iCOGS infrastructure came from: the European Community's Seventh Framework Programme under grant agreement n° 223175 (HEALTH-F2-2009-223175) (COGS), Cancer Research UK (C1287/A10118, C1287/A 10710, C12292/A11174, C1281/A12014, C5047/A8384, C5047/A15007, C5047/A10692, C8197/A16565), the National Institutes of Health (CA128978) and Post-Cancer GWAS initiative (1U19 CA148537, 1U19 CA148065 and 1U19 CA148112 - the GAME-ON initiative), the Department of Defence (W81XWH-10-1-0341), the Canadian Institutes of Health Research (CIHR) for the CIHR Team in Familial Risks of Breast Cancer, Komen Foundation for the Cure, the Breast Cancer Research Foundation, and the Ovarian Cancer Research Fund.

The PRACTICAL Consortium (http://practical.ccge.medschl.cam.ac.uk/), in addition to those named in the authors list

Rosalind Eeles [1, 2], Doug Easton [3], Zsofia Kote-Jarai [1], Ali Amin Al Olama [3], Sara Benlloch [3], Kenneth Muir [4], Graham G. Giles [5, 6], Fredrik Wiklund [7], Henrik Gronberg [7], Christopher A. Haiman [8], Johanna Schleutker [9, 10], Maren Weischer [11], Ruth C. Travis [12], David Neal [13], Paul Pharoah [14], Kay-Tee Khaw [15], Janet L. Stanford [16, 17], William J. Blot [18], Stephen Thibodeau [19], Christiane Maier [20, 21], Adam S. Kibel [22, 23], Cezary Cybulski [24], Lisa Cannon-Albright [25], Hermann Brenner [26,27], Jong Park [28], Radka Kaneva [29], Jyotsna Batra [30], Manuel R. Teixeira [31], Hardev Pandha[32]

[1] The Institute of Cancer Research, 15 Cotswold Road, Sutton, Surrey, SM2 5NG, UK, [2] Royal Marsden NHS Foundation Trust, Fulham and Sutton, London and Surrey, UK, [3] Centre for Cancer Genetic Epidemiology, Department of Public Health and Primary Care, University of Cambridge, Strangeways

Research Laboratory, Worts Causeway, Cambridge, UK, [4] University of Warwick, Coventry, UK, [5] Cancer Epidemiology Centre, Cancer Council Victoria, 615 St Kilda Road, Melbourne Victoria, Australia, [6] Centre for Epidemiology and Biostatistics, Melbourne School of Population and Global Health, The University of Melbourne, Victoria, Australia, [7] Department of Medical Epidemiology and Biostatistics, Karolinska Institute, Stockholm, Sweden, [8] Department of Preventive Medicine, Keck School of Medicine, University of Southern California/Norris Comprehensive Cancer Center, Los Angeles, California, USA, [9] Department of Medical Biochemistry and Genetics, University of Turku, Turku, Finland, [10] Institute of Biomedical Technology/BioMediTech, University of Tampere and FimLab Laboratories, Tampere, Finland, [11] Department of Clinical Biochemistry, Herlev Hospital, Copenhagen University Hospital, Herlev Ringvej 75, DK-2730 Herlev, Denmark, [12] Cancer Epidemiology Unit, Nuffield Department of Clinical Medicine, University of Oxford, Oxford, UK, [13] Surgical Oncology (Uro-Oncology: S4), University of Cambridge, Box 279, Addenbrooke's Hospital, Hills Road, Cambridge, UK and Cancer Research UK Cambridge Research Institute, Li Ka Shing Centre, Cambridge, UK, [14] Centre for Cancer Genetic Epidemiology, Department of Oncology, University of Cambridge, Strangeways Research Laboratory, Worts Causeway, Cambridge, UK, [15] Cambridge Institute of Public Health, University of Cambridge, Forvie Site, Robinson Way, Cambridge CB2 0SR, [16] Division of Public Health Sciences, Fred Hutchinson Cancer Research Center, Seattle, Washington, USA, [17] Department of Epidemiology, School of Public Health, University of Washington, Seattle, Washington, USA, [18] International Epidemiology Institute, 1455 Research Blvd., Suite 550, Rockville, MD 20850, [19] Mayo Clinic, Rochester, Minnesota, USA, [20] Department of Urology, University Hospital Ulm, Germany,

[21] Institute of Human Genetics University Hospital Ulm, Germany, [22] Brigham and Women's Hospital/Dana-Farber Cancer Institute, 45 Francis Street- ASB II-3, Boston, MA 02115, [23] Washington University, St Louis, Missouri, [24] International Hereditary Cancer Center, Department of Genetics and Pathology, Pomeranian Medical University, Szczecin, Poland, [25] Division of Genetic Epidemiology, Department of Medicine, University of Utah School of Medicine[26] Division of Clinical Epidemiology and Aging Research & Division of Preventive Oncology, German Cancer Research Center, Heidelberg Germany, [27]German Cancer Consortium (DKTK), German Cancer Research Center (DKFZ), Heidelberg Germany, [28]Division of Cancer Prevention and Control, H. Lee Moffitt Cancer Center, 12902 Magnolia Dr., Tampa, Florida, USA, [29] Molecular Medicine Center and Department of Medical Chemistry and Biochemistry, Medical University - Sofia, 2 Zdrave St, 1431, Sofia, Bulgaria, [30] Australian Prostate Cancer Research Centre-Qld, Institute of Health and Biomedical Innovation and Schools of Life Science and Public Health, Queensland University of Technology, Brisbane, Australia, [31] Department of Genetics, Portuguese Oncology Institute, Porto, Portugal and Biomedical Sciences Institute (ICBAS), Porto University, Porto, Portugal, [32]The University of Surrey, Guildford, Surrey, GU2 7XH, UK

Figure 1

Click here to download Figure Gao&Xia_Figure_1.tif

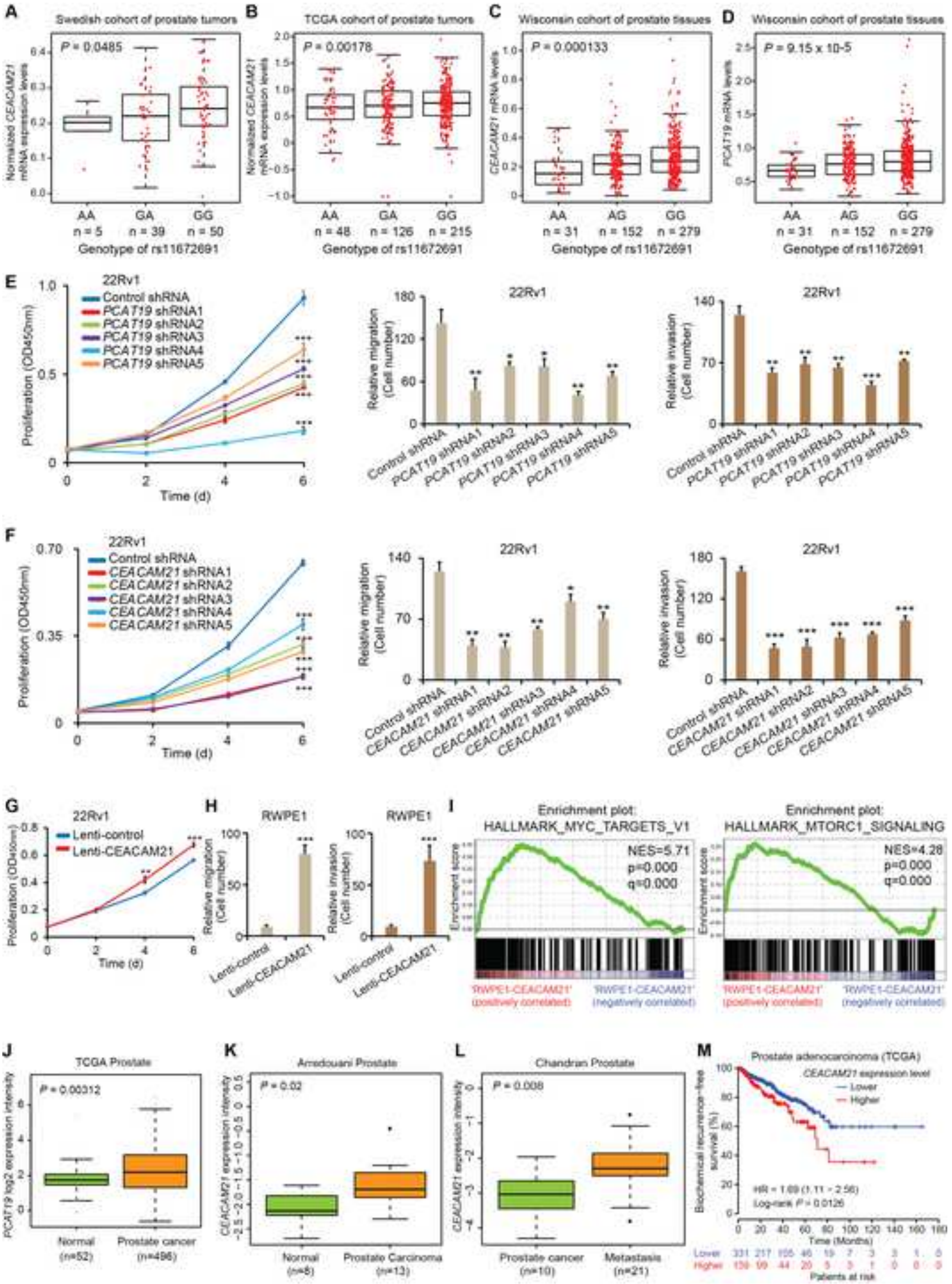

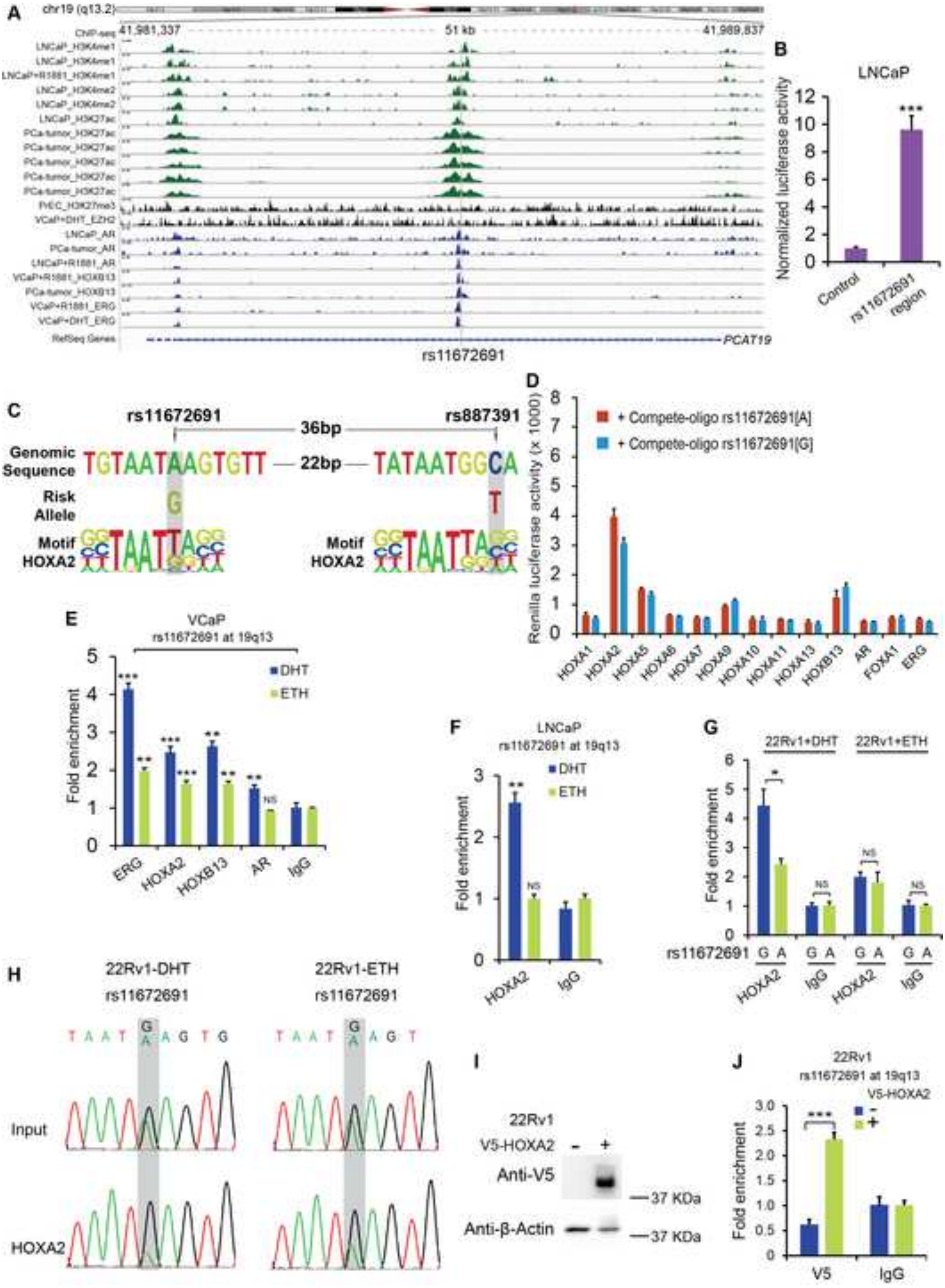
A
chr19 (q13.2)
ChIP-seq
41,981,337
51 kb
41,989,837
LNCaP_H3K4me1
LNCaP_H3K4me1
LNCaP+R1881_H3K4me1
LNCaP_H3K4me2
LNCaP_H3K4me2
LNCaP_H3K27ac
PCa-tumor_H3K27ac
PCa-tumor_H3K27ac
PCa-tumor_H3K27ac
PCa-tumor_H3K27ac
PCa-tumor_H3K27ac
PrEC_H3K27me3
VCaP+DHT_EZH2
LNCaP_AR
PCa-tumor_AR
LNCaP+R1881_AR
VCaP+R1881_HOXB13
PCa-tumor_HOXB13
VCaP+R1881_ERG
VCaP+DHT_ERG
RefSeq Genes
PCAT19
rs11672691
B
LNCaP
Normalized luciferase activity
12
10
8
6
4
2
0
***
Control
rs11672691 region
C
rs11672691
36bp
rs887391
Genomic Sequence
TGTAATAAGTGTT
22bp
TATAATGGCA
Risk Allele
G
T
Motif HOXA2
Motif HOXA2
D
Renilla luciferase activity (x 1000)
8
7
6
5
4
3
2
1
0
+ Compete-oligo rs11672691[A]
+ Compete-oligo rs11672691[G]
HOXA1
HOXA2
HOXA5
HOXA6
HOXA7
HOXA9
HOXA10
HOXA11
HOXA13
HOXB13
AR
FOXA1
ERG
E
VCaP
rs11672691 at 19q13
Fold enrichment
5
4
3
2
1
0
DHT
ETH
***
**
***
***
**
**
**
NS
ERG
HOXA2
HOXB13
AR
IgG
F
LNCaP
rs11672691 at 19q13
Fold enrichment
3
2
1
0
DHT
ETH
**
NS
HOXA2
IgG
G
22Rv1+DHT
22Rv1+ETH
Fold enrichment
6
5
4
3
2
1
0
*
NS
NS
NS
rs11672691
G A
G A
G A
G A
HOXA2
IgG
HOXA2
IgG
H
22Rv1-DHT
rs11672691
22Rv1-ETH
rs11672691
T A A T G A A G T G
T A A T G A A G T
Input
HOXA2
I
22Rv1
V5-HOXA2
-
+
Anti-V5
37 KDa
Anti-β-Actin
37 KDa
J
22Rv1
rs11672691 at 19q13
V5-HOXA2
-
+
Fold enrichment
3.0
2.5
2.0
1.5
1.0
0.5
0
***
V5
IgG

Figure 3

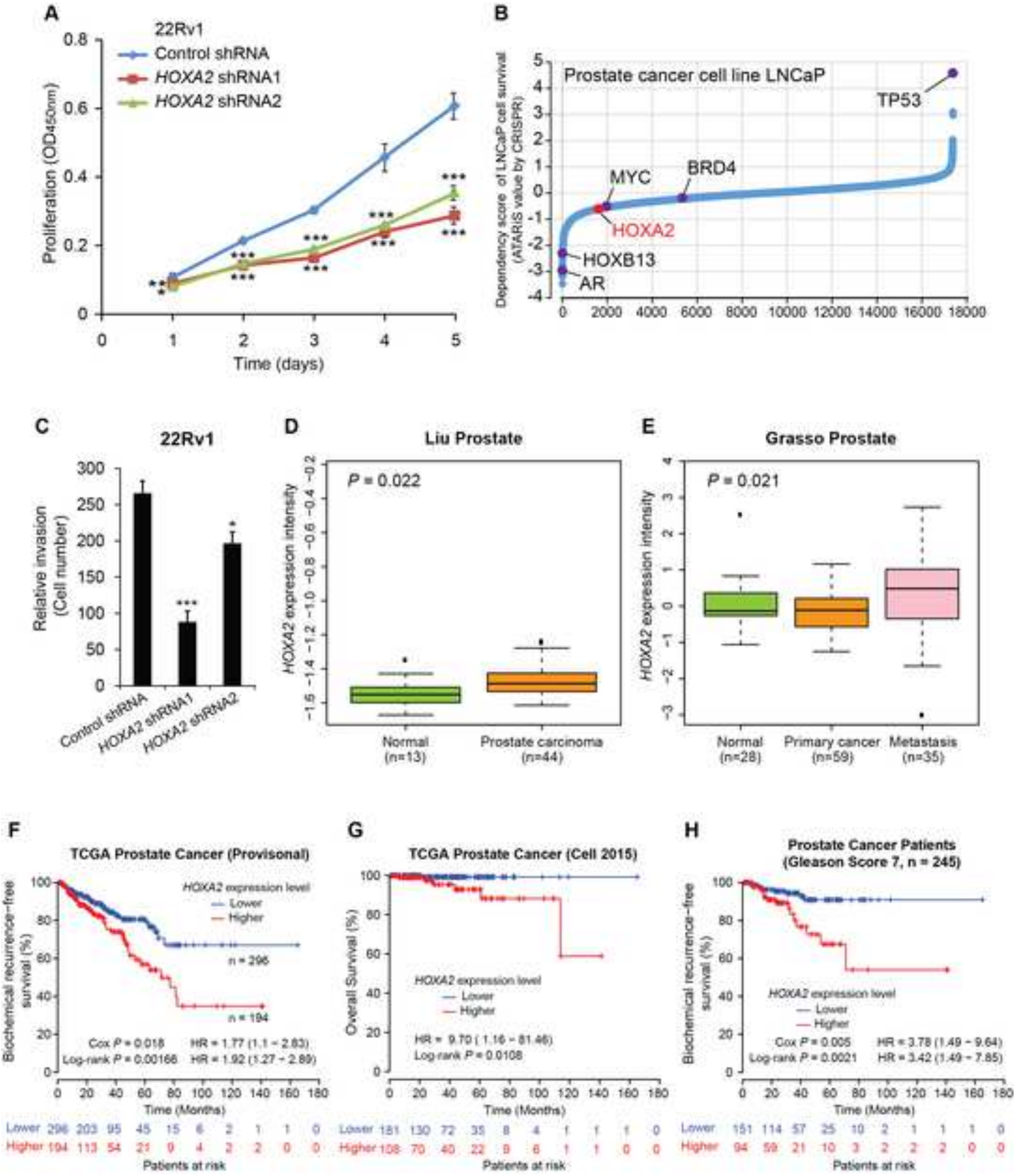
A
22Rv1
Control shRNA
HOXA2 shRNA1
HOXA2 shRNA2
Proliferation (OD450nm)
0.8
0.6
0.4
0.2
0
Time (days)
0 1 2 3 4 5
**
*
***
B
Prostate cancer cell line LNCaP
Dependency score of LNCaP cell survival (ATARIS value by CRISPR)
5 4 3 2 1 0 -1 -2 -3 -4
TP53
MYC
BRD4
HOXA2
HOXB13
AR
0 2000 4000 6000 8000 10000 12000 14000 16000 18000
C
22Rv1
Relative invasion (Cell number)
300 250 200 150 100 50 0
***
*
Control shRNA
HOXA2 shRNA1
HOXA2 shRNA2
D
Liu Prostate
P = 0.022
HOXA2 expression intensity
−0.2 −0.4 −0.6 −0.8 −1.0 −1.2 −1.4 −1.6
Normal (n=13)
Prostate carcinoma (n=44)
E
Grasso Prostate
P = 0.021
HOXA2 expression intensity
4 3 2 1 0 −1 −2 −3
Normal (n=28)
Primary cancer (n=59)
Metastasis (n=35)
F
TCGA Prostate Cancer (Provisonal)
Biochemical recurrence−free survival (%)
HOXA2 expression level
Lower
Higher
n = 296
n = 194
Cox P = 0.018 HR = 1.77 (1.1 − 2.83)
Log-rank P = 0.00168 HR = 1.92 (1.27 − 2.89)
0 20 40 60 80 100 120 140 160 180
Time (Months)
Lower 296 203 95 45 15 6 2 1 1 0
Higher 194 113 54 21 9 4 2 2 0 0
Patients at risk
G
TCGA Prostate Cancer (Cell 2015)
Overall Survival (%)
HOXA2 expression level
Lower
Higher
HR = 9.70 (1.16 − 81.46)
Log-rank P = 0.0108
Time (Months)
Lower 181 130 72 35 8 4 1 1 1 0
Higher 108 70 40 22 9 6 1 1 0 0
Patients at risk
H
Prostate Cancer Patients (Gleason Score 7, n = 245)
Biochemical recurrence−free survival (%)
HOXA2 expression level
Lower
Higher
Cox P = 0.005 HR = 3.78 (1.49 − 9.64)
Log-rank P = 0.0021 HR = 3.42 (1.49 − 7.85)
Time (Months)
Lower 151 114 57 25 10 2 1 1 1 0
Higher 94 59 21 10 3 2 2 2 0 0
Patients at risk

Figure 4

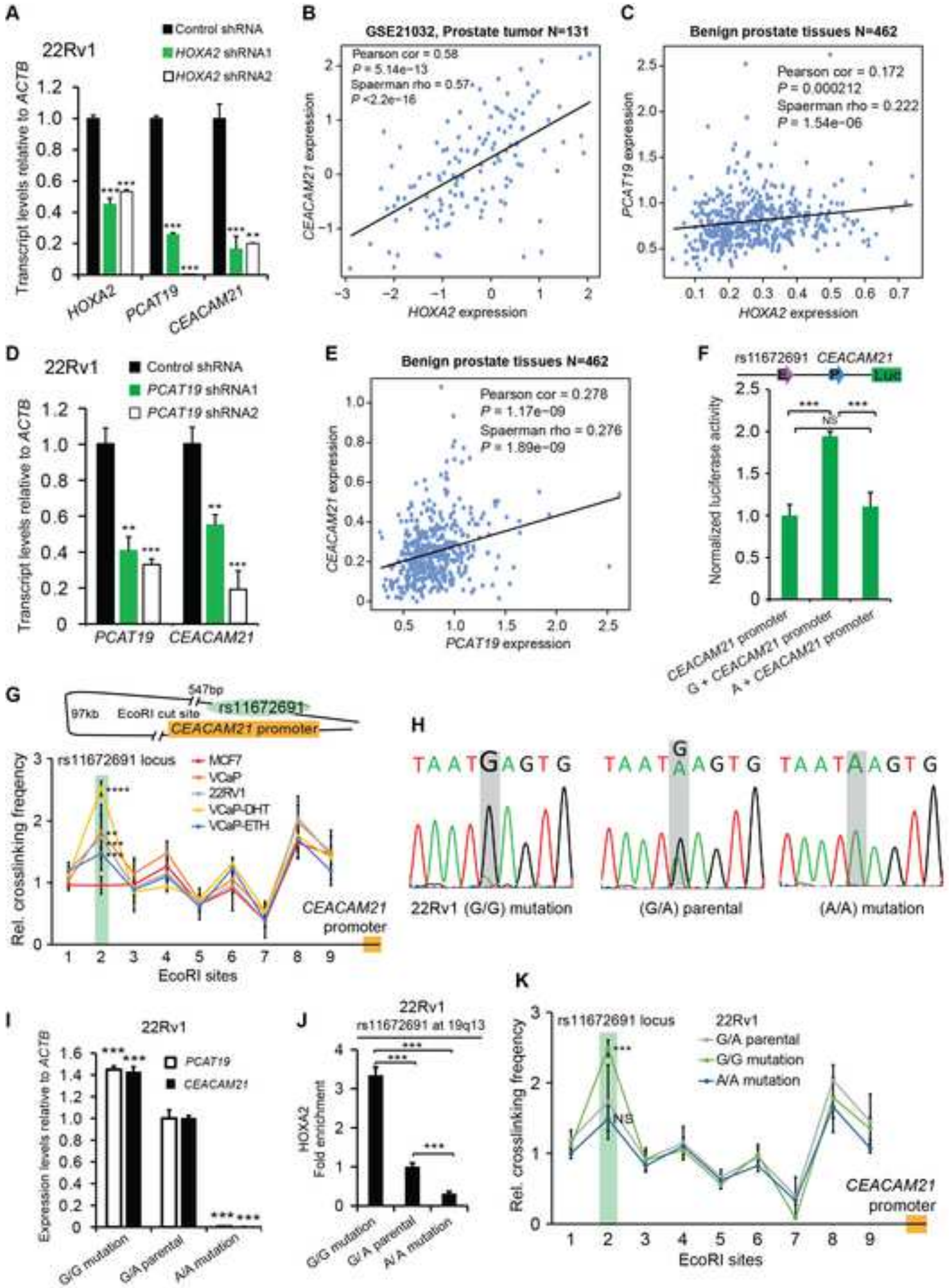
A
22Rv1
Control shRNA
HOXA2 shRNA1
HOXA2 shRNA2
Transcript levels relative to ACTB
1.2
1.0
0.8
0.6
0.4
0.2
0
***
***
***
***
***
**
HOXA2
PCAT19
CEACAM21
B
GSE21032, Prostate tumor N=131
Pearson cor = 0.58
P = 5.14e−13
Spearman rho = 0.57
P <2.2e−16
CEACAM21 expression
HOXA2 expression
−3
−2
−1
0
1
2
C
Benign prostate tissues N=462
Pearson cor = 0.172
P = 0.000212
Spearman rho = 0.222
P = 1.54e−06
PCAT19 expression
HOXA2 expression
0.1
0.2
0.3
0.4
0.5
0.6
0.7
2.5
2.0
1.5
1.0
0.5
D
22Rv1
Control shRNA
PCAT19 shRNA1
PCAT19 shRNA2
Transcript levels relative to ACTB
**
***
**
***
PCAT19
CEACAM21
E
Benign prostate tissues N=462
Pearson cor = 0.278
P = 1.17e−09
Spearman rho = 0.276
P = 1.89e−09
CEACAM21 expression
PCAT19 expression
F
rs11672691
CEACAM21
E
P
Luc
Normalized luciferase activity
***
***
NS
CEACAM21 promoter
G + CEACAM21 promoter
A + CEACAM21 promoter
G
547bp
rs11672691
97kb
EcoRI cut site
CEACAM21 promoter
rs11672691 locus
MCF7
VCaP
22RV1
VCaP-DHT
VCaP-ETH
Rel. crosslinking freqency
CEACAM21
promoter
EcoRI sites
H
TAATGAGTG
TAATAAGTG
G
TAATAAGTG
22Rv1 (G/G) mutation
(G/A) parental
(A/A) mutation
I
22Rv1
PCAT19
CEACAM21
Expression levels relative to ACTB
1.6
1.4
1.2
1.0
0.8
0.6
0.4
0.2
0
***
***
***
***
G/G mutation
G/A parental
A/A mutation
J
22Rv1
rs11672691 at 19q13
HOXA2
Fold enrichment
***
***
***
G/G mutation
G/ A parental
A/ A mutation
K
rs11672691 locus
22Rv1
G/A parental
G/G mutation
A/A mutation
***
NS
Rel. crosslinking frequency
CEACAM21
promoter
EcoRI sites

Figure 5

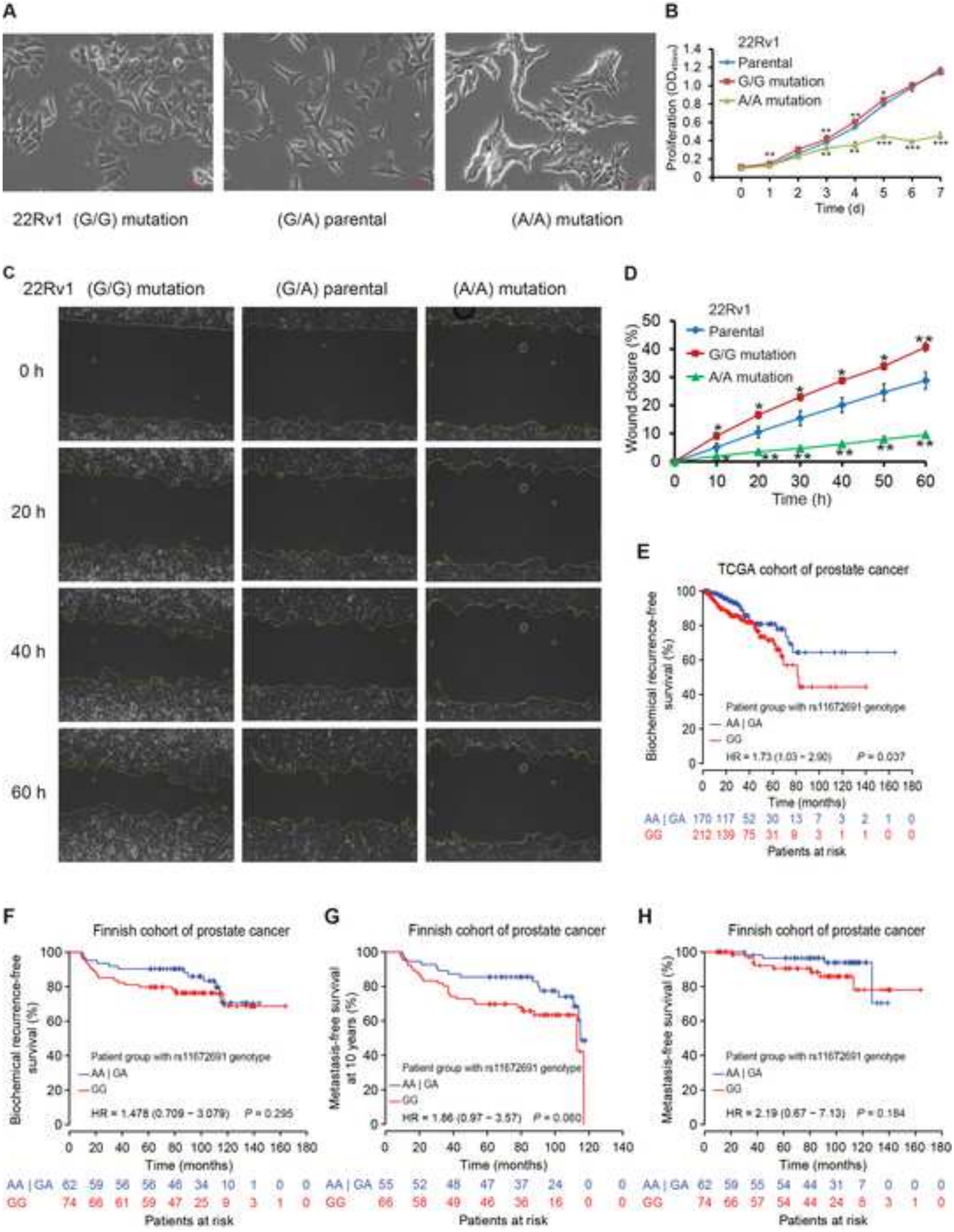
A
22Rv1 (G/G) mutation
(G/A) parental
(A/A) mutation
B
22Rv1
Parental
G/G mutation
A/A mutation
Proliferation (OD)
1.4
1.2
1.0
0.8
0.6
0.4
0.2
0
0 1 2 3 4 5 6 7
Time (d)
C
22Rv1 (G/G) mutation
(G/A) parental
(A/A) mutation
0 h
20 h
40 h
60 h
D
22Rv1
Parental
G/G mutation
A/A mutation
Wound closure (%)
50
40
30
20
10
0
0 10 20 30 40 50 60
Time (h)
E
TCGA cohort of prostate cancer
Biochemical recurrence-free survival (%)
100 80 60 40 20 0
Patient group with rs11672691 genotype
AA | GA
GG
HR = 1.73 (1.03 - 2.90)
P = 0.037
0 20 40 60 80 100 120 140 160 180
Time (months)
AA | GA 170 117 52 30 13 7 3 2 1 0
GG 212 139 75 31 9 3 1 1 0 0
Patients at risk
F
Finnish cohort of prostate cancer
Biochemical recurrence-free survival (%)
Patient group with rs11672691 genotype
AA | GA
GG
HR = 1.478 (0.709 - 3.079)
P = 0.295
0 20 40 60 80 100 120 140 160 180
Time (months)
AA | GA 62 59 56 56 46 34 10 1 0 0
GG 74 66 61 59 47 25 9 3 1 0
Patients at risk
G
Finnish cohort of prostate cancer
Metastasis-free survival at 10 years (%)
Patient group with rs11672691 genotype
AA | GA
GG
HR = 1.86 (0.97 - 3.57)
P = 0.060
0 20 40 60 80 100 120 140
Time (months)
AA | GA 55 52 48 47 37 24 0 0
GG 66 58 49 46 36 16 0 0
Patients at risk
H
Finnish cohort of prostate cancer
Metastasis-free survival (%)
Patient group with rs11672691 genotype
AA | GA
GG
HR = 2.19 (0.67 - 7.13)
P = 0.184
0 20 40 60 80 100 120 140 160 180
Time (months)
AA | GA 62 59 55 54 44 31 7 0 0 0
GG 74 66 57 54 44 24 6 3 1 0
Patients at risk

Figure 6

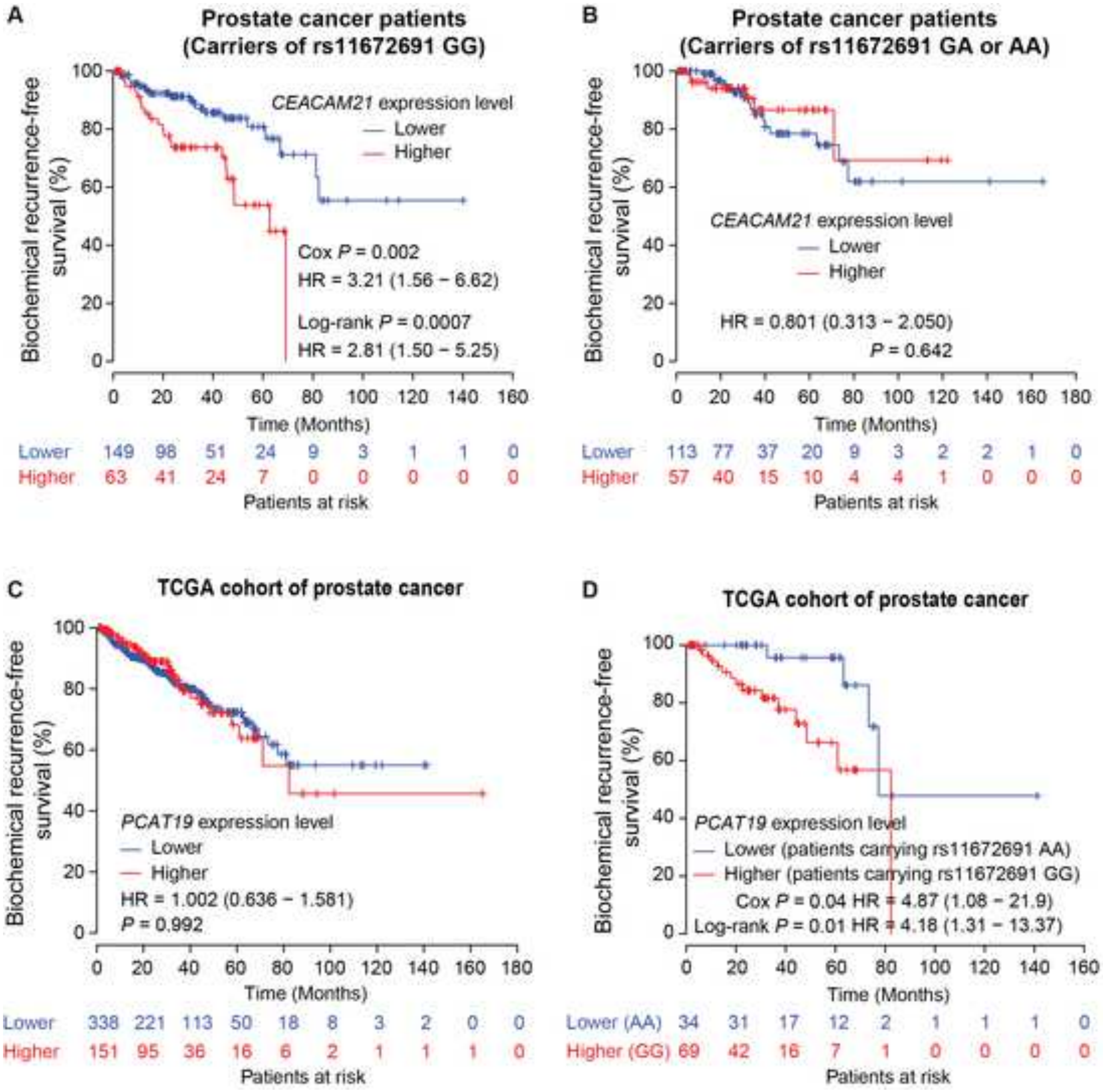
A
Prostate cancer patients (Carriers of rs11672691 GG)
Biochemical recurrence-free survival (%)
100
80
60
40
20
0
CEACAM21 expression level
Lower
Higher
Cox *P* = 0.002
HR = 3.21 (1.56 – 6.62)
Log-rank *P* = 0.0007
HR = 2.81 (1.50 – 5.25)
0 20 40 60 80 100 120 140 160
Time (Months)
Lower 149 98 51 24 9 3 1 1 0
Higher 63 41 24 7 0 0 0 0 0
Patients at risk
B
Prostate cancer patients (Carriers of rs11672691 GA or AA)
Biochemical recurrence-free survival (%)
100
80
60
40
20
0
CEACAM21 expression level
Lower
Higher
HR = 0.801 (0.313 – 2.050)
P = 0.642
0 20 40 60 80 100 120 140 160 180
Time (Months)
Lower 113 77 37 20 9 3 2 2 1 0
Higher 57 40 15 10 4 4 1 0 0 0
Patients at risk
C
TCGA cohort of prostate cancer
Biochemical recurrence-free survival (%)
100
80
60
40
20
0
PCAT19 expression level
Lower
Higher
HR = 1.002 (0.636 – 1.581)
P = 0.992
0 20 40 60 80 100 120 140 160 180
Time (Months)
Lower 338 221 113 50 18 8 3 2 0 0
Higher 151 95 36 16 6 2 1 1 1 0
Patients at risk
D
TCGA cohort of prostate cancer
Biochemical recurrence-free survival (%)
100
80
60
40
20
0
PCAT19 expression level
Lower (patients carrying rs11672691 AA)
Higher (patients carrying rs11672691 GG)
Cox *P* = 0.04 HR = 4.87 (1.08 – 21.9)
Log-rank *P* = 0.01 HR = 4.18 (1.31 – 13.37)
0 20 40 60 80 100 120 140 160
Time (Months)
Lower (AA) 34 31 17 12 2 1 1 1 0
Higher (GG) 69 42 16 7 1 0 0 0 0
Patients at risk

Table S1

Table S1. Clinical information defining aggressive prostate cancer, n=2738 (%), Related to Table 1.

Core clinical characteristics for aggressive prostate cancer	
Diagnostic PSA level, ng/mL	
High, >100	130 (4.8)
Low, ≤100	2481 (90.6)
Missing data	127 (4.6)
Gleason score	
High, ≥8	368 (13.4)
Low, <8	2005 (73.3)
Missing data	365 (13.3)
Tumour stage	
High (T3/T4)	540 (19.7)
Low (≤T2)	2090 (76.3)
Missing data	108 (3.9)
Nodus stage	
Yes (N1)	14 (0.5)
No (no N1)	2626 (95.5)
Missing data	108 (3.9)
Metastasis	
Yes (M1)	191 (7.0)
No (no M1)	2439 (89.1)
Missing data	108 (3.9)
Prostate cancer specific mortality	
yes, fatal prostate cancer	297 (10.9)
no, non-fatal prostate cancer	2441 (89.1)
Additional clinical features	
PSA progression	
Yes	785 (28.7)
No	1953 (71.3)
Castration resistance prostate cancer (CRPC)	
Yes	287 (10.5)
No	2451 (89.5)

Table S2. GSEA results for gene sets enriched in RNA-seq data from RWPE1 cells with overexpression of CEACAM21, Related to Figures 1I and S3D.

Gene Set Name	SIZE	ES	NES	NOM p-val	FDR q-val	FWER p-val
HALLMARK_MYC_TARGETS_V1	198	0.351	5.706	0	0	0
HALLMARK_MTORC1_SIGNALING	193	0.263	4.278	0	0	0
HALLMARK_MYC_TARGETS_V2	58	0.399	3.539	0	0	0
HALLMARK_UNFOLDED_PROTEIN_RESPONSE	108	0.238	2.838	0	9.26E-05	0.001
HALLMARK_CHOLESTEROL_HOMEOSTASIS	68	0.263	2.537	0	2.39E-04	0.003
HALLMARK_OXIDATIVE_PHOSPHORYLATION	198	0.142	2.313	0.002	7.21E-04	0.011
HALLMARK_PROTEIN_SECRETION	92	0.145	1.625	0.04	0.05497	0.62
HALLMARK_KRAS_SIGNALING_DN	119	0.106	1.353	0.113	0.161	0.966
HALLMARK_PI3K_AKT_MTOR_SIGNALING	94	0.116	1.325	0.16	0.16013	0.977
HALLMARK_PEROXISOME	88	0.111	1.232	0.213	0.20578	0.997

Table S3

Table S3. SNP imputation for rs11672691 with variants r2 >= 0.8, Related to Figure 2C and STAR Methods.

chr	pos (hg19)	LD	LD	variant	Within active gene regulatory elements?	Ref	Alt	dbSNP
		(r^2)	(D')					func annot
chr19	41985587	1	1	rs11672691	**YES**	A	G	intronic
chr19	41985624	0.87	1	rs887391	**YES**	C	T	intronic
chr19	41985931	0.98	0.99	rs74738513	**NO**	A	T	intronic
chr19	41986217	0.99	1	rs2079811	**NO**	T	C	intronic
chr19	41986536	0.99	1	rs2316974	**NO**	G	A	intronic
chr19	41989711	0.85	0.96	rs8112363	**NO**	C	T	intronic
chr19	41999120	0.84	0.96	rs7248215	**NO**	G	A	intronic
chr19	42001210	0.84	0.96	rs2191139	**NO**	T	C	N/A

Table S4. Enhancer Element Locator (EEL) prediction results of rs11672691 and rs887391 surrounding sequence, Related to STAR methods, Related to Figures 2C, S4B, S4C and STAR Methods.

SNP&allele	Program	PWM	Start	End	EEL score	Strand (+/-)
rs11672691G	eel	HOXA2.pfm	20	29	9.551937	-
rs11672691A	eel	HOXA2.pfm	20	29	5.647312	-
rs887391C	eel	HOXA2.pfm	18	27	6.654399	-
rs887391T	eel	HOXA2.pfm	18	27	6.000891	-
rs11672691G	eel	NKX3-1.pfm	24	32	6.368699	-
rs11672691A	eel	NKX3-1.pfm	24	32	9.936611	-

Table S5. Primer sequences for qPT-PCR and ChIP assays, Related to STAR Methods.

No.	Primer name	Sequence 5'-3'	Application
1	actin-f	AGAAAATCTGGCACCACACC	Control primer
2	actin-R	AGAGGCGTACAGGGATAGCA	
3	PCAT19-F	TGTTCTGAGCAGCGAGCCAC	Figures 4A,D,I,S1A,S6A-S6D,S6F
4	PCAT19-R	AGCTCCTCCCTTTCCTCGGG	
5	PCAT19 intron2 F	AAGCAAGGGAAGCTGCTTTGT	Figure S6F
6	PCAT19 intron2 R	CGAGACCCTTAATCGCTGGG	
7	CEACAM21-F	ATGACAACACTCTAGGCATCC	Figures 4A,D,I,S1F,S6A-S6C,S6E,S6F
8	CEACAM21-R	CAACCAGGACCCCGATCA	
9	ERG-56F	CGCAGAGTTATCGTGCCAGCAGAT	Figure S6B
10	ERG-56R	CCATATTCTTTCACCGCCCACTCC	
11	HOXB13-F	GAGTACCCCAGCCGCCCCACT	Figure S6A
12	HOXB13-R	ACGAAAGGCGCAGGCGTCAGG	
13	HOXA2-F	CTCTGCGCTCGCCTTTTTCC	Figures 4A,S5A
14	HOXA2-R	AGCGACGGCTGGCTATTGAT	
15	HOXA10-F	AGGGCTATCTGCTCCCTTCG	Figure S6C
16	HOXA10-R	CTGATGAGCGAGTCGACCAA	
ChIP-qPCR prmers			
1	ChIPNeg135-f	TGCCTCAGATTTGGAGTGCT	Control primer
2	ChIPNeg135-r	GAGAAGCCTCTGAGGAGGGA	
3	rs116-87F	CTGAATGACTTGTGCTGCTTGT	Figures 2E,2F,2J,4J,S6F-S6J
4	rs116-87R	GCTTCCCTTGCTTCTGAAATGC	
5	rs116-97f	CGACCACTTTCTCCACTAGC	Figures 2G,S4K
6	rs116Arev	CGTGAAACCGACAGAACACTT	Figure 2G
7	rs116Grev	CGTGAAACCGACAGAACACTC	Figure 2G

Table S6

Table S6. Oligos for microwell-based transcription factor-DNA binding assay and cloning of gene-specific cDNA, Related to Figures 2D, S4D, S4E, and the STAR Methods.

No.	Oligo Name	5´-> 3´Sequence
1	BioHOXA2CONf	AAAAAGTGTAATTAGTGTTCTG
2	HOXA2CONf	AAAAAGTGTAATTAGTGTTCTG
3	HOXA2CONr	CAGAACACTAATTACACTTTTT
4	HOXA2SCRf	AAAAAGGTATGTATTAGTTCTG
5	HOXA2SCRr	CAGAACTAATACATACCTTTTT
6	HOXA2f1	AAAAAGAGTAATTAGTGTTCTG
7	HOXA2f2	AAAAAGGGTAATTAGTGTTCTG
8	HOXA2f3	AAAAAGCGTAATTAGTGTTCTG
9	HOXA2f4	AAAAAGTATAATTAGTGTTCTG
10	HOXA2f5	AAAAAGTTTAATTAGTGTTCTG
11	HOXA2f6	AAAAAGTCTAATTAGTGTTCTG
12	HOXA2f7	AAAAAGTGAAATTAGTGTTCTG
13	HOXA2f8	AAAAAGTGGAATTAGTGTTCTG
14	HOXA2f9	AAAAAGTGCAATTAGTGTTCTG
15	HOXA2f10	AAAAAGTGTTATTAGTGTTCTG
16	HOXA2f11	AAAAAGTGTGATTAGTGTTCTG
17	HOXA2f12	AAAAAGTGTCATTAGTGTTCTG
18	HOXA2f13	AAAAAGTGTATTTAGTGTTCTG
19	HOXA2f14	AAAAAGTGTAGTTAGTGTTCTG
20	HOXA2f15	AAAAAGTGTACTTAGTGTTCTG
21	HOXA2f16	AAAAAGTGTAAATAGTGTTCTG
22	HOXA2f17	AAAAAGTGTAAGTAGTGTTCTG
23	HOXA2f18	AAAAAGTGTAACTAGTGTTCTG
24	HOXA2f19	AAAAAGTGTAATAAGTGTTCTG
25	HOXA2f20	AAAAAGTGTAATGAGTGTTCTG
26	HOXA2f21	AAAAAGTGTAATCAGTGTTCTG
27	HOXA2f22	AAAAAGTGTAATTTGTGTTCTG
28	HOXA2f23	AAAAAGTGTAATTGGTGTTCTG
29	HOXA2f24	AAAAAGTGTAATTCGTGTTCTG
30	HOXA2f25	AAAAAGTGTAATTAATGTTCTG
31	HOXA2f26	AAAAAGTGTAATTATTGTTCTG
32	HOXA2f27	AAAAAGTGTAATTACTGTTCTG
33	HOXA2f28	AAAAAGTGTAATTAGAGTTCTG
34	HOXA2f29	AAAAAGTGTAATTAGGGTTCTG
35	HOXA2f30	AAAAAGTGTAATTAGCGTTCTG
36	HOXA2r1	CAGAACACTAATTACTCTTTTT
37	HOXA2r2	CAGAACACTAATTACCCTTTTT
38	HOXA2r3	CAGAACACTAATTACGCTTTTT
39	HOXA2r4	CAGAACACTAATTATACTTTTT
40	HOXA2r5	CAGAACACTAATTAAACTTTTT

41	HOXA2r6	CAGAACACTAATTAGACTTTTT
42	HOXA2r7	CAGAACACTAATTTCACTTTTT
43	HOXA2r8	CAGAACACTAATTCCACTTTTT
44	HOXA2r9	CAGAACACTAATTGCACTTTTT
45	HOXA2r10	CAGAACACTAATAACACTTTTT
46	HOXA2r11	CAGAACACTAATCACACTTTTT
47	HOXA2r12	CAGAACACTAATGACACTTTTT
48	HOXA2r13	CAGAACACTAAATACACTTTTT
49	HOXA2r14	CAGAACACTAACTACACTTTTT
50	HOXA2r15	CAGAACACTAAGTACACTTTTT
51	HOXA2r16	CAGAACACTATTTACACTTTTT
52	HOXA2r17	CAGAACACTACTTACACTTTTT
53	HOXA2r18	CAGAACACTAGTTACACTTTTT
54	HOXA2r19	CAGAACACTTATTACACTTTTT
55	HOXA2r20	CAGAACACTCATTACACTTTTT
56	HOXA2r21	CAGAACACTGATTACACTTTTT
57	HOXA2r22	CAGAACACAAATTACACTTTTT
58	HOXA2r23	CAGAACACCAATTACACTTTTT
59	HOXA2r24	CAGAACACGAATTACACTTTTT
60	HOXA2r25	CAGAACATTAATTACACTTTTT
61	HOXA2r26	CAGAACAATAATTACACTTTTT
62	HOXA2r27	CAGAACAGTAATTACACTTTTT
63	HOXA2r28	CAGAACTCTAATTACACTTTTT
64	HOXA2r29	CAGAACCCTAATTACACTTTTT
65	HOXA2r30	CAGAACGCTAATTACACTTTTT

Oligos for cloning into pGEN-MCS-Renilla vector

No.	Oligoes name	Sequence 5' to 3'	Restriction site
1	HOXB13-F	gtCTCGAGatggagcccggcaattatg	XhoI/AscI
2	HOXB13-R	tGGCGCGCCaggggtagcgctgttcttc	
3	HOXA1-F	gaaGGATCCATGGACAATGCAAGAATGAAC	BamHI/AscI
4	HOXA1-R	taGGCGCGCCGTGGGAGGTAGTCAGAGTG	
5	HOXA2-F	gtCTCGAGatgaattacgaatttgagcgag	XhoI/AscI
6	HOXA2-R	tGGCGCGCCGTAATTCAGATGCTGCAAG	
7	AR-F	gaaGGATCCATGGAAGTGCAGTTAGGGC	BamHI/AscI
8	AR-R	taGGCGCGCCCTGGGTGTGGAAATAGATGG	
9	ERG-F	GTGAAGCTTATGATTCAGACTGTCCCGG	HindIII/NheI
10	ERG-R	GTGGCTAGCAAGTAGTAAGTGCCCAGATGA	
11	HOXA5-F	gaaGGATCCATGAGCTCTTATTTTGTAAACTCATTT	BamHI/AscI
12	HOXA5-R	taGGCGCGCCGGGACGGAAGGCCCCTC	
13	HOXA6-F	gaaGGATCCATGAGTTCCTATTTTGTGAATCC	BamHI/AscI
14	HOXA6-R	taGGCGCGCCCTCGCCCGCCTTTGCCTC	
15	HOXA7-F	gaaGGATCCATGAGTTCTTCGTATTATGTGAAC	BamHI/AscI
16	HOXA7-R	taGGCGCGCCTTCCTCCTCGTCTTCCTC	
17	HOXA9-F	gtCTCGAGatggccaccactggggccc	XhoI/AscI

18	HOXA9-R	tGGCGCGCCCTCGTCTTTTGCTCGGTC	
19	HOXA10DBD-F	gaagaGAATTCATGAACTGGCTCACGGCAAAGAG	EcoRI/AscI
20	HOXA10DBD-R	taGGCGCGCCCTCCCGGATCCGGTTTTC	
21	HOXA11DBD-F	gaaGGATCCATGCAACGCACCCGCAAAAAG	BamHI/AscI
22	HOXA11DBD-R	taGGCGCGCCTGCTGAGTAGTACTGTAAACGGTC	
23	FOXA1-F	gaaGGATCCATGTTAGGAACTGTGAAGATGG	BamHI/NheI
24	FOXA1-R	atcttGCTAGCccGGAAGTGTTTAGGACGGGTC	
25	HOXA13DBD-F	cccAAGCTTATGGTCTCCCATCCCTCG	HindIII/NheI
26	HOXA13DBD-R	CTAGCTAGCAAACTAGTGGTTTTCAGTTTGT	

Table S7. Primers for quantitative analysis of chromosome conformation capture assays (3C-qPCR), Related to Figures 4G,4KS6H, and the STAR Methods.

No.	Oligoname	Sequence	Cut site on chr19 (hg19)	Function
1	ECO-rs116-Tagman probe	5'FAM-ACATGCCCCCAACTGAAACCAG-3'TAMRA		Tagman probe
2	Reverse primer	TCAGTGCTTGCCATGTGT		ECORI 3C reverse primer
3	Cut site 1	TGCCATCATCCTTCTGGATT	41982282	ECORI 3C Forward primer
4	Cut site 2	GAGTTCCGTTGGTACATTCC	41986134	ECORI 3C Forward primer
5	Cut site 3	AGCTGTCTTCCCCTGAATG	41987947	ECORI 3C Forward primer
6	Cut site 4	GCCATCATCCTTCTGGATTTT	42001261	ECORI 3C Forward primer
7	Cut site 5	CTGTAGGTCTTTTCCAAGGGA	42001803	ECORI 3C Forward primer
8	Cut site 6	CTGGACAGGATTCACGAAGA	42005004	ECORI 3C Forward primer
9	Cut site 7	ACGGAATTCAAGAATGCATTAAAA	42033648	ECORI 3C Forward primer
10	Cut site 8	ATGTTTTCCATGGACTTGCTT	42056323	ECORI 3C Forward primer
11	Cut site 9	TGCCAAAAGGAAGGTAAAGAAG	42062588	ECORI 3C Forward primer
12	ERCC3-Tagman probe	5'FAM-ACAGAATCAACCCAAGTTTTCTGCA-3'TAMR		Tagman probe
13	ERCCC-3C Forward primer	TACTACAAGGGCTCCCTATC		ERCC3 control pri-mer
14	ERCCC-3C reverse primer	TGGTGGATGGTAGTAAACTCA		
15	Cut site 1-F	CACAGAAGGGTGTACACTTCC	41982282	BAC primer

16	Cut site 1-R	AAGTCATCATCCTTCATCCAGT		
17	Cut site 2-F	TGTTCTGTCGGTTTCACGTA	41986134	BAC primer
18	Cut site 2-R	GGACTTGAGAAGTGCTGTGA		
19	Cut site 3-F	GGGAAAACTCTTCTGGTCATT	41987947	BAC primer
20	Cut site 3-R	ACACGGCTCTGTGTATCTGA		
21	Cut site 4-F	TTGCAGAATGTTCTGATGGG	42001261	BAC primer
22	Cut site 4-R	TCCTTGCCAACTTCTGCCT		
23	Cut site 5-F	CACAGAGGAGAGAGGTTCAC	42001803	BAC primer
24	Cut site 5-R	GGGGTATAAGGAGGTGACAC		
25	Cut site 6-F	TCCGTGTGACAAAGAGTTCA	42005004	BAC primer
26	Cut site 6-R	TCTTCCATAGTGCCACTCAC		
27	Cut site 7-F	TCCACTAAAGAAAAGCCCGG	42033648	BAC primer
28	Cut site 7-R	CCTCAAGCGCTGCATTATTT		
29	Cut site 8-F	TGCAGGACACAGGTATTAGC	42056323	BAC primer
30	Cut site 8-R	TCTGTGCATATTCATGCTGC		
31	Cut site 9-F	CTCTCAGCCATCTCCAAACT	42062588	BAC primer
32	Cut site 9-R	CTCTATGGTCAGAAGTCGGC		
33	ERCC3-F	CACTCGGCAAAAGACCACTAT		BAC primer
34	ERCC3-R	TGTATTTGGAGACTCCCTAGC		
35	ECO-rs116D7-61F	CTGTGAGCATAGAATCCGGC		Digest efficiency
36	ECO-rs116D7-61R	TTTCAGTTGGGGGCATGTTG		
37	rs11-88-81F	AAGCAAGGGAAGCTGCTTTGT		Control of digest efficiency and loading adjustments primer
38	rs11-88-81R	CGAGACCCTTAATCGCTGGG		

Figure S1

Click here to download Supplemental Figure Gao&Xia_Figure_S1.tif

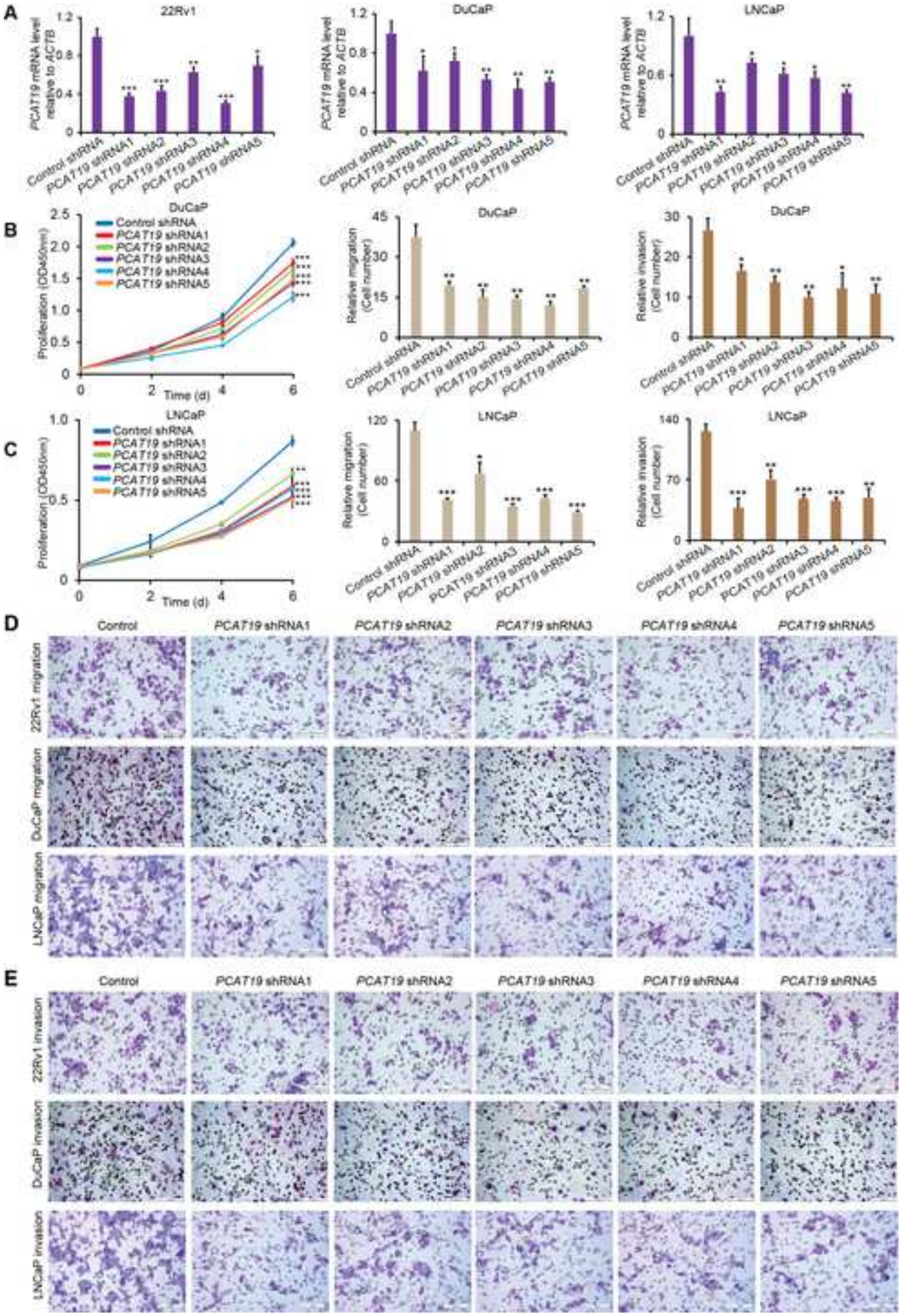

Figure S1 continued

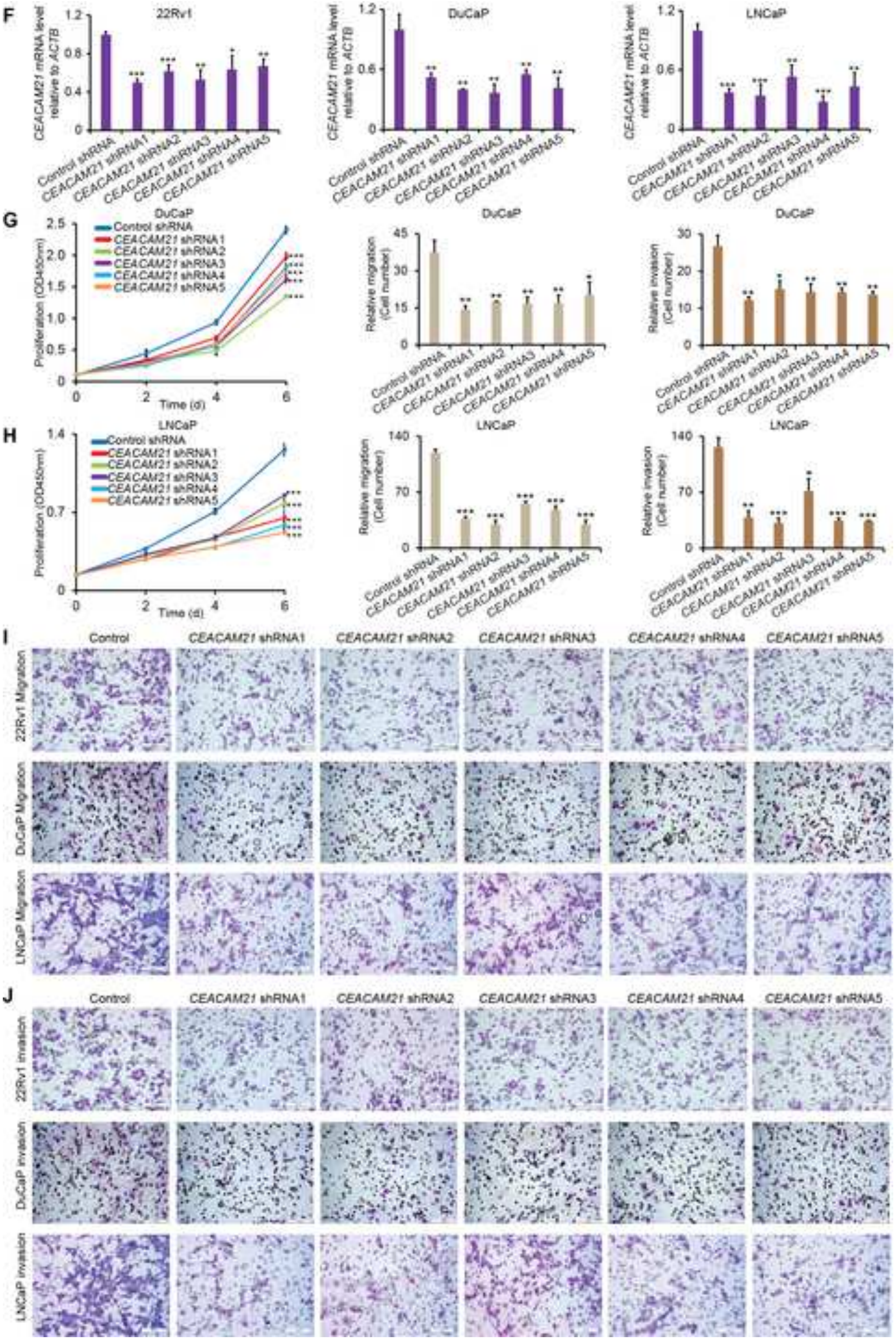

Figure S2

Click here to download Supplemental Figure Gao&Xia_Figure_S2.tif

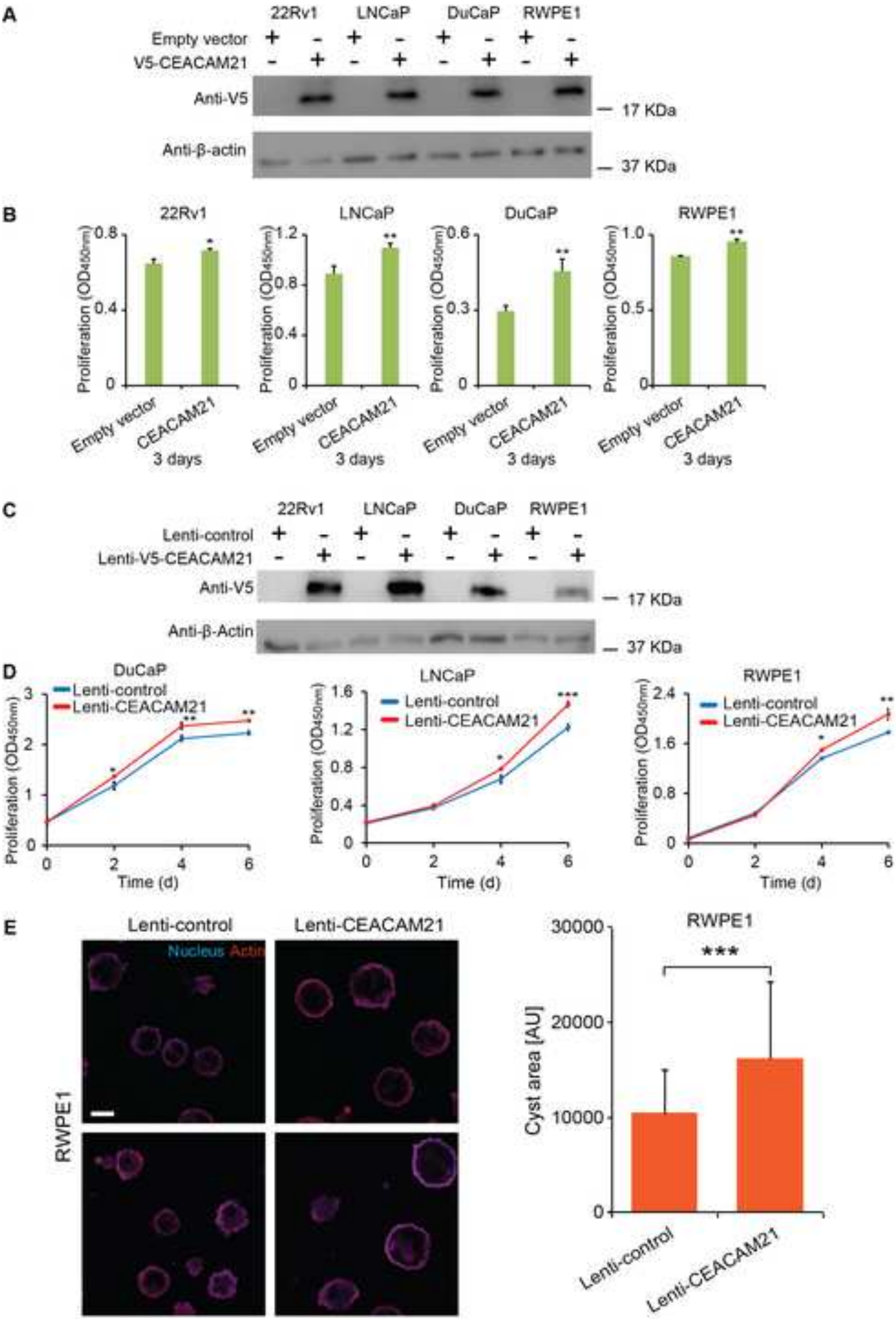

Figure S2 continued

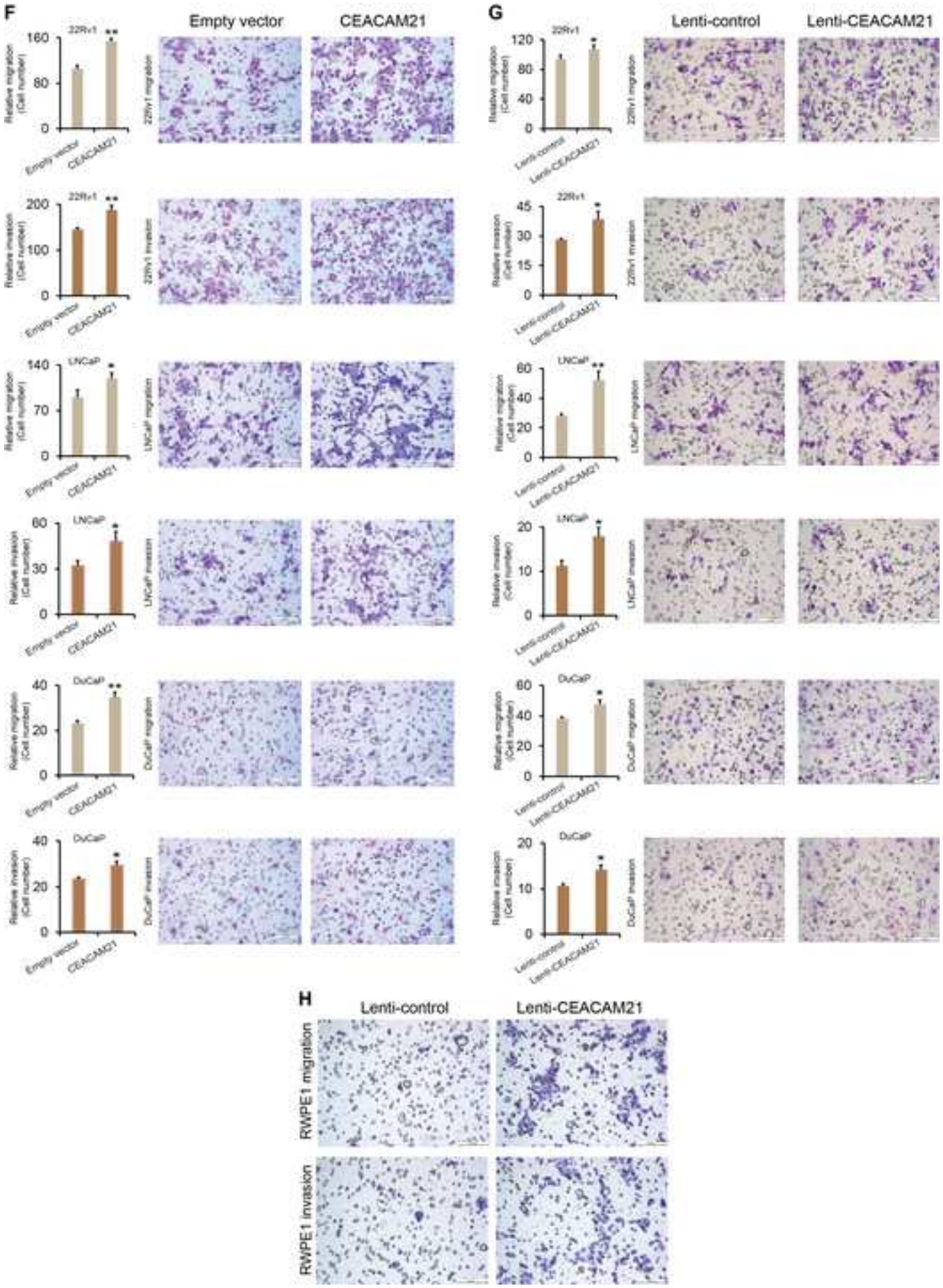

Figure S3

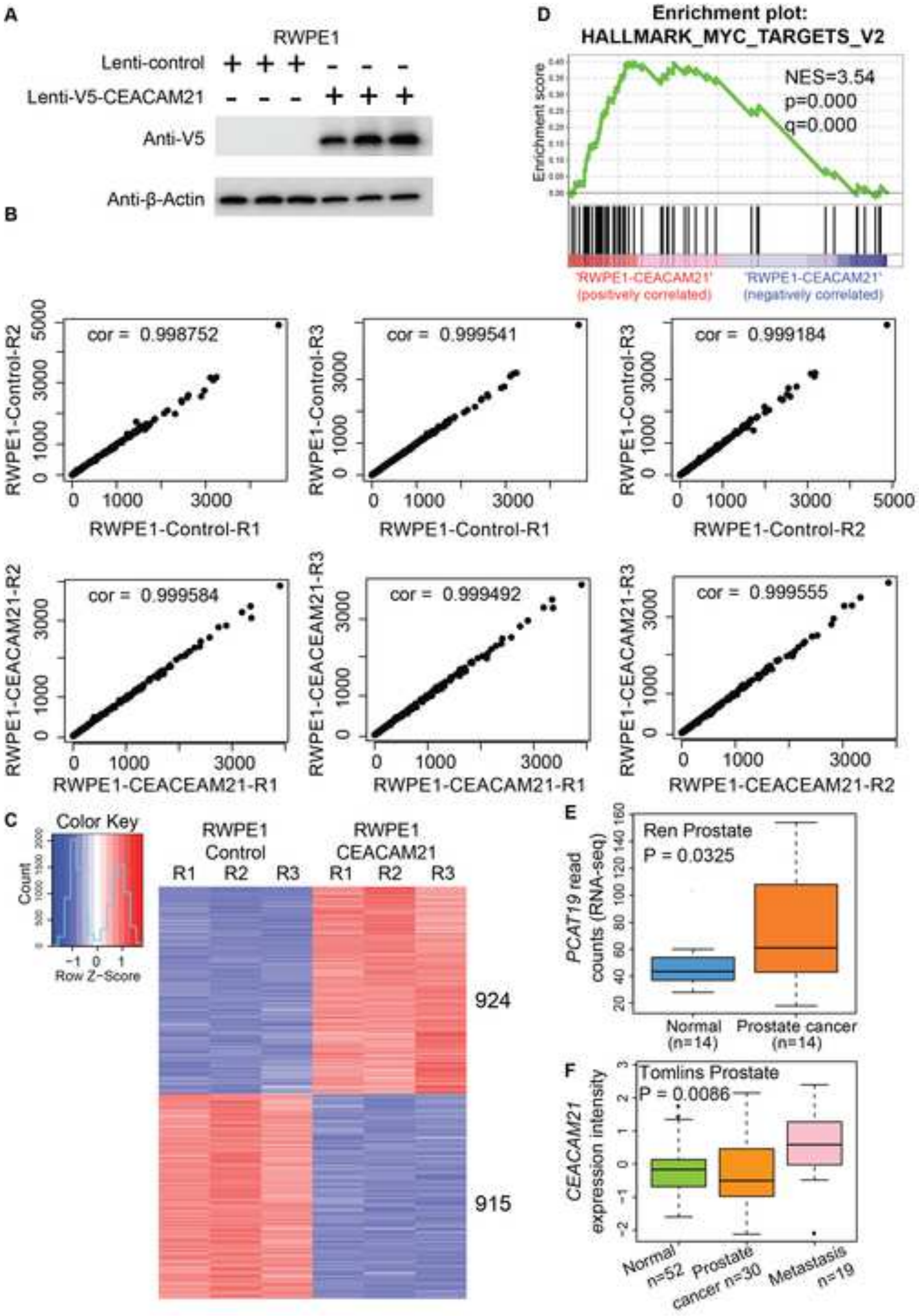
A
RWPE1
Lenti-control + + + - - -
Lenti-V5-CEACAM21 - - - + + +
Anti-V5
Anti-β-Actin
B
cor = 0.998752
RWPE1-Control-R2
RWPE1-Control-R1
cor = 0.999541
RWPE1-Control-R3
RWPE1-Control-R1
cor = 0.999184
RWPE1-Control-R3
RWPE1-Control-R2
cor = 0.999584
RWPE1-CEACAM21-R2
RWPE1-CEACEAM21-R1
cor = 0.999492
RWPE1-CEACAM21-R3
RWPE1-CEACEAM21-R1
cor = 0.999555
RWPE1-CEACAM21-R3
RWPE1-CEACEAM21-R2
0
1000
3000
5000
C
Color Key
Count
Row Z-Score
-1 0 1
RWPE1 Control
RWPE1 CEACAM21
R1 R2 R3 R1 R2 R3
924
915
D
Enrichment plot: HALLMARK_MYC_TARGETS_V2
Enrichment score
NES=3.54
p=0.000
q=0.000
'RWPE1-CEACAM21' (positively correlated)
'RWPE1-CEACAM21' (negatively correlated)
E
Ren Prostate
P = 0.0325
PCAT19 read counts (RNA-seq)
20 40 60 80 100 120 140 160
Normal (n=14)
Prostate cancer (n=14)
F
Tomlins Prostate
P = 0.0086
CEACAM21 expression intensity
-2 -1 0 1 2 3
Normal n=52
Prostate cancer n=30
Metastasis n=19

Figure S4

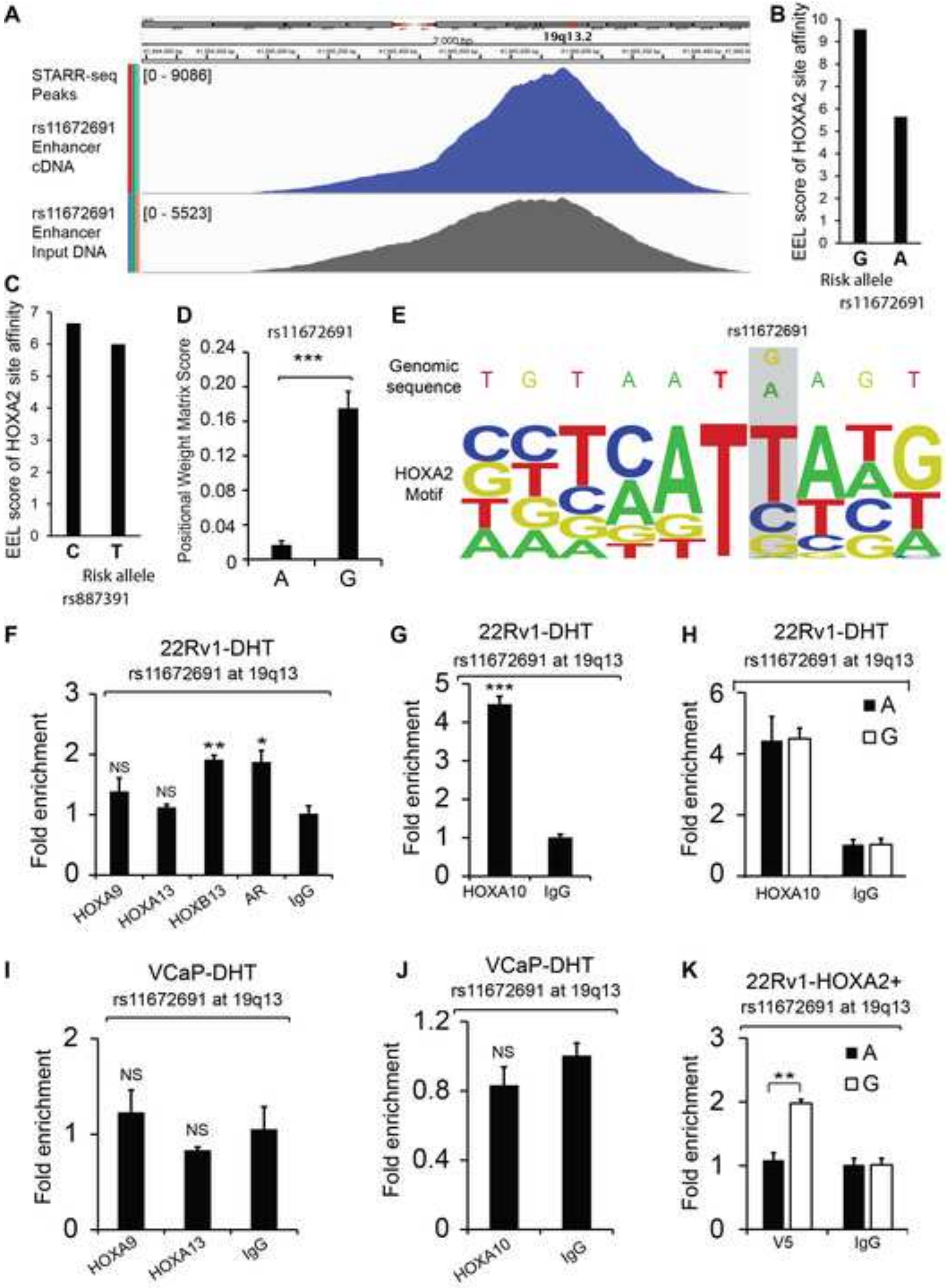
A
19q13.2
2,000 bp
STARR-seq Peaks
[0 - 9086]
rs11672691 Enhancer cDNA
rs11672691 Enhancer Input DNA
[0 - 5523]
B
EEL score of HOXA2 site affinity
0 1 2 3 4 5 6 7 8 9 10
G A
Risk allele
rs11672691
C
EEL score of HOXA2 site affinity
0 1 2 3 4 5 6 7
C T
Risk allele
rs887391
D
rs11672691
***
Positional Weight Matrix Score
0 0.04 0.08 0.12 0.16 0.20 0.24
A G
E
rs11672691
Genomic sequence
T G T A A T G A A G T
HOXA2 Motif
F
22Rv1-DHT
rs11672691 at 19q13
Fold enrichment
0 1 2 3
NS NS ** *
HOXA9 HOXA13 HOXB13 AR IgG
G
22Rv1-DHT
rs11672691 at 19q13
Fold enrichment
0 1 2 3 4 5
***
HOXA10 IgG
H
22Rv1-DHT
rs11672691 at 19q13
Fold enrichment
0 2 4 6
■ A
□ G
HOXA10 IgG
I
VCaP-DHT
rs11672691 at 19q13
Fold enrichment
0 1 2
NS NS
HOXA9 HOXA13 IgG
J
VCaP-DHT
rs11672691 at 19q13
Fold enrichment
0 0.4 0.8 1.2
NS
HOXA10 IgG
K
22Rv1-HOXA2+
rs11672691 at 19q13
Fold enrichment
0 1 2 3
■ A
□ G
**
V5 IgG

Figure S5

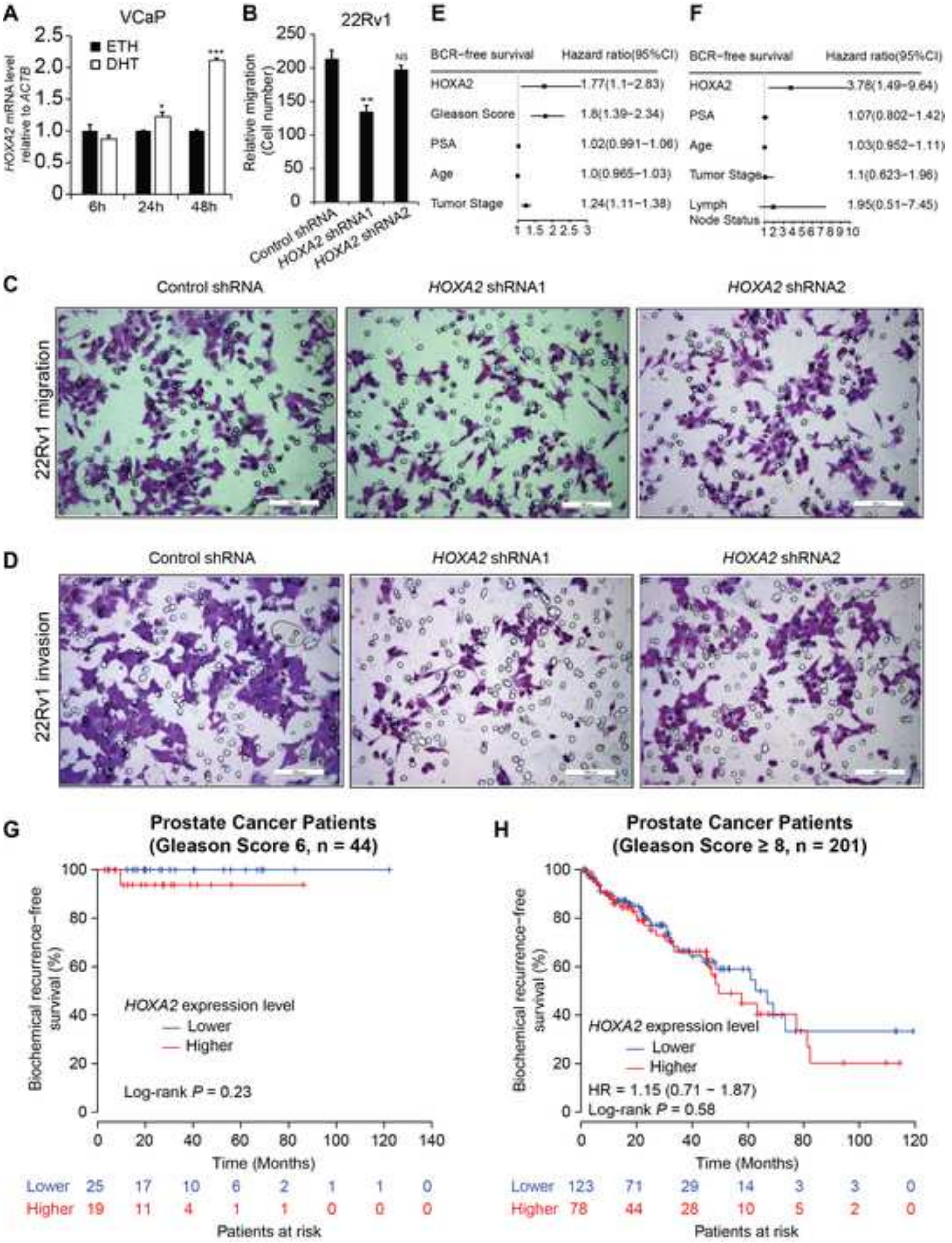
A
VCaP
HOXA2 mRNA level relative to ACTB
2.5
2.0
1.5
1.0
0.5
0
■ ETH
□ DHT
*
***
6h
24h
48h
B
22Rv1
Relative migration (Cell number)
250
200
150
100
50
0
**
NS
Control shRNA
HOXA2 shRNA1
HOXA2 shRNA2
E
BCR-free survival
Hazard ratio(95%CI)
HOXA2
1.77(1.1-2.83)
Gleason Score
1.8(1.39-2.34)
PSA
1.02(0.991-1.06)
Age
1.0(0.965-1.03)
Tumor Stage
1.24(1.11-1.38)
1 1.5 2 2.5 3
F
BCR-free survival
Hazard ratio(95%CI)
HOXA2
3.78(1.49-9.64)
PSA
1.07(0.802-1.42)
Age
1.03(0.952-1.11)
Tumor Stage
1.1(0.623-1.96)
Lymph Node Status
1.95(0.51-7.45)
1 2 3 4 5 6 7 8 9 10
C
22Rv1 migration
Control shRNA
HOXA2 shRNA1
HOXA2 shRNA2
D
22Rv1 invasion
Control shRNA
HOXA2 shRNA1
HOXA2 shRNA2
G
Prostate Cancer Patients (Gleason Score 6, n = 44)
Biochemical recurrence-free survival (%)
100
80
60
40
20
0
HOXA2 expression level
Lower
Higher
Log-rank P = 0.23
0 20 40 60 80 100 120 140
Time (Months)
Lower 25 17 10 6 2 1 1 0
Higher 19 11 4 1 1 0 0 0
Patients at risk
H
Prostate Cancer Patients (Gleason Score ≥ 8, n = 201)
Biochemical recurrence-free survival (%)
100
80
60
40
20
0
HOXA2 expression level
Lower
Higher
HR = 1.15 (0.71 − 1.87)
Log-rank P = 0.58
0 20 40 60 80 100 120
Time (Months)
Lower 123 71 29 14 3 3 0
Higher 78 44 28 10 5 2 0
Patients at risk

Figure S6

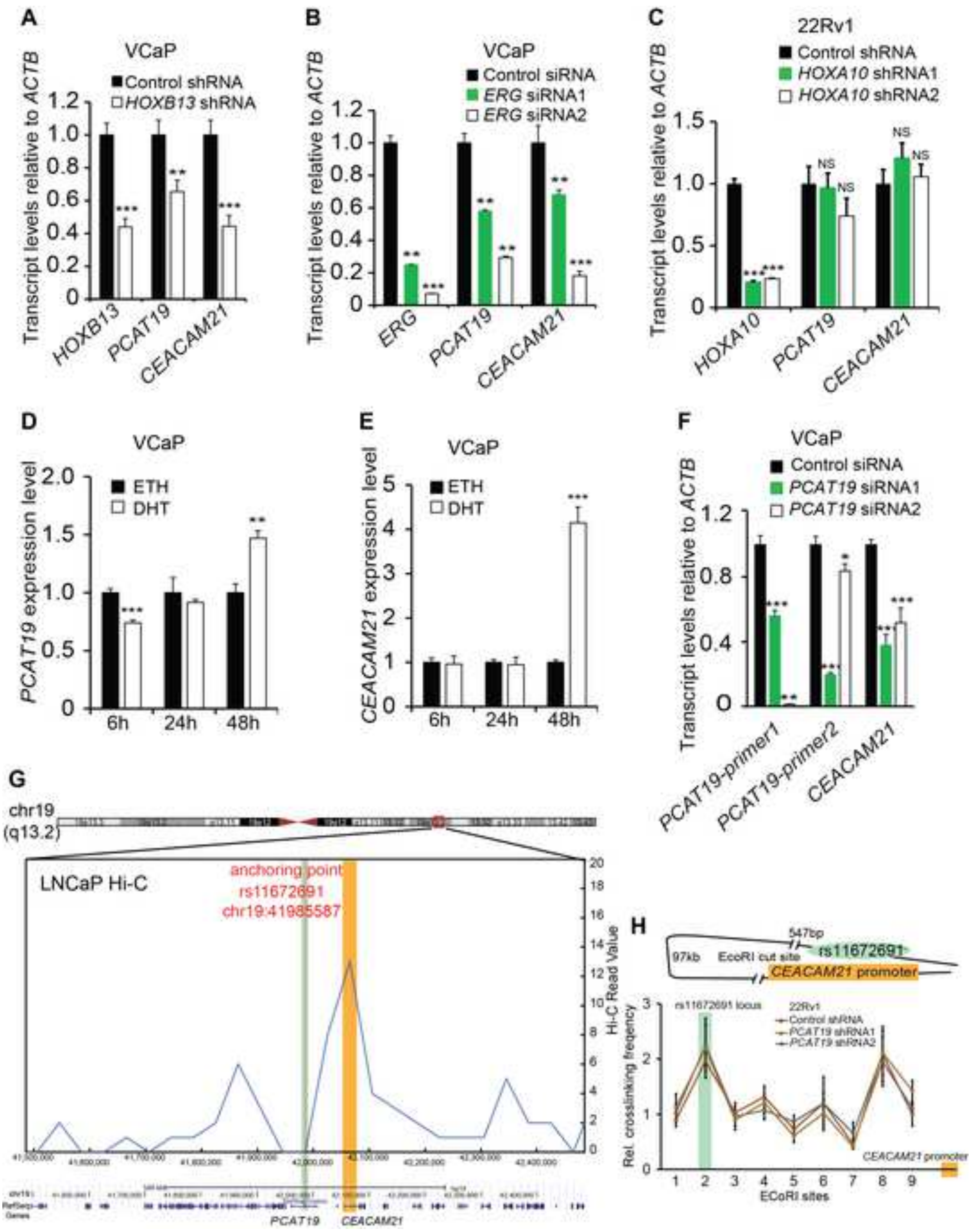
A
VCaP
Control shRNA
HOXB13 shRNA
Transcript levels relative to ACTB
1.2
1.0
0.8
0.6
0.4
0.2
0
***
**
***
HOXB13
PCAT19
CEACAM21
B
VCaP
Control siRNA
ERG siRNA1
ERG siRNA2
Transcript levels relative to ACTB
**
***
**
**
**
***
ERG
PCAT19
CEACAM21
C
22Rv1
Control shRNA
HOXA10 shRNA1
HOXA10 shRNA2
Transcript levels relative to ACTB
1.5
1.0
0.5
0
***
***
NS
NS
NS
NS
HOXA10
PCAT19
CEACAM21
D
VCaP
ETH
DHT
PCAT19 expression level
2.0
1.5
1.0
0.5
0
***
**
6h
24h
48h
E
VCaP
ETH
DHT
CEACAM21 expression level
5
4
3
2
1
0
***
6h
24h
48h
F
VCaP
Control siRNA
PCAT19 siRNA1
PCAT19 siRNA2
Transcript levels relative to ACTB
1.2
0.8
0.4
0
***
**
***
*
***
***
PCAT19-primer1
PCAT19-primer2
CEACAM21
G
chr19
(q13.2)
LNCaP Hi-C
anchoring point
rs11672691
chr19:41985587
Hi-C Read Value
20
18
16
14
12
10
8
6
4
2
0
41,500,000
41,600,000
41,700,000
41,800,000
41,900,000
42,000,000
42,100,000
42,200,000
42,300,000
42,400,000
chr19:
RefSeq Genes
PCAT19
CEACAM21
H
547bp
rs11672691
97kb
EcoRI cut site
CEACAM21 promoter
rs11672691 locus
22Rv1
Control shRNA
PCAT19 shRNA1
PCAT19 shRNA2
Rel. crosslinking frequency
3
2
1
0
1
2
3
4
5
6
7
8
9
EcoRI sites
CEACAM21 promoter

Figure S7

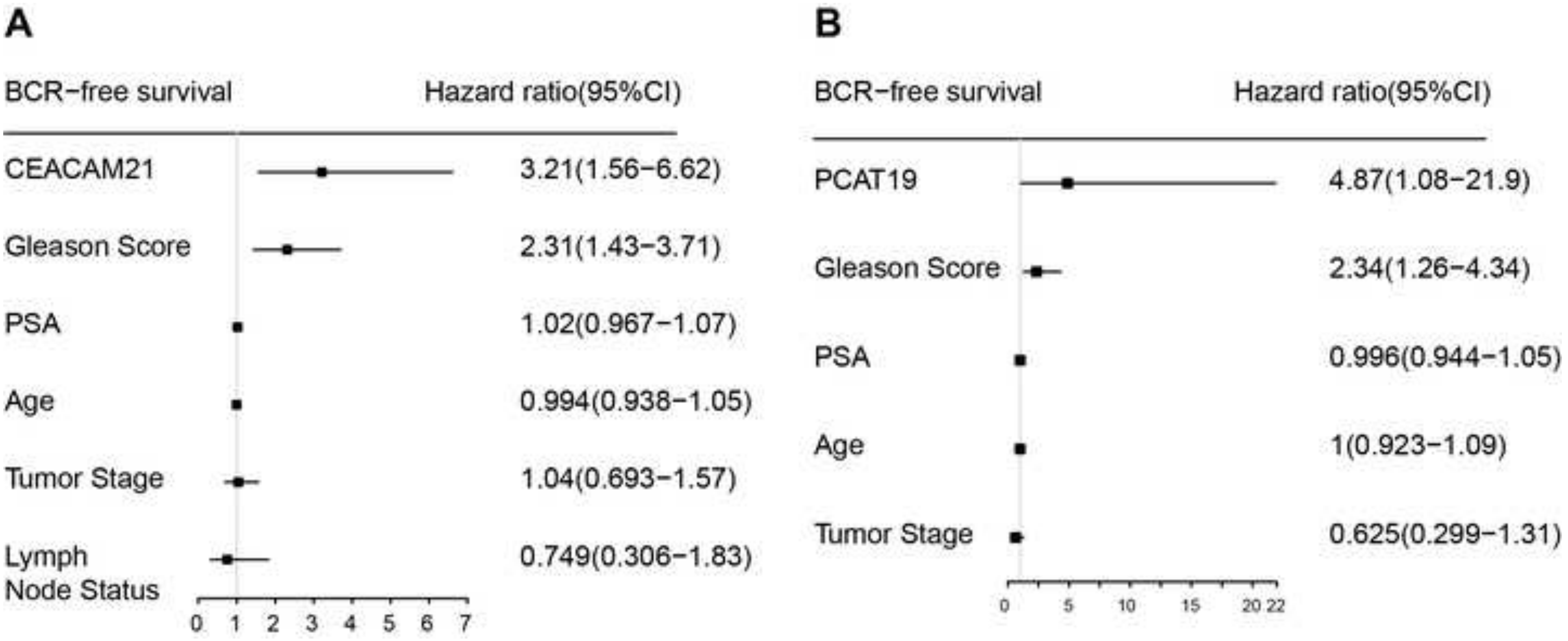
A
BCR−free survival
Hazard ratio(95%CI)
CEACAM21
3.21(1.56−6.62)
Gleason Score
2.31(1.43−3.71)
PSA
1.02(0.967−1.07)
Age
0.994(0.938−1.05)
Tumor Stage
1.04(0.693−1.57)
Lymph Node Status
0.749(0.306−1.83)
0
1
2
3
4
5
6
7
B
BCR−free survival
Hazard ratio(95%CI)
PCAT19
4.87(1.08−21.9)
Gleason Score
2.34(1.26−4.34)
PSA
0.996(0.944−1.05)
Age
1(0.923−1.09)
Tumor Stage
0.625(0.299−1.31)
0
5
10
15
20
22